Water as a coolant of cities

Solcerova, Anna

DOI
10.4233/uuid:ce45b39c-4a28-46a5-a90f-fab989b132ce

Publication date
2018

Document Version
Final published version

Citation (APA)
Solcerova, A. (2018). *Water as a coolant of cities*. [Dissertation (TU Delft), Delft University of Technology]. https://doi.org/10.4233/uuid:ce45b39c-4a28-46a5-a90f-fab989b132ce

WATER AS A COOLANT OF CITIES

WATER AS A COOLANT OF CITIES

Proefschrift

ter verkrijging van de graad van doctor
aan de Technische Universiteit Delft,
op gezag van de Rector Magnificus prof. dr. ir. T.H.J.J. van der Hagen,
voorzitter van het College voor Promoties,
in het openbaar te verdedigen op vrijdag 26 oktober 2018 om 10:00 uur

door

Anna SOLCEROVÁ

Master of Science in Earth en Environment
Wageningen University & Research
en
Engineer of Environmental Modelling
Czech University of Life Sciences

geboren te Ústí nad Labem, Tsjechië.

Dit proefschrift is goedgekeurd door de

promotor: prof. dr. ir. N. C. van de Giesen
copromotor: dr. ir. F. H. M. van de Ven

Samenstelling promotiecommissie:

Rector Magnificus	voorzitter
Prof. dr. ir. N. C. van de Giesen	Technische Universiteit Delft
Dr. ir. F. H. M. van de Ven	Technische Universiteit Delft
Onafhankelijke leden:	
Prof. dr. Č. Maksimović	Imperial College London
Prof. dr. A. A. M. Holtslag	Wageningen University
Prof. dr. ir. S. C. Steele-Dunne	Technische Universiteit Delft
Dr. ir. A. M. J. Coenders-Gerrits	Technische Universiteit Delft
Prof. dr. ir. A. van Timmeren	Technische Universiteit Delft

Keywords: urban heat island, climate adaptation, water management, evaporation, heat stress mittigation

Printed by: Ipskamp Printing

Front & Back: Yozef van 't Klooster

ISBN 978-94-028-1215-2

An electronic version of this dissertation is available at
http://repository.tudelft.nl/.

SUMMARY IN ENGLISH

Since more than half of the world population already lives in cities, it is important to understand the urban climate and its particularities. One of the typical aspects of urban areas is that cities are generally warmer than their rural surrounding. This phenomenon was first time described 200 years ago in the case of London and is commonly referred to as the *Urban Heat Island* (UHI).

Urban heat island roots from a wide scale of factors typical for cities. Increased heat storage caused by higher specific heat capacities of construction materials together with darker color of urban surfaces, lack of vegetation and open water bodies, anthropogenic heat added by industry, traffic or air-conditioning, or the specific geometry of the street canyons are just few examples of how cities become warmer than rural areas. One of the often suggested ways to mitigate UHI is increasing evaporation by reintroducing vegetation and open water back to urban areas.

One of the possible ways to decrease air temperature is to increase evaporation by open water, such as ponds, channels, or fountains. Comparative studies have shown that from all the urban land use types, open water is the most efficient in reducing UHI at a local scale. This is because urban ponds and channels reduce the air temperature in two ways: they store the heat and increase its own temperature, and they use the incoming solar energy to evaporate the water.

The heat that an open water body accumulates during daytime is then released at night. We have analyzed the magnitude of turbulent - latent and sensible - heat fluxes in comparison to radiative and ground fluxes in order to further understand in what form the heat leaves the water. A detailed vertical temperature profile was measured in an urban pond in Delft (NL) using Distributed Temperature Sensing (DTS) method. This method allows for high temporal and spatial resolution. In our case, we measured a 2 m tall temperature profile with 2 mm vertical resolution. The results show that, from the recorded total of 2.7 MJm^{-2} of heat released on average by the pond every summer night, 43 % of the thermal energy is emitted as longwave radiation, 39 % as latent energy, and 11 % as sensible heat. Sensible heat is the only flux that increases the air temperature. An additional 0.1 - 0.3 MJm^{-2} is transferred into the bottom of the lake.

During the measurements done in Delft we have also observed a thin layer of surface water that is colder than the water beneath it. This phenomenon is known as the skin effect and was previously described in oceanography and verified in lab measurements. Nonetheless, only a few measurements have been done on the skin effect in field conditions, and therefore this phenomenon is relatively unknown. We have compared the measurements obtained in Delft with measurements from two different fresh water bodies, in Israel and in Ghana, and analyzed the magnitude of the temperature difference and the thickness of the skin layer. The results suggest that the skin effect of fresh water bodies is predominantly a daytime phenomenon and only occurs during low to zero wind speeds. The thickness of the skin effect was measured to be an order of mag-

nitude larger than the previously assumed maximum of 1 mm. Despite the testing of several potential reasons, no solid explanation could be found for the observed depth of the skin layer.

Air temperature is also cooled by evaporation from water intercepted on paved surfaces. Cooling efficiency of interception was investigated using a 17^{th} century Japanese tradition, uchimizu, in which water is sprinkled around houses to cool the ground surface and the air and to settle the dust. Though the method is widely used and its benefits are agreed on, the number of published studies that have quantified the cooling effects of uchimizu are limited, and only report measurements of the surface temperature, or of an air temperature at a single height, as a measure of the cooling effect. We have used a dense three-dimensional DTS setup to measure air temperature with high spatial and temporal resolution within one cubic meter of air above an urban surface. Six experiments were performed to systematically study the effects of (1) applied water amount, (2) initial surface temperature, and (3) shading of the pavement on the cooling effect of uchimizu. The measurements showed a decrease in air temperature up to 1.5 °C at 2 m height, and up to 6 °C for near-ground temperature. The strongest cooling was measured in the shade experiment. There was no clear difference in cooling effect for an amount of water applied of 1 l/m^2 and 2 l/m^2, but after application of a large amount of water (>5 l/m^2), the strong near-ground cooling effect was approximately twice as high as when only 1 mm of water was applied. The dense measurement grid used in this research also enabled us to detect the rising turbulent eddies created by the heated surface.

Next to open water and wetted paved surfaces, evaporative cooling can also be provided via transpiration of vegetation. One of the repeatedly suggested measures to moderate the urban heat island are green roofs. We have investigated several extensive sedum-covered green roofs in Utrecht (NL) and their effect on air temperature right above the roof surface. Temperature was measured 15 and 30 cm above the roof surface and also in the substrate. We showed that under well-watered conditions, the air above the green roof, compared to the white gravel roof, was colder at night and warmer during the day. This suggests that, if well-watered, extensive sedum-covered green roofs might help decrease air temperatures at night, when the urban heat island is strongest, but possibly contribute to high daytime temperatures. The average 24 hour effect of sedum-covered green roof was a 0.2°C increase of air temperature 15 cm above the sedum surface. During a dry year the examined green roof exhibited behavior similar to conventional white gravel roof and even exhibited slight cooling effect in late afternoon. Interestingly, the pattern of soil temperature remained almost the same for both dry and well-prospering green roofs, colder during the day and warmer at night.

SAMENVATTING IN HET NEDERLANDS

Omdat al meer dan de helft van de wereldpopulatie in steden woont, is het belangrijk om het klimaat in stedelijke omgevingen goed te begrijpen. Een van de typische aspecten van verstedelijkte gebieden, is dat deze over het algemeen warmer zijn dan de landelijke gebieden rondom steden. Dit fenomeen werd al 200 jaar geleden beschreven in Londen en staat bekend als het Urban Heat Island (stedelijke hitte-eilandeffect).

Urban Heat Islands (UHI) worden veroorzaakt door een scala typische karakteristieken van steden. Veelgebruikte materialen in stedelijke gebieden hebben donkere kleuren en hogere specifieke warmtecapaciteiten en veroorzaken daardoor een verhoogde warmteopslag. Ook zijn er in steden vaak minder planten en open water te vinden. Daarnaast voegen menselijke warmtebronnen zoals industrie, verkeer, airconditioning en geometrie van straten nog extra hitte toe aan de stad in vergelijking tot rurale gebieden. Een van de gesuggereerde manieren om UHI's tegen te gaan is door de verdamping te vergroten door middel van het herintroduceren van planten en open water in stedelijke gebieden.

Luchttemperatuur kan verlaagd worden door middel van hogere verdamping van water uit vijvers, kanalen of fonteinen. Vergelijkende studies hebben al laten zien dat open water het meest efficiënte manier is op UHI's tegen te gaan op kleinere schaal. Open water verlaagd luchttemperatuur op twee manieren: het kan zelf warmte opslaan en ze onttrekken energie door water te laten verdampen.

De warmte die accumuleert in open water gedurende de dag wordt 's nachts weer uitgestoten. In deze dissertatie zijn de groottes van turbulente (latente en voelbare) warmtefluxen in vergelijking tot de warmtestraling vanuit de bodem geanalyseerd om beter te begrijpen hoe de warmte het open water verlaat. Hiervoor zijn temperatuurprofielen van in totaal twee meter van de lucht boven een open waterlichaam in Delft (Nederland) met hoge ruimtelijke resolutie (2mm) gemeten. Hieruit is gebleken dat in totaal 2.7 MJ/m^2 aan warmte wordt uitgestoten boven een vijver elke nacht tijdens de zomer, waarvan 43% als warmtestraling, 39% als latente energie en 11% als voelbare energie. De voelbare energie is de enige flux die de luchttemperatuur doet stijgen. Daarnaast is 0.1 – 0.3 MJ/m^2 aan warmte overgegaan in de bodem van de vijver.

Tijdens de metingen in Delft is ook waargenomen dat een dunne laag van het wateroppervlak kouder is dan het water daaronder. Dit fenomeen staat bekend als het skineffect en is reeds beschreven in de oceanografie en bevestigd tijdens laboratoriumexperimenten. Echter, slechts weinig metingen van het skineffect zijn gedaan in het veld en daardoor is er nog steeds veel onbekend over dit fenomeen. In dit proefschrift zijn metingen van het skineffect vergeleken onder veldomstandigheden in Delft, Ghana en Israël, met name de grootte van het verschil in temperatuur tussen de koude laag en

het onderliggende water en de dikte van deze koudere laag. De resultaten laten zien dat het skineffect van zoetwaterlichamen voornamelijk tijdens de dag plaatsvindt en alleen tijdens momenten met weinig tot geen wind. De dikte van deze koude laag is een ordegrootte groter dan de tot dusver aangenomen 1mm. Ondanks het testen van verschillende hypotheses is er nog geen eenduidige verklaring gevonden voor de dikte van de koude laag.

Luchttemperatuur wordt ook gekoeld door water dat verdampt van verhard oppervlakte (interceptie) in de stad. De koelefficiëntie van interceptie is onderzocht door middel van het gebruik van een 17e-eeuwse Japanse traditie uchimizu, waarbij water rondom huizen wordt gesprenkeld om de bodem te koelen en om het stof in de lucht te laten neerdalen. Alhoewel deze methode alom wordt gebruikt en men het eens is over de voordelen zijn er weinig studies gepubliceerd die de koeling van uchimizu gekwantificeerd hebben. Daarnaast rapporteren de enige beschikbare studies alleen het effect op de oppervlaktetemperatuur of op de luchttemperatuur op een enkele hoogte. Dit proefschrift presenteert data van een driedimensionale Distributed Temperature Sensing¬-opstelling (DTS), waarbij luchttemperatuur met hoge ruimtelijke en temporele resolutie binnen een kubieke meter boven een stedelijk verhard oppervlak gemeten is. Er zijn zes experimenten uitgevoerd om systematisch te bestuderen wat de effecten zijn van (1) de hoeveelheid besprenkeld water, (2) de aanvankelijke oppervlaktetemperatuur en (3) de mate van schaduw op de koelende werking van uchizmizu. De metingen laten zien dat de luchttemperatuur gekoeld kan worden met 1.5 graden op een hoogte van 2 meter, tot 6 graden dichtbij de grond. De sterkste koeling werd gemeten tijdens het experiment met de meeste schaduw. Er was geen duidelijk verschil tussen het koeleffect bij een besprenkelde hoeveelheid van 1L/m^2 en 2L/m^2, maar bij besprenkeling met een hoge hoeveelheid water (>5L/m^2), de sterkte koeling dichtbij de bodem was ongeveer twee keer zo hoog als bij besprenkeling met slechts 1 L/m^2. De gebruikte meetopstelling met hoge dichtheid van kabels stelde ook in staat om opkomende turbulente wervels, gecreëerd door het verhitte oppervlakte, te detecteren.

Behalve open water en bewaterde verharde oppervlaktes kan koeling middels verdamping ook vergroot worden door transpiratie van water door vegetatie. Een van de veelvoorkomende suggesties om UHI's tegen te gaan zijn groene daken. Dit proefschrift heeft het effect van met sedum bedekte groene daken in Utrecht op de luchttemperatuur boven deze daken onderzocht. De luchttemperatuur is gemeten op 15 en 30 cm boven het oppervlakte, alsmede in het substraat van het dak. Tijdens goed bewaterde omstandigheden is de lucht boven het groene dak 's nachts kouder en overdag warmer vergeleken met een wit, met gravel bedekt, dak. Dit suggereert dat, indien goed bewaterd, daken die met sedumplanten bedekt zijn helpen om de luchttemperatuur 's nachts, wanneer het UHI het sterkste is, te koelen, maar mogelijk leiden tot een hogere luchttemperatuur overdag. Het middelde 24-uurseffect van sedumdaken was een verhoging van de luchttemperatuur met 0.2 C op 15cm boven het dak. Tijdens een droog jaar gedraagt een sedumdak zich nagenoeg gelijk als een wit graveldak en laat zelfs een licht koelend effect zien in de namiddag. De dynamiek van bodemtemperatuur op een groen dak is nagenoeg hetzelfde tijdens droge en natte omstandigheden; kouder tijdens de dag en warmer tijdens de nacht.

CONTENTS

1

INTRODUCTION

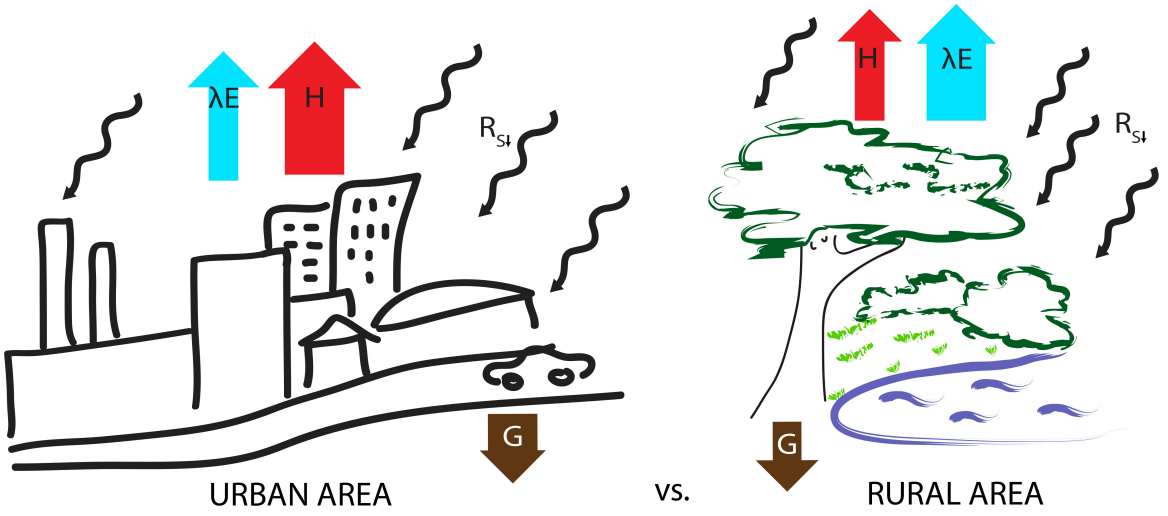

1

During the last decades, solutions involving combinations of vegetation and water became increasingly popular for rain water management in cities [Liao et al. (2017)]. Incorporating vegetated areas and water detention facilities for drainage and peak flow reduction after strong rainfalls has several benefits compared to the traditional gray solutions, e.g. for improvement of storm water quality. These so called blue-green solutions – blue for water, green for vegetation – are easier to adapt for changing rain intensities, they are more aesthetically pleasing, and they provide additional ecosystem services, such as habitats for various species of fish, birds, invertebrates, and also plants. Additionally, many blue-green solutions have claimed effect on urban climate, reducing extreme heat by up to several degrees. This thesis focuses on the cooling effect of urban water and vegetation.

Generally, blue-green solutions are adaptation measures that incorporate water, vegetation, and combinations of the two. Examples include urban ponds, green roofs [Santamouris (2014); Berardi et al. (2014)], bioswales [Allen et al. (2015); Leroy et al. (2016)], or rain gardens [Li et al. (2016); Tang et al. (2015)]. Utilizing blue green solutions not only minimizes the water shortage for vegetation during heat stress, but also enhances storage capacity and reduces peak flows during and after heavy rainfall events [Voskamp and Van de Ven (2015)]. Anther advantage is that they can be specifically designed for each location.

Extreme heat is a common problem in the urban environment. A problem that is intensified by a phenomenon called the Urban Heat Island (UHI) and by projected climate change. Due to climate change, the average air temperature rises and the frequency and intensity of heat waves is predicted to increase [Perkins et al. (2012)]. This will not be without consequences, as several studies have shown that higher temperatures can lower the quality of sleep, and increase the risk of respiratory illnesses and cardiovascular mortality [e.g. Changnon et al. (1996); Patz et al. (2005); Tan et al. (2007); Peng et al. (2011)]. For example, at high temperatures (as defined by Baccini et al. (2008) for different climate zones) the mortality increases by 20 % to 35 % [Paravantis et al. (2017)].

Thermal comfort, or perceived temperature, refers to the way people experience their environment. Many studies focused on thermal comfort of indoor environments and the effect of, for example, air-conditioning, or presence of plants [e.g. Frontczak and Wargocki (2011); Baird and Field (2013)]. Outdoor thermal comfort of urban areas is related to many different factors. Some of the most important and often studied factors include air temperature, radiative temperature, relative humidity, wind speed, but also age, gender, clothing, or general fitness [Djongyang et al. (2010); Rupp et al. (2015)].

Temperatures in cities are almost always higher than those in the surrounding rural areas. This is a consequence of many factors, including the presence of high specific heat capacity materials used for construction of buildings and roads, lower albedo of urban surfaces, and heat added by human activities. This difference in temperature between cities and rural areas was first time described almost 200 years ago in the case of London [Howard (1820)], but was more intensively studied only during the last two decades.

The UHI is generally defined as the difference between temperature in the city and in the rural (surrounding) area. This, however, leaves space for interpretation. The UHI can be approached from different perspectives: (1) daytime vs nighttime UHI, (2) surface vs urban canopy vs boundary layer UHI, (3) point measurements vs average values. Surface

UHI is usually referred to, when large remote sensing datasets are used. This is particularly useful for studying differences between average UHI for different neighbourhoods [Huang and Cadenasso (2016)], land uses [Jenerette et al. (2016)], or whole cities [Zhou et al. (2014)]. Urban canopy UHI is usually associated with point measurements of air temperature, or with case studies investigating the effect of a particular adaptation measure on the air temperature [e.g. van Hove et al. (2015)]. Boundary layer UHI is relatively less common in literature, since it requires complex measurement techniques such as meteorological towers, aircraft measurements, or lidar [Barlow (2014)]. In this thesis we focus on the urban canopy UHI.

In recent years, much attention has been given to finding solutions to mitigate the urban canopy UHI. Many studies have focused on quantifying the cooling effects of certain measures. Those measures can be, in general, divided into solutions that aim to reduce the heating through structural and architectural changes, such as a higher albedo [Salamanca et al. (2012)] or a reduced sky view factor [Wang et al. (2011)], and those solutions that aim at cooling through increased evaporation [Theeuwes et al. (2013)].

Blue-green solutions are part of the solutions that aim to decrease extreme temperature by increased evaporation [Rozos et al. (2013); Voskamp and Van de Ven (2015)]. Green roofs and green walls, vegetated swales, urban parks, water retentive paving materials, and open water bodies, have all been studied in order to quantify their cooling performance. Nonetheless, majority of the published research results were case studies only focusing on a performance of one particular blue-green solution at one particular location.

This thesis focuses on quantifying the role water plays in the cooling effect of blue-green solutions in urban environments. We performed several measurement campaigns and analyzed the results in a way that is adaptable for and transferable to other cases. For example: instead of asking "How does this green roof influence the air temperature?", we aim to answer a more basic question of "What is the influence of soil moisture on thermal performance of a green roof?".

The aim of this introduction is to elaborate on the role of water in the different components of natural cooling processes of urban areas. We focus on the relationship between water and energy, on how the energy balance of cities is shifted from latent heat towards sensible heat, and ground flux, which are the components that cause increase in air and surface temperature respectively. As evaporation and energy are inevitably linked, we discuss the role water plays in the energy balance of urban area and the effectiveness of using blue-green elements as cooling solutions. Knowledge gaps will be identified to create the basis for the leading research questions for this thesis and its under-laying research.

1.1 ENERGY BALANCE

Within the surface energy balance, net radiation (R_n [Wm^{-2}]) can be expressed as sum of incoming shortwave radiation (R_S) and incoming longwave radiation (R_L), minus energy emitted:

$$R_n = (1-\alpha)R_S + (1-\epsilon)R_L - \epsilon\sigma T^4 \tag{1.1}$$

Where α is albedo [-] of the surface, ϵ is emissivity [-], σ is Stefan Boltzmann constant [Wm^2K^{-4}], and T is temperature [K]. This balance can be also expressed as

$$R_n = H + E + G \tag{1.2}$$

Where H [Wm^{-2}] represents sensible heat flux, E [Wm^{-2}] latent heat flux due to evaporation of water, and G [Wm^{-2}] ground flux. Sensible heat flux is what warms up the air above a dry surface. For instantaneous values, Equation 1.1 represents the available amount of energy at any given moment, while Equation 1.2 represents how the available energy is portioned to different fluxes.

Cities generally transform the incoming solar radiation more into sensible heat than into latent heat - their Bowen ratio (H/E) is higher. Due to dryer conditions, the ability of urban areas to convert radiation into latent heat is lower than that of rural areas. Consequently, the ground heat flux and the amount of energy released in the form of sensible heat is magnified [Oke (1982)].

The latent heat flux - evaporation - is an important component of the energy balance. Globally, evaporation, including transpiration of plants, consumes almost 22 % of available solar energy [Qiu et al. (2013)]. The average net incoming radiation on a partly cloudy summer day in the Netherlands is between 200 and 300 Wm^{-2}, or about7 - 12 MJm^{-2}. Energy necessary to evaporate one liter of water equals 2260 kJ, which means that to evaporate just 2 mm of water requires up to about half of the energy provided by solar radiation per day. Consequently, this energy is no longer available for heating up the air. Lack of water for evaporation is one of the drivers of differences in the energy balance in urban areas compared to rural areas. A detailed water balance study of a 2 hectare, 47 % paved housing area and a 93 % paved, 0.76 ha parking lot in the city of Lelystad (NL) over the period 1970 - 1984 showed an annual evaporation of 312 mm/y (42 % of total precipitation) and 138 mm/yr (18 %) respectively [Van de Ven (1990)]. In comparison Verhagen et al. (2014) reported an average actual evaporation of a deciduous forest located some 70 kilometers away from Lelystad equal to 609 mm/y and 681 mm/yr for a coniferous forest over 1951 - 2013. Elbers et al. (2010) reports an annual actual evaporation of two grassland sites located in the center of Holland of 567 ± 89 mm/yr in 2006 (73 % of annual precipitation) and 548 ± 60 mm/yr in 2003/2004 (81 %). Although no direct comparison can be made, it could be argued that the actual annual evaporation of a "regular" housing area is some 200 - 250 mm less than the evaporation of a "regular" rural area. For the paved parking lot this difference is in the order of 370 - 420 mm/yr.

We may hypothesize that this difference is created during warm and dry spring and summer days, not throughout the wet, humid and colder fall and winter season. The difference in actual evaporation between rural and urban environment will be the largest on warm and dry days during the growing season, ranging from May - September. Under the assumption that this period contains about 100 - 125 "summer" days per year the difference in evaporation is at least about 1.5 - 2 mm/d for the housing area or about 3.5 - 4.5 $MJm^{-2}day^{-1}$. This is on average a quarter to one third of the daily net incoming solar radiation. Similarly, for the parking lot these figures are 3 - 4 mm/d of reduced evaporation or about half to equal to the average net solar radiation. No wonder that the urban area runs hot on sunny days.

1.2 MITIGATING HEAT STRESS

In particular since the beginning of this century, heat stress in urban areas has been recognized as a serious problem, as shown above. Hence, urban planners, designers and landscape architects, urban climate specialists, and hydrologists have been looking for effective measures to mitigate heat stress and the UHI in particular.

1.2.1 LATENT HEAT

Comparative studies have shown that open water is the most efficient of all the city land use types in reducing UHI in its surrounding [Rinner and Hussain (2011); Olah (2012)], although disputed by CPC-Consortium (2014). Another effective remedy is evaporation of vegetation. From various different vegetated surfaces commonly found in cities, grass showed the highest evaporation rate [Peters et al. (2011)]. However, trees have several degrees higher cooling effect than grassy surfaces, which suggests that the contribution of shading cannot be neglected either [Olah (2012)]. Other sources of evaporation in the city are evaporation (drying) of intercepted water on vegetation, roofs, and paved surfaces after rainfall or other wetting.

OPEN WATER BODIES

Open water evaporation from urban surface water bodies such as ponds, lakes, canals, and rivers have a direct effect on the latent energy component of the energy balance. Even presence of a swimming pool in a garden resulted in lower temperatures in the area [Halper et al. (2012)]. Literature about cooling effect of ponds is however relatively scarce, often just part of a larger assessment of the UHI and possibilities of its mitigation [i.e. Kleerekoper et al. (2012); Taleghani (2017); Völker et al. (2013)]. Literature about urban ponds and lakes mostly focuses on investigation of other functions, such as urban water storage [Furumai (2008)], flood protection [Meierdiercks et al. (2010)], water treatment [Martin (1988)], decorative purposes[Nasar and Li (2004)], or even energy harvesting [Aparicio Medrano (2008); de Graaf et al. (2008)]. Storing water locally not only can help reduce ambient temperature. It is also beneficial during extreme rainfall events to avoid flooding, and during dry spells to lower the costs for irrigation, which would normally be done with high-quality potable water [Coutts et al. (2012)]. There are also several studies considering the temperature regime of the water body itself and its impact on water quality [Jacobs et al. (1997); Hester and Bauman (2013)].

Limiting factors to evaporative cooling caused by a water surface include humidity and wind speed. If relative humidity reaches 100%, an equilibrium between evaporation and condensation is established. This can happen in a thin layer above water during calm summer days [Hisatake et al. (1993)] and significantly restrict evaporation. Therefore, a determining factor is wind speed, as this is a powerful engine behind convective vapor transport from water into the higher atmosphere.

VEGETATION

Compared to the effect of urban surface water bodies, the effect of green areas on city temperature is better researched. There is a relatively wide spectrum of articles addressing cooling by the different types of green spaces in urban area such as, green roofs [e.g. Berardi et al. (2014); Peri et al. (2013)], grassy areas [Wu et al. (2014)], parks [Shishegar

(2014)], and trees [Taleghani (2017)]. Evaporation by the vegetation suggests to be of great importance for cooling. The presence of vegetation indeed shows a negative correlation with temperature [Gabor and Jombach (2010)]. Bowler et al. (2010) summarized articles that measured the effect of the aforementioned categories of urban green space on air temperature. They concluded that incorporating green areas always lowers air temperature at least at a local scale. However, the magnitude of the effect is hard to estimate, since it depends on many factors such as specific species, soil moisture availability, and local climate. Specific species are often generalized to categories such as 'grass', 'coniferous trees', or 'broad-leaf trees', which makes it hard to investigate potentially relevant differences in cooling effect between plant species. However, the evaporation rates of various species of trees and turf grasses in urban areas were quantified by several studies [e.g. Bush et al. (2008); Zhang et al. (2007)] and show that cold-season grasses have the highest evaporation rate. Peters et al. (2011) measured the evaporation fluxes from residential and recreational areas in a city and concluded that the relative contribution of vegetation types to evaporation rate depends on the season. For example, broad-leaf trees reach their maximal potential during late summer, but grass in spring and fall. Grass is also the most common vegetation cover in urban areas, both irrigated and non-irrigated and therefore contributes the most to the evaporation component of the urban water budget and hence to cooling.

Actual evaporation of vegetation depends on the availability of water in the root zone. Depth of the root zone is species and soil type dependent. Trees tend to have a deeper and wider root system than most grasses, thus can sustain evaporation better in periods of drought than grass. Limited soil moisture content during drought also influences opening of the stomata in leaves and thus evaporation. Some plants - like Sedum - can stop transpiring to save water and survive dry spells due to an adapted photosynthesis mechanism. Data on soil conditions, groundwater depth, on the root zone depth, and vegetation species are therefore important to estimate actual evaporation, and thus latent energy flux.

Green roofs can be considered a special case in urban greening for two reasons. First, the effect of green roofs is not sensible at the street level as is the case for other urban greening. Second, sedum - which is a commonly used plant for extensive green roofs - behaves differently than other types of plants, the metabolism of sedum is highly resistant to drought and requires only minimum maintenance through irrigation [Nagase and Dunnett (2010); Kircher (2002); Monterusso et al. (2005)]. Drought resilience is achieved by limiting the transpiration during daytime hours and postponing it until night. Hence, sedum is expected to have a cooling effect on nighttime air temperatures, but not during the day.

INTERCEPTED WATER

Water from rainfall or sprinkler irrigation is intercepted by vegetation and on paved surfaces and roofs. Several techniques are available to mitigate heat this way. For example in Japan, where water is sprinkled on the pavement. This tradition is called uchimizu and is still used today as immediate cooling technique during hot summer days [Matsubara and Sawashima (1993)]. The effect of such a measure is local and time limited, but it can temporarily decrease the local air temperature by several degrees [Slingerland (2012)].

Other methods utilizing intercepted water are blue roofs and water retentive pavements. They too can help reduce the sensible heat flux [Takebayashi and Moriyama (2007)]. Utilizing intercepted water by harvesting in a retentive pavement can cool the environment by 3 °C at night and up to 8 °C during day [Yamagata et al. (2008)]. Similar principles hold for blue roofs, with the additional benefit of indoor cooling and reduction in air conditioning energy consumption [Pisello (2017)].

The cooling effect of evaporating intercepted water is temporal, for short periods following rainfall, as the volume of water is limited; during longer dry spells this reservoir is empty. Additionally, evaporation from bare soil and paved surfaces is at an absolute minimum or non-existent during droughts, unless water is supplied from an external source.

1.2.2 ALBEDO

Albedo ("whiteness") is the fraction of solar shortwave radiation reflected by the surface of a material. The part of the radiation that is not reflected is adsorbed by the surface. The albedo value determines how much incoming solar energy becomes available as heat and is consequently extremely important for the thermal control of the urban environment. Simply painting all roofs with a reflecting color - cool roofs - can decrease the overall UHI up to 33% [Oleson et al. (2010)]. Many urban surfaces, however, have a lower albedo than natural surfaces and therefore produce more heat. Although expected otherwise, data on albedo of urban surface materials are limited. Table 1.1 contains albedo values for urban surfaces retrieved from literature as well as values from own observations in Delft.

As can be seen in Table 1.1, the albedo of urban surfaces strongly depends on type and state of the surface cover. Wet pavements tend to have a lower albedo than dry ones - a phenomenon hardly ever mentioned in literature. Given the diversity of the surface cover in urban areas, heat production can vary largely from place to place.

Albedo is also an important parameter influencing the amount of heat storage in the surface water. Albedo of surface water is generally considered relatively low during summer day (ca 6%) when the zenith angle is low. Field observations of a highly turbid urban pond in Delft in the summer of 2014 showed values of approximately 3%. With sun closer to the horizon albedo of water surface increases.

1.2.3 SHADING

High evaporative rates of grasses would suggest that grass has the strongest evaporative cooling power. However, grassy surfaces show several degrees lower cooling effect than trees 0.5 m above ground [Shashua-Bar et al. (2009)]. This addresses yet another important parameter, the role of shading. Especially in tropical climates, shading is one of the leading factors in cooling effect of vegetation during daytime [Oke (1989)]. Shading certain areas reduces sky view factor, thereby lowering the peak in local air temperature at street level [Hien and Jusuf (2010); Wang and Akbari (2016); Zölch et al. (2016)]. On the other hand, just shading a certain area may have the opposite effect of what is expected, i.e. increased ambient air temperature. According to a study comparing several identical courtyards with different amounts and types of vegetation cover, simply covering the area to provide shade can increase the air temperature and also reduce the ventilation

Table 1.1: Albedo values reported in literature [Psiloglou and Kambezidis (2009); Rutgers (1998)] and measured in Delft [Romeijn (2014)]

Surface	**Details**	**Albedo**		
		Literature	Measured Delft	
			wet	dry
Soil	dark and wet	0.05 -	-	-
	light and dry	0.4	-	-
Forest	deciduous	0.15-0.20	-	-
Water	small zenith angle	0.03 - 0.10	0.05 - 0.07	-
	large zenith angle	0.10 - 1.00	0.80 - 1.00	-
Sand		0.15 - 0.45	0.22	0.22
Grass		0.16 - 0.26	0.17	0.18
Asphalt		0.05 - 0.20	0.07	0.07
Concrete		0.10 - 0.35	0.19	0.23
Brick		0.20 - 0.40	-	-
	mixed	-	0.06	0.07
	red	-	0.07	0.07
	gray	-	0.13	0.15
Gravel		-	0.30	0.28
Paving	smooth	-	0.12	0.15
	coarse	-	0.09	0.11
Natural stones		-	0.35	0.51
Artificial stones		-	0.15	0.16

by wind by 50% [Shashua-Bar et al. (2009)]. The combination of higher temperature and lower wind speed results in significantly lower thermal comfort than if the place would be well ventilated.

Shading caused by vegetation has a different effect in different climates and even in different positions with respect to buildings and other vegetation. While parks provide cooling during both night and day, trees planted along roads in between buildings can prevent nighttime cooling due to reduced ventilation, leading to higher nighttime temperatures than in streets without vegetation [Hien and Jusuf (2010)]. Shading provided by trees in between buildings reduces the outgoing long-wave radiation at night and therefore prevents radiative cooling [Yamashita et al. (1986)]. A study by McPherson et al. (1988) showed consequences of vegetative shading on use of heating and air conditioning. While west wall shading in a tropical city can lower electricity consumption for air conditioning, the same positioning of trees in cold regions will prevent sun irradiation and increase the demand for heating. Correspondingly, wind speed reduction is more welcome in cold regions than in tropical ones.

1.2.4 HEAT STORAGE IN SURFACE WATER

Measurements previously done by Slingerland (2012) in a stagnant urban canal in Rotterdam showed fluctuations of the top 0.20 m of water by more than two degrees during the day (6am till 10pm). Since heating one liter of water by 1 K requires 4190 J of energy, heating up one square meter of 20 cm layer of water (200 liters/m^2) by two degrees requires 1676 kJ of energy. The recorded incoming solar radiation that day (28 July 2011) was 12800 kJ/m2. This implies that over 13% of incoming solar energy was absorbed by the top layer of the canal with total depth of 1,1 m [Slingerland (2012)]. Unfortunately, no information was provided on the turbidity of this water, nor on the temperature increase below this 0.20 m top layer.

Turbidity of the water plays a role when it comes to radiation absorption. The net incoming solar radiation in turbid waters is converted to heat in the top layer. In contrast, radiation can penetrate deeper in cleaner waters and the incoming energy (heat) is distributed more equally over the depth of the water column. So, in the case of turbid water the top layer becomes hotter than it would for clean water, likely leading to a higher evaporation rate.

Surface water absorbs solar radiation very well and hence can effectively be used as a solar heat collector, as demonstrated in Paleiskwartier in 's-Hertogenbosch (The Netherlands) where an urban pond is used to feed the warm well of an Aquifer Thermal Energy System for heating of surrounding apartment and office buildings [Aparicio Medrano (2008)].

The ability of urban surface water bodies to store solar heat brings up the discussion about when and how this heat is released. During winter periods open water surfaces are the warmest areas in the city, and their warming effect is also visible at night, when the water temperature is higher than the air temperature in the city area [Hathway and Sharples (2012); Theeuwes et al. (2013); Steeneveld et al. (2014)]. This release of stored heat can enhance the UHI-effect by increasing minimum temperatures during summer nights [Albers et al. (2015); Jacobs et al. (1997)]. The same phenomenon is observed for road pavements and buildings. However, due to their smaller heat capacity and high

thermal conductance the effect on air temperature might be smaller than for urban surface water. The only way for buildings and pavements to cool at night is by long wave radiation and sensible heat flux from solid material to air, while surface water bodies continue to evaporate as well. Investigations on the ratio between cooling at night-time by long wave radiation versus cooling by evaporation versus cooling by a sensible heat flux were not found.

1.3 DISCUSSION

The link between the availability of water and ambient temperature in urban areas is recognized but not yet well understood. Several factors are subject of scientific debate.

VEGETATION

There are not many studies that in practice investigating the effect of a park beyond its boundary to quantify their zone of thermal influence. Existing studies have often contradicting conclusions. Most conclusions are based on modelling results. Chen and Wong (2006) showed that cooling effect of a park can extend to its surrounding and influence nearby built up area, but the effect dissipates rapidly with distance. The cooling effect disappears even faster when we consider the thermal comfort of inhabitants. By simply crossing the street when exiting a park perceived temperature (as defined by Höppe (1999)) can rise by up to 15 K [Heusinkveld et al. (2011)].

A lack of measurements of physical causes of cooling effect can be seen for urban vegetation. It is disputable if, for example, green roofs will still have a cooling effect, when transpiration is restricted by water stress. Modelling studies have shown contradictory results. While some suggest that the cooling effect will disappear when the soil moisture is limited [e.g. Suter et al. (2017)], other predict cooling also for low moisture content [Li et al. (2014)].

OPEN WATER BODIES

The highest cooling effect of lakes can be also observed close to the shore and several studies show that the effect mitigates after few tenths of meters [Xu et al. (2010)]. However, minor effects of a big enough lake can be expected even several kilometers far [Theeuwes et al. (2013)]. Factors such as the size of the water body, its shape, location in the city, and water temperature have an impact on the cooling effect of urban surface water. When it comes to size, it seems that bigger areas of open water have stronger effects on the surroundings. However, the drop in temperature caused by presence of a water body decreases with increased area [Sun et al. (2012)].

It has been proven that a water body not only evaporates, but also stores heat, but it stays unclear what is the ratio of these processes both during the day and night. Research on possible warming effect of water bodies on ambient air caused by releasing heat at night is also very scarce [e.g. Theeuwes et al. (2013)]. The observed cooling of a surface water body at night could also, at least partly, be the result of evaporation. The contributions of urban water bodies to the increased minimum temperatures during summer nights is yet to be investigated.

SIZE

Several smaller blue or green areas may be more beneficial than one large park or pond due to its oasis effect [Armson et al. (2012)].There is a limiting factor to the size. It was found that only parks bigger than 2 ha had continuous effect greater than 1.5 degrees (Nagoya, Japan) [Cao et al. (2010)]. Two hectares is also the optimal size for ponds. Although small water bodies of several square meters showed influence on surrounding temperature, optimal effect can be reached around 2 ha of size. Large lakes have only slightly greater cooling effect [Xu et al. (2010)].

THERMAL COMFORT

One can argue, that higher humidity caused by additional evaporation can lower the perceived cooling effect by decreasing the thermal comfort of inhabitants [Saneinejad et al. (2014)]. Yet, Saaroni and Ziv (2003) concluded that, during most of the day, a lake does not contribute to the air humidity more than a grassy area or park. Later in the afternoon, a lake seems to evaporate more than grassy surfaces but altogether significantly less than during the hottest part of the day. This suggests that the effect of open water on thermal comfort may not be noticeable. Presence of trees or grass does not seem to have a strong influence on the air humidity either. A small increase of humidity was found only up to half a meter above grassy surface, or high in the canopy of trees [Shashua-Bar et al. (2009)]. This suggests that the actual drop of thermal comfort due to higher humidity may be unnoticeable to inhabitants. Local humidity changes due to evaporation will depend on mixing processes in the lower atmosphere and thus on wind speed. This relation with the canopy boundary layer and urban boundary layer has hardly been investigated in urban areas.

BLUE-GREEN SOLUTIONS

Research has been done on the micro-climatological effects of vegetation and water bodies on urban areas, but the physical basis of these effects is hardly researched and largely just assumed. Hence, unresolved remains how much influence blue-green solutions have on ambient air temperatures in the urban environment.

1.4 RESEARCH QUESTIONS

It can be argued that a substantial part of urban heat stress and the urban heat island phenomenon is caused by a lack of water, resulting in a reduction of the latent energy flux and an increase in the sensible heat flux. The total latent energy flux (total evaporative flux) from common urban areas is substantially smaller than from vegetated rural areas. The city is unable to "sweat" properly which makes it run hotter. Boosting evaporation seems an effective strategy to reducing ambient air temperatures in an urban environment in hot and dry periods. For a hot summer day an additional 2-3 mm/day of evaporation in urban areas would bring the evaporative water consumption - hence the latent energy flux - on the same level as in rural areas (for moderate sea climate as in the Netherlands).

Literature analysis revealed the need for further understanding of the role water plays in cooling of urban ares. The main research questions addressed in this thesis are as

follows:

The cooling effect of urban surface water, in particular during night-time, is unclear. There is a discussion in literature of the possible downsides of the large heat storage capacity of water bodies for nightly air temperatures. Investigating the radiative, sensible, ground, and the latent heat flux from a surface water body around the clock could contribute to better understanding of how this body influences ambient air temperatures during day and night. And, as nightly minimum air temperatures are extremely important for the size and consequences of the UHI, we have have concentrated on the nightly energy fluxes.

- What is the effect of open water bodies on nighttime ambient air temperature above water surface?
  Effect of open water on daytime temperature has been often addressed in UHI mitigation research all over the world. It has also been postulated that the heat that water stored during daytime is released at night and heats up the air. In Chapter 4, we investigate the ways heat leaves the water body during night, and discuss the potential effect on air temperature.

Also, the effect of intercepted water on air temperature was hardly investigated in previous research. Yet, providing an additional source of evaporation by sprinkling water on urban roofs and paved surfaces might prove to be a simple, yet effective, way towards mitigating UHI.

- What is the cooling effect of intercepted water on paved surfaces?
  Rain water is intercepted by both vegetation and paved surfaces. Chapter 5 presents the effect of evaporation of water from a wet paved surface in Dutch climate when using an old Japanese water sprinkling technique.

Actual evaporation of urban vegetation is strongly related to the availability of water in the root zone. We found no studies investigating this relation. Vegetation was irrigated if serious water shortage could occur. In urban environments the relation between the amount of water that was supplied, depth and size of the root zone, soil moisture content of the root zone, the soil type in the root zone, the type (species) of vegetation, and actual evaporation remains to be investigated.

Green roofs have been mainly installed for storm water management and for their positive effect on indoor temperatures. However, they have been also promoted for their possible role in mitigating the UHI. This has been mostly proven for irrigated intensive green roofs and green gardens. The potential cooling effect of extensive green roofs was studied to a lesser degree, and always under relatively well watered conditions.

- What is the influence of soil moisture on thermal performance of an extensive green roof?
  Several green roofs were investigated under different soil moisture conditions, including an extreme case of drought, in order to quantify the effect of water availability on outdoor air temperature. Results of this study are presented in Chapter 6.

In the course of investigating these main research questions and their components, two supplementary research issues arose. The cooling effect of urban surface and intercepted water was investigated with Distributed Temperature Sensing (DTS). This technique uses a glass fibre for detail and precise monitoring of temperature [Selker et al. (2006)]. When using the DTS for daytime air temperature measurements we found a distinct pattern caused by effect of solar radiation.

- What is the effect of solar radiation on temperature measurements using Distributed Temperature Sensing?
  Chapter 2 deals with the effect of solar radiation on the measurement set up used in chapter four and five, and, consequently, with the effect of radiation on temperature measurements using DTS.

And second, when measuring water temperature in order to assess the energy balance of urban pond, a cold layer of water at the surface of warmer water was frequently observed. This temperature anomaly should be relatively unstable, yet it prevailed for several hours on almost all measurement days.

- What is the diurnal evolution and the thickness of skin effect of fresh water bodies?
  Chapter 3 introduces a typical temperature profile of air-water interface measured during daytime. This profile usually includes a ca 1.5 °C temperature drop near the water surface, the skin effect. We provide a first analysis based on high-resolution field measurements from three different measurement campaigns.

2

EFFECT OF RADIATION ON DTS MEASUREMENTS

Parts of this chapter have been published in Geoscientific Instrumentation: Methods and Data Systems (Hilgersom et al., 2016b)

2.1 INTRODUCTION

Distributed Temperature Sensing (DTS) became increasingly popular in recent years. Beside studies focusing on temperature measurements of water [Selker et al. (2006); Vogt et al. (2010); Westhoff et al. (2007a); Vercauteren et al. (2011); Van Emmerik et al. (2013)] or soil [Steele-Dunne et al. (2010); Jansen et al. (2011); Ciocca et al. (2012)], DTS has been also used for monitoring of air temperature [Thomas et al. (2012); **?**); De Jong et al. (2015)].

DTS is based on Raman scattering of laser beam travelling through a fiber-optic cable. Decrease in wavelength of the back-scattered light is temperature sensitive and is referred to as the anti-Stokes signal. Decrease in wavelength is relatively temperature insensitive and is referred to as Stokes signal. Combination of the travelling time of the signal up and down the cable and ratio of the Stokes and anti-Stokes signal is used to determine the temperature along the cable.

Solar radiation heats up the fiber optic cable and the auxiliary construction, which can lead to inaccuracies in DTS temperature measurements. The effect of solar radiation on the cable was already reported by De Jong et al. (2015). This chapter discusses the air temperature measurements errors introduced by the tubular structure on which the cable is mounted, based on measurement results. The datasets were acquired using different types of auxiliary construction, which allowed an analysis of the influence of solar radiation for different constructions on DTS temperature measurements in relation to the openness of the auxiliary construction and the amount of incoming radiation.

2.2 METHODS

Influence of the auxiliary construction on the temperature measurement is generally neglected. This assumption might not hold when the auxiliary construction used for fixing the cable has high thermal mass or different thermal properties than the measured medium. In such cases, fast changes in temperature will not be correctly reported due to the thermal inertia of the tube. This problem is for example apparent in measurements of air temperature, where there is both rapid fluctuation and low heat content. When measuring air temperature, one must also consider the effect of radiation on the probe [e.g., Vercauteren et al. (2011); Oldroyd et al. (2013)]. Color of the cable coating and direct exposure to solar radiation can have influence on the temperature measurement up to several degrees [De Jong et al. (2015)], and is also relevant underwater [Neilson et al. (2010)].

For the assessment of the influence of the construction material on DTS temperature measurements, we compare three datasets acquired between 2011 and 2014. All experiments used different auxiliary constructions on which the fiber optic cables were mounted. The construction types varied between an almost imperforated transparent PVC tube to an open hyperboloid PVC construction (Table 2.1).

IMPERFORATED PVC TUBE, DELFT (THE NETHERLANDS)

From 25 to 30 June, 2012, the temperature profile in and above a ditch in Delft (51.996°N, 4.377°E) was measured using a Sensornet Oryx (Sensornet Ltd., Hertfordshire, UK), with a 2 m intrinsic machine resolution and 1 min temporal resolution. The cable (AFL 1.6 mm simplex 50/125, white) was wrapped around a 1.8 m long transparent PVC tube with

Table 2.1: Details of the data from three fieldwork experiments in small reservoirs used in this study: (a) Delft (Netherlands) using an imperforated construction, (b) Delft (Netherlands) using a perforated construction, and (c) Binaba (Ghana) using an open construction.

Site	Measurement period	Sensor	Machine resolution	Coil resolution	Temporal resolution	Construction type
Delft	5 - 30 June, 2012	Sensornet Oryx	2 m	0.02 m	1 min	Imperforated
Delft	9 July - 7 August, 2014	Silixa Ultima-S	0.3 m	0.004 m	5 min	Perforated
Binaba	23 - 27 October, 2011	Sensornet Halo	4 m	0.008 m	1 min	Open

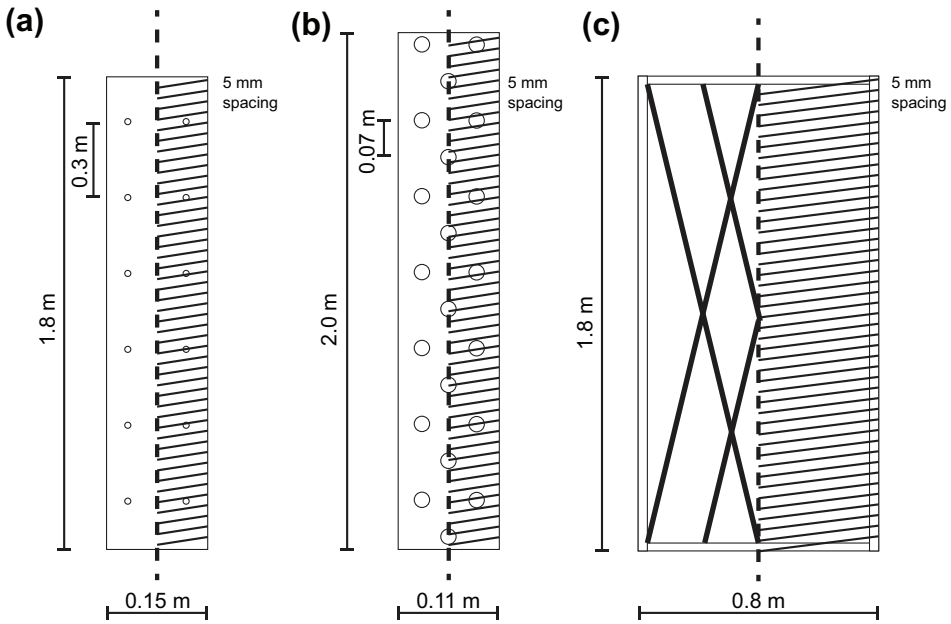

Figure 2.1: Used measurement setups for the three experiments, (a) in Delft from 25 – 30 June, 2012, (b) in Delft from 9 July – 7 August, 2014 and (c) 23 – 27 October, 2011.

a diameter of 0.15 m, and a wall thickness of 5 mm. Small holes (5 mm diameter) were made on four sides of the tube, every 30 cm in the vertical direction. The tube is considered as imperforated, as 99.9% of the cable was in contact with the tube. The cable was wrapped around the tube with 5 mm spacing, resulting in a 0.01 m coil resolution, see Figure 2.1a.

PERFORATED PVC TUBE, DELFT (THE NETHERLANDS)

From 9 July to 7 August, 2014, the temperature profile in a shallow urban pond in Delft (52.007°N, 4.375°E) was measured using a Silixa Ultima-S (Silixa Ltd., Hertfordshire, UK), with a 0.3 m intrinsic machine resolution and set to report with 5 min temporal resolution. The cable (AFL 1.6 mm simplex 50/125, white) was wrapped around a 2.0 m long transparent PVC tube with a diameter of 0.11 m, and a wall thickness of 5 mm. The tube was perforated with 2 cm diameter openings on four sides, every 7.5 cm in the vertical direction (covering approximately 5% of the total area of the tube). From the total cable, 95.0% was in contact with the PVC tube. At heights where the perforations are centered, 77.1% of the cable was in contact with the PVC tube. The cable was wrapped around the coil with 5 mm spacing, resulting in a 0.002 m vertical coil resolution, see Figure 2.1b.

OPEN CONSTRUCTION, BINABA (GHANA)

From 23 to 27 October, 2011, the temperature profile in the shallow Lake Binaba (10.781°N, 0.479°W) was measured using a Sensornet Halo (Sensornet Ltd., Hertfordshire, UK), with a 4 m intrinsic machine resolution and set to 1 min temporal resolution. The cable (AFL 1.6 mm simplex 50/125, white) was wrapped around a 1.8 m hyperboloid frame, that consisted of six PVC tubes (25 mm diameter). In these tubes, grooves were made to mount the cable easily with equal spacing. The open construction was designed to minimize radiation absorption by the construction and allow water and air to flow freely through the construction. For more details on the construction, see van Emmerik et al. (2013). Because of the open construction, only 3.1% of the cable was in contact with PVC. The cable was wrapped around the construction with 5 mm spacing, resulting in a 0.004 m coil resolution (Figure 2.1c).

The three data sets are compared for their air temperature profile measurements above the water surface. The perforated setup was used to quantify the radiation effect on the temperature measurements through the auxiliary construction. The temperature profile was separated into (1) measurement points that were only in contact with the tube (T_{tube}) and (2) measurement points that were in contact with both air and the tube (T_{air}). The spatially averaged difference between T_{air} and T_{tube} was used as a measure of radiation influence. Please note that since T_{air} was still partially influenced by the construction, the real deviation between temperature at the tube and in the air might be underestimated.

2.3 RESULTS

Figure 2.2 shows typical vertical profiles of air temperature at 12 P.M. during a clear day. Figure 2.2a shows a relatively smooth profile for the imperforated PVC tube. For the perforated profile (Figure 2.2b), one can see a clear pattern in the vertical profile. A drop in temperature was observed about every 7 cm, corresponding with the locations of the

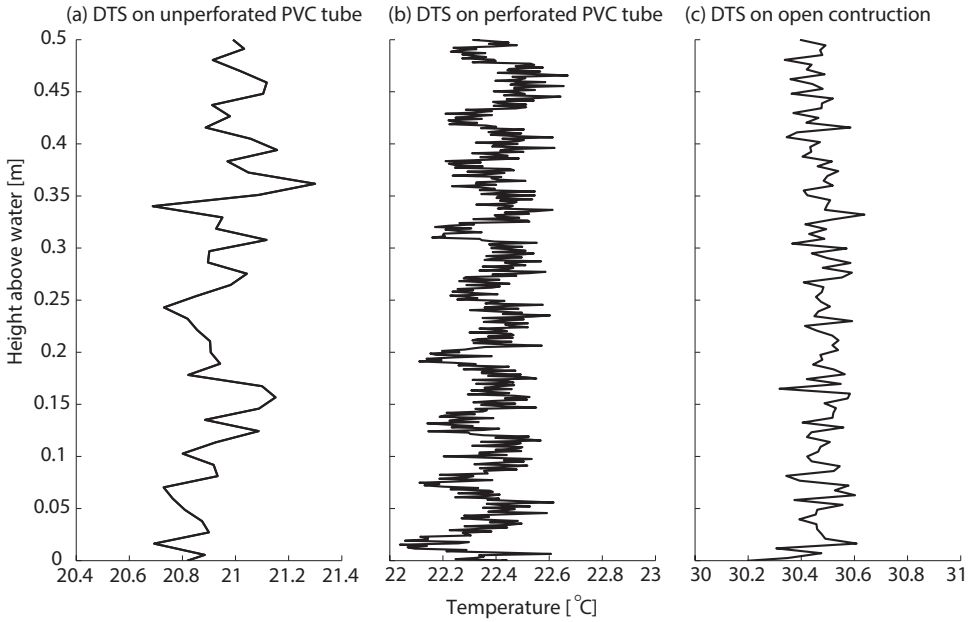

Figure 2.2: Typical air temperature profiles measured by DTS on (a) an imperforated PVC tube in Delft, (b) a perforated PVC tube and (c) an open construction. All profiles were taken on a cloudless day at 12PM.

holes. This profile demonstrates the temperature difference between cable that is only in contact with the tube, and cable that is in contact with both air and the tube. In the case of the open construction, where only 3.1% of the cable was in contact with the PVC, the temperature profile reflects mainly air temperature and direct radiation (Figure 2.2c).

Due to very high sampling resolution of measurements, and the high precision of the temperature measurements (0.01 °C) in Figure 2.2b, we can also observe the influence of direct solar radiation exposure (the shaded versus the exposed side of the column) as smaller (up to 0.2 °C) fluctuations in temperature. A clear influence of incoming shortwave radiation on the temperature data is visible for our various measurement setups, especially those with PVC tubes employed as the basis of construction. The profiles in Figure 2.2a and 2.2c look similar at first. However, because of the differences in construction, the temperatures were influenced by different processes, of which the effect is demonstrated in Figure 2.2b. The PVC tube influences the heat transfer processes from air and radiation to the cable, which causes a deviation between the cable temperature and actual air temperature.

The temperature measured by the cable that was placed over the perforations was up to 0.5 °C lower than the temperature measured by cable that was glued to the construction (Figure2.2b). Note that the machine resolution is 0.3 m, and the perforations are 0.02 m in diameter. The temperature that was assumed as air temperature is therefore still influenced by the tube, and hence the temperature difference between the cable in the air and attached to the tube is underestimated. Similar patterns can be seen throughout the whole measurement period. Our method to determine T_{air} is a conservative estimation,

and the real effect on the DTS temperature might be even higher.

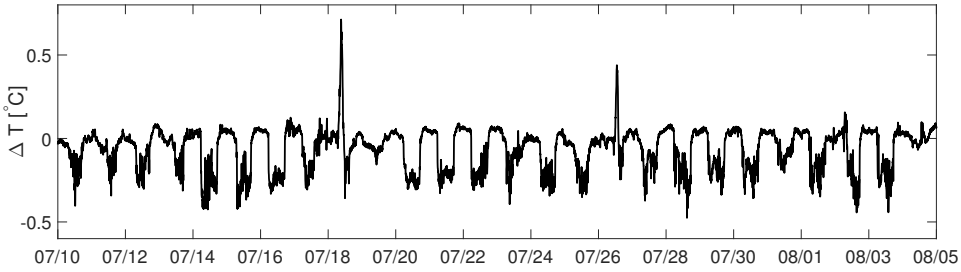

Figure 2.3: Measured temperature differences between temperature measured over the holes and over PVC ($T_{air} - T_{tube}$) during July and beginning of August 2014 including two cases of a morning dew on 18 and 26 July, 2014.

A relatively open construction (i.e., a low mass density) instead of a 5% perforated tube significantly reduces the radiation effects (Figure 2.2c). In this case, it is important to allow air/fluid circulation to prevent delayed temperature signals, which are likely to cause delayed response, and thus hysteresis patterns.

Figure 2.4a shows the relation between solar radiation and difference in temperature measured over the perforations and temperature measured on the tube. Different colors depict wind speed. For points with no (or very low) effect of wind (dark blue), we observe a relation between temperature difference and radiation. The temperature difference is smaller during the night than it is during the day. Presence of wind makes the influence of the tube on the DTS measurement less predictable. With winds higher than 0.5 m/s, the influence on temperature varies from 0 to 0.4 °C without any relation to radiation. The only exception is night (radiation equals 0 Wm^{-2}). At night, all temperature differences scatter around zero and even reach slightly positive values (up to 0.1 °C).

More complex patterns occur during morning and evening transitions, thus between 0 and 500 Wm^{-2}. During clear days, with almost no cloud cover, we observed hysteresis between morning and evening behavior of the temperature differences. Figure 2.4(b) shows the temperature differences on 14 and 18 July, 2014. For a sunny day (18 July, 2014), the temperature difference reaches relatively high values already early in the morning, when radiation is still quite low (0.25 °C difference by 50 Wm^{-2}). In the evening of the same day, T_{air} and T_{tube} reach the same values already with radiation values around 500 Wm^{-2}. Similar, but less pronounced, behavior can be observed also for more cloudy days (14 July, 2014).

2.4 OUTLOOK

Earlier work that used PVC tubes for coil-wrapped DTS setups discussed the heating effect of auxiliary constructions due to solar radiation [e.g.,Selker et al. (2006); Suárez et al. (2011); Vercauteren et al. (2011); Van Emmerik et al. (2013)]. Although our findings show that solar radiation causes temperature deviations up to 0.5 °C, transparent or light colored PVC is still the best choice for minimizing the radiation effect. It is advisable to use a radiation model prior actual measurements to estimate possible effect

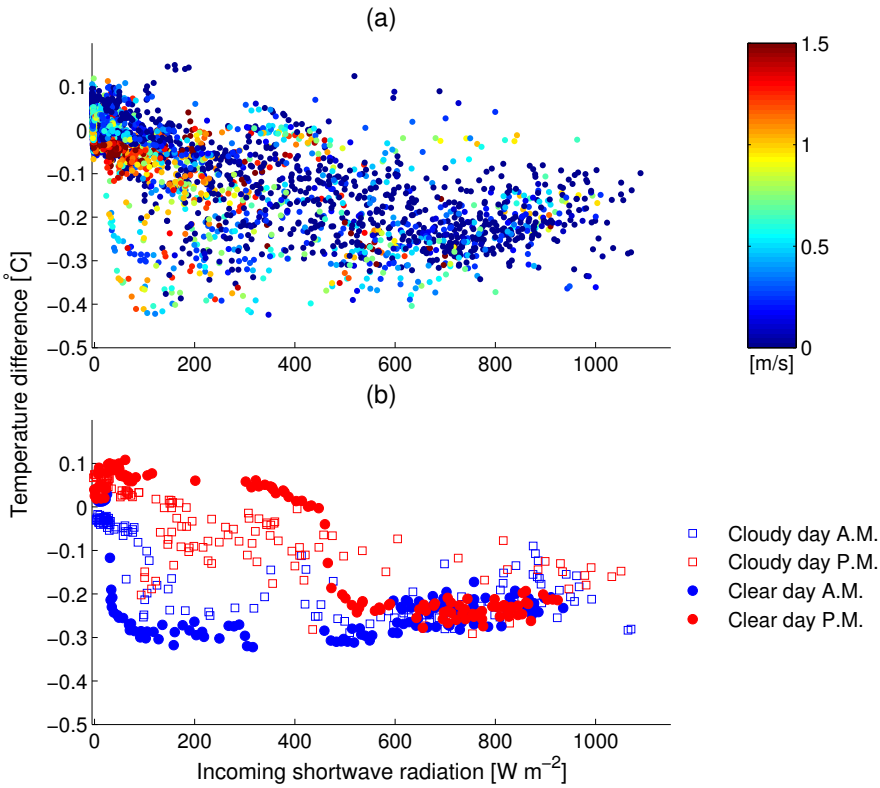

Figure 2.4: (a) Relation between temperature differences ($T_{air} - T_{tube}$), solar radiation, and wind speed (shown on color scale in m/s), (b) hysteresis in morning and evening transition in relation between temperature differences ($T_{air} - T_{tube}$) and solar radiation

of radiation driven heating on temperature measurements. Similarly, discoloring of the cables and construction by algae growth or environmental depositions likely increases temperature errors. In outdoor applications it is advised to apply ecologically sound anti-fouling paint to prevent discoloring of the cable.

One might also employ auxiliary construction design that shades the fiber wrapped around it, such as included in the installation of Vercauteren et al. (2011). Making setups like these from PVC tubes, however, is more complicated. The emerging 3D printing technique may make such approaches more feasible.

2.5 CONCLUSIONS

Our results show that using PVC auxiliary constructions can cause temperature measurement deviations up to 0.5 °C. This can be even higher for other set-ups and/or conditions.

Daily temperature deviations show a clear hysteresis pattern during clear days. The slow warm-up of the PVC cools the cable in the morning, and the heat-retaining PVC warms the cable in the afternoon.

3

TEMPERATURE PROFILE OF AIR-WATER INTERFACE

Parts of this chapter were published in Water (Solcerova et al., 2018a).

3.1 INTRODUCTION

Estimations of the energy balance of lakes and reservoirs are important to determine their heating and cooling processes, as the (thermo)dynamics of lakes and reservoirs and their water balance are significantly influenced by the surface energy fluxes [Henderson-Sellers (1986); Tanny et al. (2008); Van Emmerik et al. (2013); Nordbo et al. (2011)]. Previous studies showed a clear temperature drop at the air–water interface [Van Emmerik et al. (2013); Solcerova et al. (submitted.); Vercauteren et al. (2011); Selker et al. (2006)]. At first, we assumed that this was in fact the wet bulb temperature due to splashing of water on the measurement setup. However, the lower temperatures are below the water surface, which suggests the occurrence of a radiation and evaporation driven skin effect.

The skin effect refers to a thin, more or less stable layer of surface water that is colder than the water beneath it due to radiative and latent energy loss that exceeds the replenishment of energy via shortwave absorption or thermal diffusion from the lower water. As the energy transfer from water to atmosphere (evaporation, long-wave radiation, or sensible heat) happens at the surface, a thin cold layer is created (the skin effect) [Minnett et al. (2011); Fairall et al. (1996)]. In natural lakes, the upwelling long-wave radiation dominates long-wave energy transfer. This is due to the surface supplying all outgoing long-wave energy, while incoming shortwave energy is absorbed through the first meters of the water column. The thickness of the skin layer is hypothesised to be regulated by conductive and diffusive heat processes [Saunders (1967)]. Detailed analysis about the heat exchange and energy transfer over the water surface can be found in Edinger et al. (1974).

Existence of a skin effect results from low turbulence close to the water surface compared to the layers below. In cases where density is inverted and far from interfaces in water, heat is most rapidly transferred by turbulent mixing. Close to the surface, however, low Reynolds numbers suppress turbulence, and thus viscous forces and molecular processes prevail. Thus, the heat from lower water layers is only transferred to the laminar top layer by molecular conduction, which is an order of magnitude less efficient than turbulent mixing [Ward and Minnett (2002)].

A colder layer of water on the surface is a documented phenomenon in oceanography and most research about the skin effect of water bodies has been focused on oceans [Minnett et al. (2011); Ridley et al. (1997); Kang et al. (2015)]. The greater of research focussed on skin effect in oceanography as compared to fresh water reservoirs is related to the fact that the surface of oceans is particularly interesting from biological and chemical perspective. The top 0–1 mm of ocean surfaces contains a higher concentration of bacteria and larvae, as well as having elevated concentrations of non-polar molecules attracted to the air–water interface [Hardy (1982); Bidleman and Olney (1974)].

A few studies measured the skin effect in lakes as well [Woodcock and Stommel (1947); Wilson et al. (2013)]. Available studies on the skin effect agree that the colder layer can be present during both day and night, and that the temperature difference between the skin and the temperature of underlying water (ΔT_{water}) is highest during the daytime [Schluessel et al. (1990); Wilson et al. (2013)]. However, to date, there have been few analyses that have investigated under which conditions it occurs, and what affects the skin effect magnitude. In this paper, we use novel measurements to also analyze and discuss the timing of occurrence of the skin effect.

Although the skin effect has been previously measured [e.g., Jessup and Branch (2008); Schluessel et al. (1990); Kang et al. (2015); Ridley et al. (1997)], the measurements of the skin effect thickness remain scarce. Previous work on the skin effect thickness suggested that the effect is limited to about one millimeter. However, until now, no measurements of skin effect of fresh water were done under field conditions. For example, Grassl (1976) derived the thickness of the skin effect mathematically, Duan et al. (2008) used saturation vapour pressure measurements from funnel measurements, and Hisatake et al. (1993) performed measurements under laboratory conditions by lowering a thermocouple into water and then retrieving it again. In laboratory conditions, one could never reach the prevailing outgoing longwave radiation, as is typical for open sky. Our paper presents a first analysis based on high-resolution field measurements obtained from three different measurement campaigns.

This chapter aims to quantify the skin effect of natural water bodies. We present high-resolution temperature measurements of air–water interface from three different locations using Distributed Temperature Sensing (DTS), and discuss potential explanations for the observed phenomena.

3.2 MATERIALS AND METHODS

Goals of the methodology are to obtain high-resolution measurements of the skin effect and link them to the development of the skin temperature. In this section, we first introduce the measurement technique and the way we defined the variables such as the skin temperature and thickness; later, we describe the specifics of each measurement site.

3.2.1 HIGH-RESOLUTION MEASUREMENTS

DTS was used to measure vertical temperature profiles at very high-resolution in three different locations. DTS is a method that allows for high-resolution temperature measurements in air [**?**De Jong et al. (2015)], water [Van Emmerik et al. (2013); Westhoff et al. (2007b); Sebok et al. (2013a)], and soil [Steele-Dunne et al. (2010); Bense et al. (2016a)]. The method is based on backscatter of light traveling through a fiber optic cable. The ratio between backscatter of various wavelengths is indicative of the temperature along the cable. More details about the DTS method can be found in [Selker et al. (2006); Tyler et al. (2009)].

The resolution of DTS can be increased by wrapping the fibre optic cable around an auxiliary construction [Selker et al. (2006); Hilgersom et al. (2016a)]. In this research, we are using two types of auxiliary constructions, both allowing for measuring the vertical temperature with sub-centimeter resolution. However, attaching cables to a construction can introduce an error in observed air temperature values. The effect of the construction on the measurements can be found in Hilgersom et al. (2016b).

3.2.2 MEASURED AND CALCULATED VARIABLES

Continuous measurements of air–water interface resulted in temperature profiles similar to the one seen in Figure 3.1a. We define the bulk water temperature (T_{water} [°C]) as the average temperature over ~0.10 m below the water surface, air temperature (T_{air} [°C]) as the average temperature over ~0.10 m above the water surface, and the skin tem-

perature as the measured minimum temperature (T_{min} [°C]).

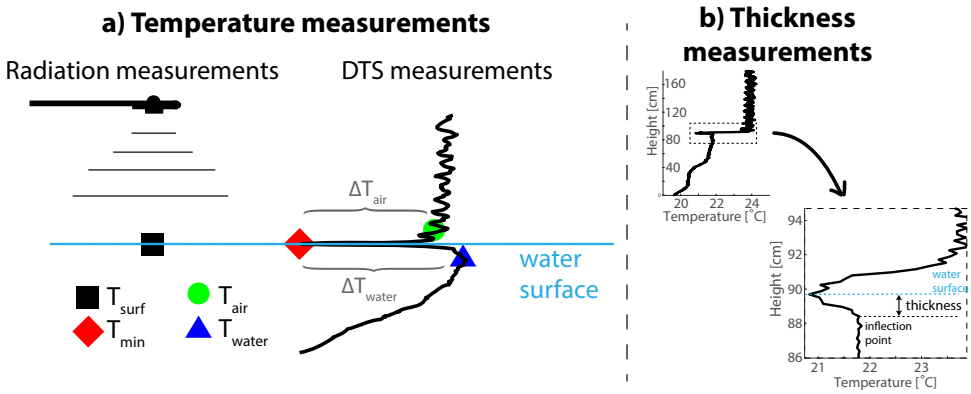

Figure 3.1: (**a**) schematization of temperatures used in Equations (1)–(4). T_{surf} was calculated from outgoing longwave radiation measurements. T_{air}, T_{min}, and T_{water} are temperatures measured with the DTS setup; thickness of the skin effect shown on temperature measurement in Delft 15 July 2014 at 3:00 p.m.

ΔT_{water} represents the difference between the bulk temperature of water (T_{water}) and the measured minimum temperature (T_{min}). ΔT_{air} represent the difference between the bulk temperature of air (T_{air}) and the measured minimum temperature (T_{min}):

$$\Delta T_{air} = T_{air} - T_{min}, \tag{3.1}$$

$$\Delta T_{water} = T_{water} - T_{min}. \tag{3.2}$$

We define the temperature drop as the smaller of the two thermal gradients found in the water ΔT_{water} and air ΔT_{air} immediately above and below the air–water interface:

$$\Delta T_{drop} = min(\Delta T_{water}, \Delta T_{air}). \tag{3.3}$$

When there is no thermal skin layer ($\Delta T_{drop} = 0$), T_{min} is defined as equal to the surface temperature.

A second important parameter measured at the water surface was the thickness of the skin layer. The thickness was defined as the distance between the minimum measured temperature (T_{min}) and the point where the local numerical derivative of the water temperature changed from negative to positive values (Figure 3.1b); in other words, the place where the water temperature does not increase any more compared to the above laying measurement.

3.2.3 MEASUREMENT LOCATIONS AND MONITORING EQUIPMENT

Three datasets were used in this research, one from an urban pond in Delft (The Netherlands), one from Lake Binaba in Ghana, and one from Lake Kinneret in Israel. All three datasets included a high-resolution temperature profile of water–air interface. Data from Delft and Israel also included meteorological observations. In the following, the measurements setups will be discussed briefly. More detailed descriptions can be found in Hilgersom et al. (2016b) and Van Emmerik et al. (2013).

DELFT POND

Measurements took place from 12 July through 7 August 2014 in a shallow urban pond at the Amalia van Solmslaan in Delft, the Netherlands (52.007° N, 4.375° E). The climate of Netherlands is moderate oceanic with summer starting in June and ending mid-September. Average water depth in the pond is 0.7 m and the average area of water surface is 3627 m^2.

For DTS, a Silixa Ultima (Silixa Ltd., Hertfordshire, UK) with spatial resolution of 0.3 m was used. The sampling resolution in the glass fibre cable was set to 0.126 m (to satisfy the Nyquist criteria for spatial resolution) and the temporal resolution 5 min. Double ended calibration [Van De Giesen et al. (2012a)] was used including two calibration baths, one with unheated water and one with water heated to ~35 °C. The temperatures in the calibration baths were measured with two Pt100 temperature probes built into the DTS.

A vertical temperature profile was measured at two locations in the northeast corner of the pond. An optical cable (AFL 1.6 mm simplex 50/125, white) was wrapped around a 200 cm long transparent PVC tube with 11 cm diameter resulting in ~2 mm vertical resolution of the temperature measurements (Figure 3.2a). To ensure ventilation, four 2 cm diameter holes were drilled into the tube every 6–8 cm. Each temperature profile covered ~20 cm of the mud on the bottom of the pond, 70 cm of water, and 110 cm of air. The same type of optical cable was used for all three measurement locations.

More details about the setup used in Delft can be found in previous chapter; see Figure 2.1b.

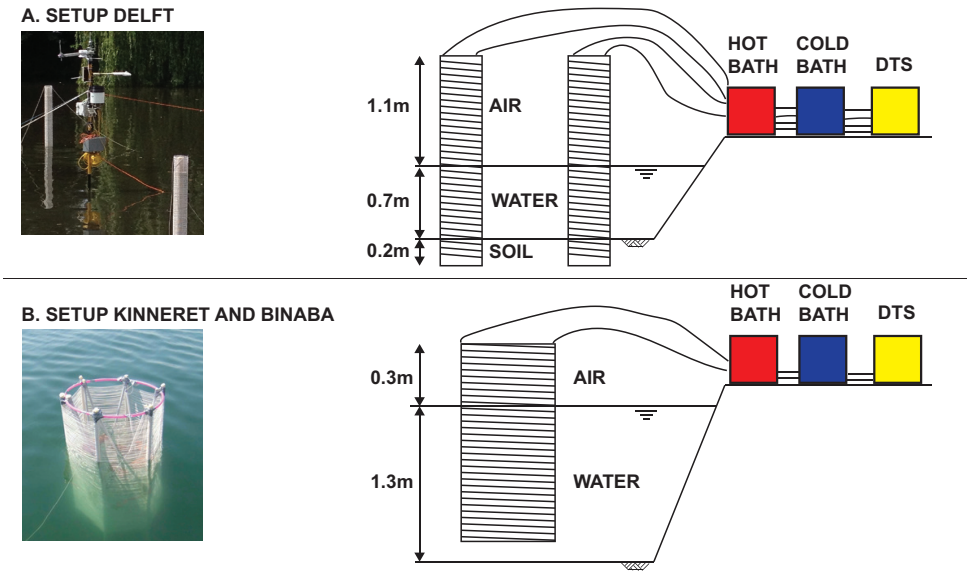

Figure 3.2: DTS measurement setup used in (**A**) Delft, and (**B**) Kinneret and Binaba.

Air temperature, relative humidity, wind speed, wind direction, and precipitation were measured using a standard HOBO weather station (Onset Computer CO., Bourne,

MA, USA) in the middle of the pond. Additionally, incoming and outgoing short- and long-wave radiation were measured using a CNR4 net radiometer (Kipp & Zonen, Delft, The Netherlands).

The measurements in Delft also included longwave outgoing radiation, which allowed for calculation of the surface temperature (T_{surf}) using the Stefan–Boltzmann law:

$$Rl_{out} = \sigma \epsilon T_{surf}^4, \tag{3.4}$$

where Rl_{out} is the measured outgoing longwave radiation [Wm^{-2}], T is the surface temperature [K], $\epsilon = 0.98$ [-] is the emissivity of water Wen-Yao et al. (1987) and $\sigma = 5.67 \times 10^{-8}$ $Wm^{-2}K^{-4}$ is the Stefan–Boltzmann constant.

A parameter influencing the calculated surface temperature is the emissivity of the water. Emissivity decreases with higher sediment concentration in water; for highly turbid salty water, it can drop down to 0.95 [Wen-Yao et al. (1987)]. The turbidity of the urban pond in Delft was not measured. Therefore, we performed a sensitivity analysis of the surface temperature to emissivity. With decreasing emissivity values, the calculated surface temperatures increased. As a consequence, the T_{surf} could change by up to 2.8 K depending on the chosen emissivity value. For this analysis, the value 0.98 was chosen based on the fact that the measurements were taken in and above highly turbid fresh water body, as suggested in the literature Wen-Yao et al. (1987).

LAKE BINABA

Measurements in Lake Binaba were taken between 24 and 28 October 2011. The climate of northern Ghana (10.78° N, 0.48° W), where the lake is located, is tropical with a dry and wet season. During the rainy season, April to September, the lake is fed by runoff via natural streams. Lake Binaba is a small artificial lake with average depth 3 m and lake surface 4.5 km^2. Water from the lake is used for small-scale irrigation and domestic water use.

A four-meter resolution Halo DTS Sensor (Sensornet, Hertfordshire, UK) was used at this site. The sampling resolution was 2.03 m and temporal averaging 2 min. Double-ended calibration was used including two calibration baths, one with unheated water and one with water heated to ~35 °C. Two HOBO Tidbit Mini Underwater Temperature Data loggers (Onset Computer CO.) with a logging interval of 1 min were used to measure the temperature in the calibration baths.

Vertical temperature profiles were measured in the pond using an open construction. A fiber-optic cable was wrapped around a PVC hyperboloid frame (Figure 3.2b) constructed from PVC pipes. Extra weight was added to the bottom of the frame to counteract the buoyancy caused by air trapped in the PVC pipes. The open construction of the setup ensured low influence of direct solar radiation, and free flow of water and air through the construction. The vertical resolution created by wrapping the wire around the construction was ~4 mm.

More details about the setup used in Ghana can be found in previous chapter; see Figure 2.1c.

LAKE KINNERET

Measurements in Lake Kinneret (32.78° N, 35.59° E) took place between 6 and 9 October 2011. Climate of northern Israel is warm Mediterranean with a colder rainy season between October and April. Lake Kinneret has an average lake surface of 166 km^2. During the experiment, a northwesterly sea breeze formed each afternoon and usually peaked at 3:00 p.m. local time with wind speed of ~5–10 m/s. The wind was significantly lower for the rest of the day: <2 m/s from 8:00 p.m. until 12:00 p.m. the following day.

An Oryx (Sensornet) with two-meter resolution was used to record the temperature with spatial samples averaging 1.03 m and temporal averaging 1 min. Single ended calibration [Hausner et al. (2011)] was used including two calibration baths. Temperature in the calibration baths, as well as the temperature measurement method, was the same as for the measurements taken in Lake Binaba. Additionally, the setup used was the same for both Binaba and Kinneret. However, a higher sampling resolution of the Oryx DTS machine resulted in vertical resolution of ~2 mm.

A meteorological station was placed in the middle of Lake Kinneret. Air temperature, relative humidity (both probe model 43372C, R.M. Young), wind speed and wind direction (MA-05106 wind monitor, R.M. Young) were measured in 10 min intervals.

3.3 RESULTS

3.3.1 SURFACE TEMPERATURE

Comparison of the calculated surface temperature (T_{surf}) and two temperatures measured using DTS (T_{water} and T_{min}) can be seen in Figure 3.3a. At night, T_{surf} followed the measured water temperature (T_{water}); however, during the day, T_{surf} reached on average 0.6 K higher values than T_{water}. Average temperature of T_{surf} and T_{water} over the whole measurement period was 23.3 °C and 23.0 °C, respectively. Average measured T_{min} reached only 20.6 °C. This might suggest that T_{water} is a better approximation of the surface temperature than T_{min}. However, T_{min} followed the variation of T_{surf} and the amplitude of its diurnal change almost exactly, with an offset of 2.7 K. The minimum temperature (T_{min}) measured proved to be well correlated with the surface temperature (T_{surf}) calculated from outgoing longwave radiation measurements for the Delft location using Equation (4). The offset of 2.7 K is well in the accuracy range of the pyrgometer that recorded the outgoing longwave radiation used for the calculation of the surface temperature. Figure 3.3b shows a scatter plot of the calculated surface temperature (y-axis) and T_{min} and T_{water}. Correlation coefficients of T_{surf} and the two temperatures measured using DTS were 0.86 for T_{min} and 0.68 for T_{water}.

All measurements showed a temperature decrease close to the water surface during the day (Figure 3.4). In general, the temperature drop followed a diurnal pattern at all three locations. Maximum values were reached between 12:00 p.m. and 4:00 p.m. in Delft and between 11:00 a.m. and 2:00 p.m. in Kinneret. At the Binnaba location, the maximum temperature differences occurred at a different time on each of the four measurement days. At night, the anomaly disappeared.

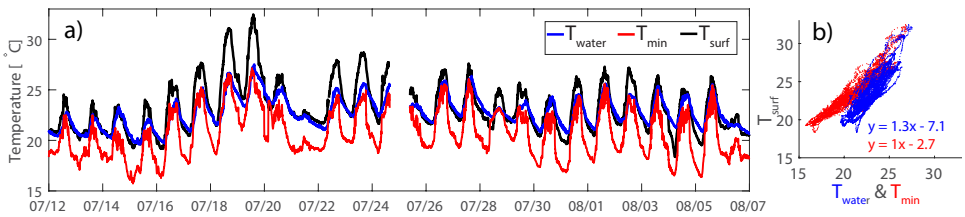

Figure 3.3: (**a**) temperature of water surface calculated from measured longwave radiation in Delft, and temperatures measured by DTS (see Figure 3.1) at the same location; (**b**) scatter plot of T_{water} and T_{min} (x-axis) and T_{surf} (y-axis).

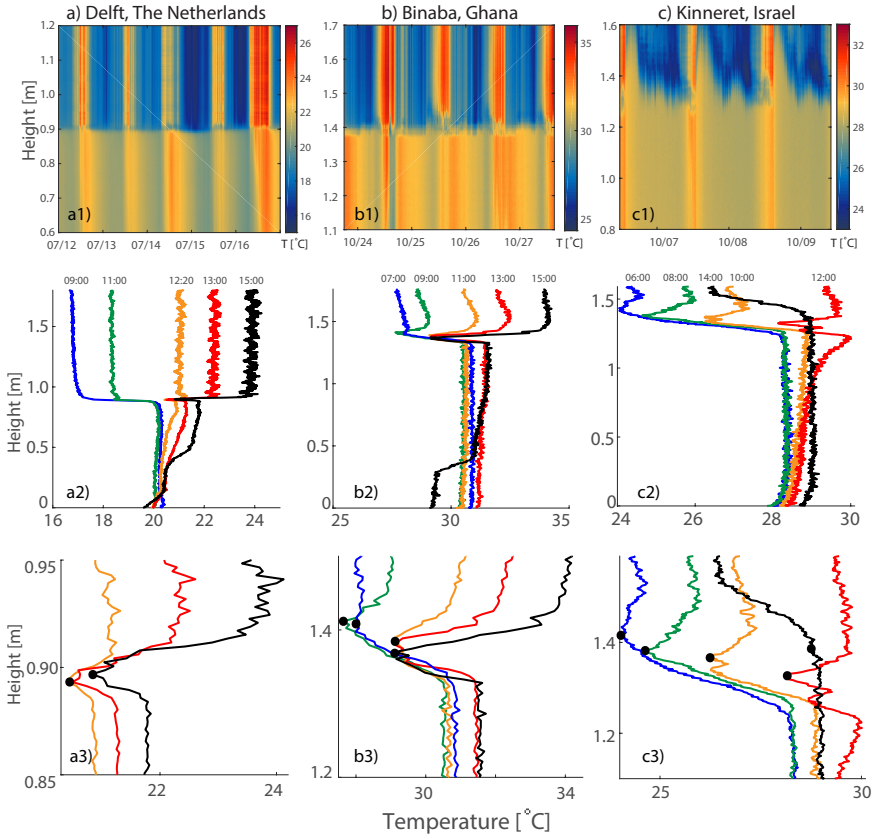

Figure 3.4: Temperature profiles of water–air interface in time for three measurement locations: (**a**) Delft, (**b**) Binaba, and (**c**) Kinneret. Subplots (1) show the instantaneous temperature profiles for all time steps. Note the different temperature scales. Subplots (2) show five chosen time steps during one day for each location. The chosen days were 15 July 2014 for Delft, 25 October 2011 for Binaba, and 7 October 2011 for Kinneret, local times are shown above each profile. Subplots (3) show the same chosen time steps but are zoomed in on the water surface (black dot).

3.3.2 ENERGY BALANCE OF WATER SURFACE

The observed total thickness of the colder layer of water was measured to be up to 3 cm (Figure 3.5). Existence of a colder layer of water on top of warm water creates instability. The cold layer will periodically mix with the warmer water below through finger-like structures Hilgersom et al. (2017).

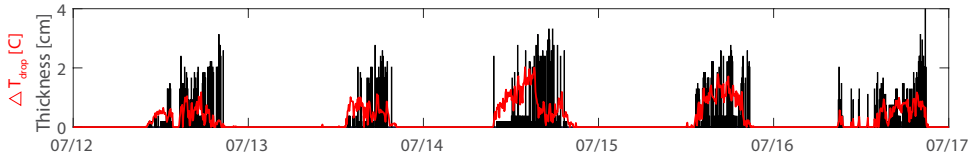

Figure 3.5: Thickness and size of the temperature drop at water surface measured in Delft.

The creation of a colder layer of water near the water surface can be approached from the energy-balance point of view. If the average temperature drop (ΔT_{drop}) of the top 3 cm is ~1 K, and the heat capacity of water equals 4.2 kJ $kg^{-1}K^{-1}$, the energy deficit compared to the water below is about 126 kJm^{-2}. The heat flux Q [Wm^{-2}] between the warm and cold water layer can be calculated using:

$$Q = -K_{water} * A * \frac{dT}{dz}, \tag{3.5}$$

where K_{water} = 0.58 $Wm^{-1}K^{-1}$ is the thermal conductivity of water, A = 1 m^2 is the unit area, and $\frac{dT}{dz}$ [Km^{-1}] is temperature gradient over depth. With a temperature gradient of ~1 K over 3 cm, the flux is ~20 Wm^{-2}.

The average net longwave radiation measured at the location in Delft during a day was –50 Wm^{-2}, meaning there was a radiative flux from water to the air. If we assume the water was cooled by the radiative flux only and the flux from water to the top layer is 20 Wm^{-2}, the time to extract 126 kJ by a 30 Wm^{-2} flux is computed to be 70 min. Indeed, the temperature difference of the top layer shows fluctuations in time. Local minima in the temperature difference (ΔT_{drop}) occurred on average once every 25 to 95 min (Figure 3.6). The instantaneous differences in time periods are caused by turbulent fluxes: evaporation and sensible heat, which were not investigated in this research.

3.4 DISCUSSION

We have presented measurements of a localized, transient surface temperature drop found at the air–water interface at different locations with three different climates. For the Delft case, we have compared it to the surface temperature calculated from long wave radiation observations. Our measurements suggest that this temperature anomaly is the skin effect, as the minimum temperature occurs at the water–air interface.

A skin effect is not the only possible explanation for occurrence of a temperature drop close to the water surface. Another possible explanation is a measurement artifact caused by the splashing of water on our sensor systems. Small waves could continuously wet the optical fiber of the measurement setup, which would consequently record temperature similar to wet bulb temperature. Waves on the water surface of lakes and ponds

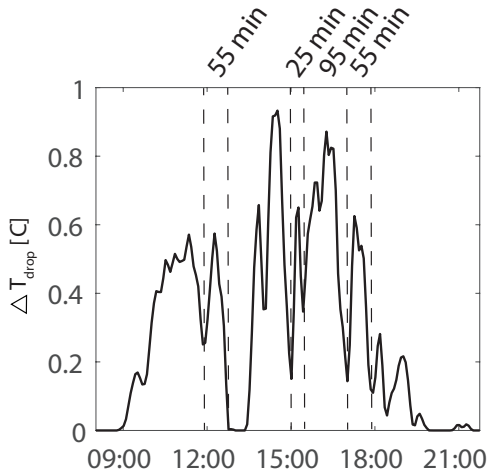

Figure 3.6: Time series of the temperature drop (ΔT_{drop}) on 12 July 2014 in Delft.

are generally created by wind. Figure 3.7 shows a daily occurrence of the temperature drop, and its size (ΔT_{drop}), and the wind speed. Both data sets show that, with higher wind speeds, the temperature difference decreased, or even disappeared totally.

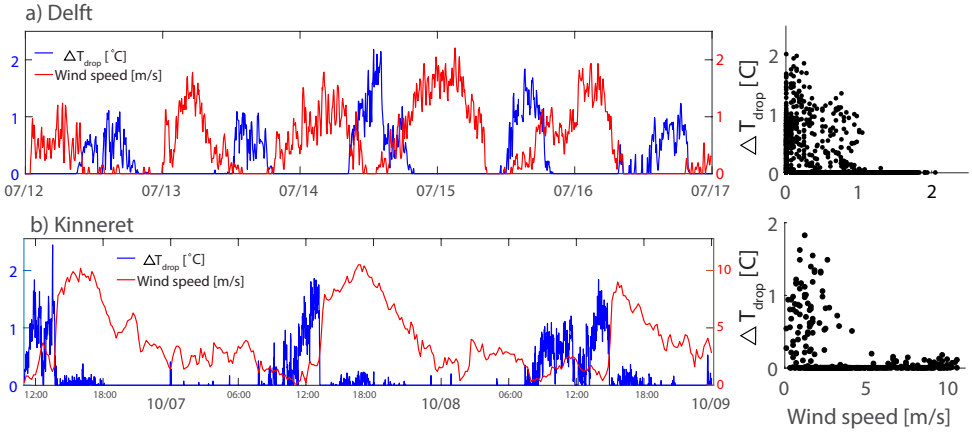

Figure 3.7: Size of the temperature drop (ΔT_{drop}) in relation to wind speed for measurements in (**a**) Delft, and (**b**) Kinneret.

Figure 3.7 convincingly illustrates that the recorded minimum is not related to splashing water or wet bulb temperature. It is possible that, at some occasions, especially during moments with wind speeds above zero (e.g., Figure 3.7a in the evening of 14 July), splashing of water is what is causing the temperature to appear colder close to water surface. This also corresponds with the fact that the correlation of the minimum temperature measured by DTS in Delft (T_{min}) with calculated water surface temperature

(T_{min}) was weaker at times with higher wind speeds.

Interestingly though, the calculated water surface temperature had an offset of 2.7 K compared to the measured skin temperature. As mentioned before, this offset is within the range of precision of the pyrgeometer used. Nonetheless, the proximity of the buildings surrounding the pond might have had an additional effect on the radiation measurements as well. During the daytime and especially early evening hours, the surface temperature of the buildings was higher than the temperature of the pond. The additional longwave radiation from the walls of the buildings could have contributed to the recorded longwave radiation of the pond.

However, it remains to be investigated how weather conditions and the physical properties of the water body influence the occurrence, size, and disappearance of the temperature drop. For example, although the temperature drop was predominantly measured during daytime, occasionally it persisted over night. This situation was mostly visible during very warm nights, when the air temperature stayed higher than the water temperature. This suggests that creation and existence of this temperature drop is dependent on the differences between the water and air temperature. A similar conclusion can be drawn by observing the temperature profile in Figure 3.4. The decrease in temperature (ΔT_{drop}) appeared when the air temperature reduced the water temperature.

Another aspect that seems to play an important role is the wind. Our measurements show that during periods with high wind speed, the skin effect disappeared. This might seem contradictory to the assumption that evaporative cooling contributes to creation of the skin effect, as wind would enhance evaporation. On the other hand, high wind speed can disturb the surface layer and promote better mixing throughout the top few centimeters of water.

There seem to be a difference in the thickness of the skin effect between the urban pond in Delft (ca 1.5 cm) and the two bigger lakes. This could be caused by several factors, such as transparency of the water, depth, or possible wave formation on the bigger lakes. These variables were not measured at either location. More research is needed to investigate what drives the thickness of the skin effect.

DTS proved to be a suitable method for measuring the skin effect. Wrapping the optical fiber in a more compact method and by increasing the diameter of the auxiliary construction allowed for higher resolution. Another advantage of this method is the continuity of the measurements allowing for a fuller observation of temporal changes in the skin effect and temperature gradient over the top layer of water. A simple energy balance calculation showed that the measured timescale and magnitude of the energy exchange is indeed comparable to the calculated values for the temperature gradient measured in Delft.

When using fiber optic cable for near water surface measurements, one needs to be aware of its tendency to absorb solar radiation, despite its white colour. This effect can be partly visible in Figures 3.1a and 3.4c3, where the DTS is measuring higher temperature just below the surface compared to the air temperature. The effect of radiation on DTS measurements in air and water close to the water surface was described in Hilgersom et al. (2016b) and Vercauteren et al. (2011), respectively. Nonetheless, even with this effect, skin is still detected, but it may, on some occasions, appear thicker due to the way the thickness is defined.

Further research of the skin effect in fresh water is necessary in order to understand how, and under what conditions, is the cold layer created, and when it mixes with the underlying warmer water. It is possible that the auxiliary construction of the DTS setup created a preferential flow during the moments when the cold layer mixed. This would cause the measured cold layer to appear thicker than the actual skin layer. Nonetheless, the thickness of the skin layer still needs to be investigated in more detail, as there are only few references available [Duan et al. (2008); Hisatake et al. (1993)]. Additionally, higher vertical resolution of the temperature measurements should be employed in future investigations. The 2 mm resolution, as used in this study, could not detect features at the sub-millimeter scale, so we cannot directly relate our measurements to features in the skin layer of less than 1 mm, as mentioned in Minnett et al. (2011); Fairall et al. (1996); Wilson et al. (2013); Schluessel et al. (1990).

3.5 CONCLUSIONS

Analysis of data collected from three different measurement locations confirmed that the measured temperature drop could be attributed to the skin effect, rather than wet bulb temperature due to splashing of water. For the first time, the skin effect was measured consistently under field conditions in fresh water bodies. Our data suggest that the skin effect of fresh water bodies is predominantly a daytime phenomenon and only occurs during low to zero wind speeds.

The high-resolution DTS measurements provided an important insight into the surface energy balance dynamics of water bodies by allowing observation of the temperature drop below the air–water interface during the three field studies.

Measurements presented in this study suggest that the thickness of the skin effect is larger than the previously assumed 1 mm or less [Minnett et al. (2011); Wilson et al. (2013); Hisatake et al. (1993)]. It was observed to be on the order of 3 cm in thickness. This sheds a new light on the energy balance dynamics around the air–water interface of water bodies. Specifically, our measurements suggest that inaccurate description of the skin effect layer might result in errors in modelling water body energy and heat fluxes, as they differ for the water body itself and for the skin layer.

4

NIGHTTIME COOLING OF AN URBAN POND

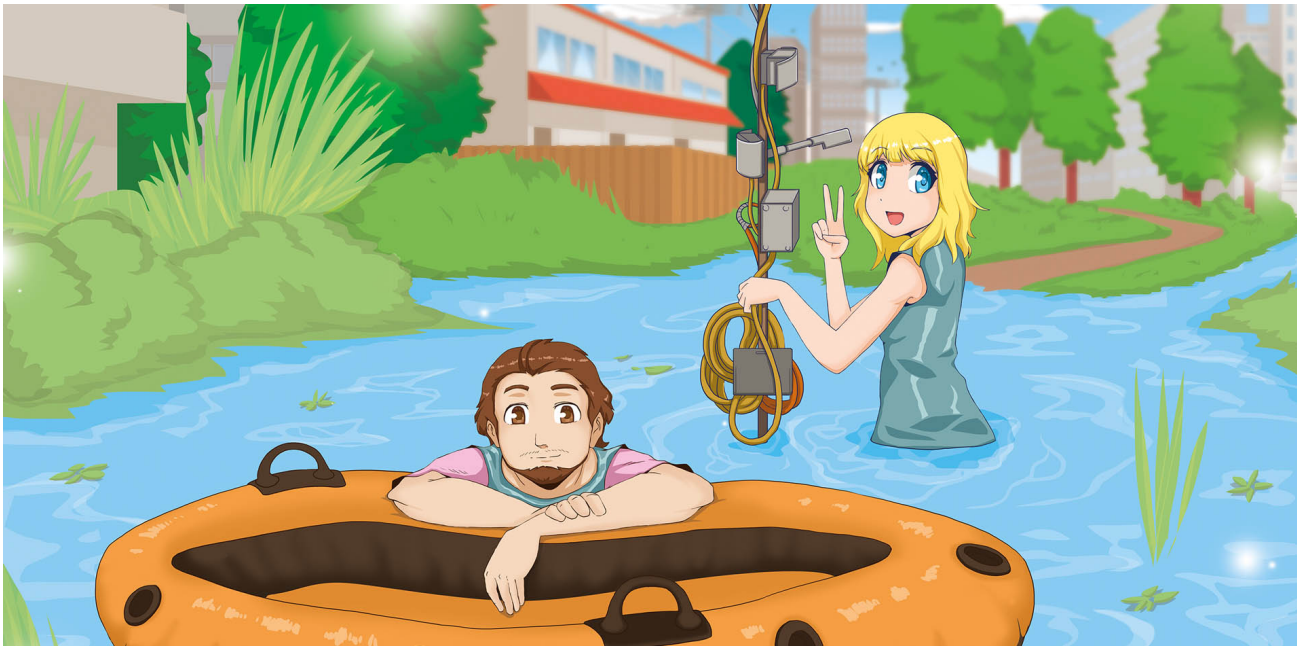

Parts of this chapter submitted to Frontiers: Hydrosphere journal (Solcerova et al., submitted.).

4.1 INTRODUCTION

High air temperatures can have a negative effect on human health and well-being. Several studies have shown that higher temperatures can lower the quality of sleep, and increase the risk of respiratory illnesses and cardiovascular mortality [e.g. Patz et al. (2005); Tan et al. (2007)]. Impact of extreme heat on humans is especially visible in cities, because urban areas generally experience higher temperatures than rural areas. Such Urban Heat Islands (UHI) are mostly caused by different heat capacities and albedo of urban surfaces, lower evaporation, anthropogenic heat production, and the specific geometry of street canyons [Oke et al. (1991); Lee (1993); Ryu and Baik (2012); Gago et al. (2013)].

One of the possible ways to decrease air temperature in the urban environment is to increase evaporation by open water, such as ponds, channels, or fountains. Comparative studies have shown that from all the urban land use types, open water is the most efficient in reducing UHI at a local scale [e.g. Rinner and Hussain (2011); Olah (2012)]. Already a small pond can reduce temperature in its surroundings up to several degrees [Halper et al. (2012)], especially in the morning, when the evaporative cooling effect is the strongest [Hathway and Sharples (2012)]. Most pronounced influence of open water on temperature was measured close to the shore [Xu et al. (2010)] and an effect of a big enough lake can be observed even at several kilometers [Theeuwes et al. (2013)]. Several studies agreed that proximity to open water dampens the diurnal temperature pattern [e.g. CPC-Consortium (2014); Theeuwes et al. (2013); Steeneveld et al. (2014); Wang et al. (2011)].

Strongest UHI is generally measured at night [Oke (1982)]. Although the absolute temperatures are lower at night, the differences between urban and rural temperatures are at its maximum. In contrast to their daytime cooling effect, urban water bodies might contribute to higher air temperatures at night [Albers et al. (2015)]. Water has a high thermal inertia, which causes water bodies to have relatively high temperature at the end of a night compared to other urban land use types [Oswald et al. (2012); Yang and Zhao (2015)]. Nonetheless, some studies concluded that water bodies provide cooling effect also at night, although to a limited extent [Coutts et al. (2012); Syafii et al. (2016)].

The way urban water bodies influence air temperature at night has not been extensively studied so far and reported measurements show contradictory results. A comprehensive literature review by Manteghi et al. (2015) identified a lack of research about the potential night-time heating effect of urban water bodies, and a need for understanding the mechanisms.

This research aims to contribute to the understanding of thermal behavior of an urban pond during summer nights. This chapter provides an analysis of temperature measurements and meteorological data from an urban pond in Delft, The Netherlands. We quantify the energy balance over the night, hence the magnitude of turbulent, sensible and latent, heat fluxes in comparison to radiative and ground fluxes, and the total decrease in temperature of the water.

4.2 METHODS

4.2.1 MEASUREMENT LOCATION

The measurements took place from 12 July till 7 August, 2014 in a shallow urban pond in Delft, The Netherlands (52.007 °N, 4.375 °E). The climate of The Netherlands is a moderate oceanic climate with summer starting in June and ending mid-late September. We chose a representative urban setting with an office building to the north and a residential building to the south. Several family houses with small gardens were located in the north-western direction from the setup and to the east was a quiet street with four floor residential buildings. The water was stagnant, except for rain conditions when the runoff from the streets was redirected to the pond. Water depth was ± 70 cm, and the bed of the pond was covered with a soft layer of decomposing leaves. The pond had grassy embankments.

A vertical temperature profile was measured in the pond using Distributed Temperature Sensing (DTS). DTS is based on the backscatter of a laser beam traveling through a fiber optic cable and can be used for high-resolution temperature measurements. More information about this method can be found in Selker et al. (2006) and Tyler et al. (2009). Two DTS setups were placed in the north-east corner of the pond, each in the form of a 200 cm long transparent PVC tube with a diameter of 11 cm. To ensure ventilation, four 2 cm diameter holes were drilled every 6 - 8 cm in the tube. An optical cable was wrapped around the perforated tube with 0.50 cm spacing (see Figure 4.1). Temperature was measured every 5 minutes using a Silixa Ultima (Silixa Ltd., Hertfordshire, UK) with 0.126 m sampling resolution. Resulting measured vertical resolution of the described set-up was 0.18 cm. One column (right one in Figure 4.1a) was used for the analysis. The other column was used to study potential spatial differences in the pond.

A fully equipped HOBO weather station (Onset Computer CO., Bourne, MA, USA) was placed in between the two DTS columns. A full set of atmospheric variables was monitored during the whole experiment including atmospheric pressure, air temperature, relative humidity, wind speed and wind direction, and precipitation. Additionally, incoming and outgoing short- and long-wave radiation was measured using a CNR4 radiometer (Kipp & Zonen, The Netherlands).

4.2.2 ANALYSIS METHODOLOGY

The analysis focuses only on the night-time. Night-time was defined as the time when incoming shortwave radiation equalled zero for all the days of the measurement period. After adjusting for different sunset and sunrise times the night was defined as the period between 23:00 and 5:00 CEST.

Conditions above an urban pond at night are predominantly unstable; the water is warmer than the air. On top of that, during our experiment the wind speeds were very low, up to 2.5 ms^{-1}. Due to these circumstances the standard calculation of sensible and latent heat flux using bulk aerodynamic method [Hicks (1975)] was not possible. The wide scale of measured meteorological variables and a detailed temperature profile allowed us to calculate the Bowen ratio (B [-], Bowen (1926); Barr et al. (1994)) and

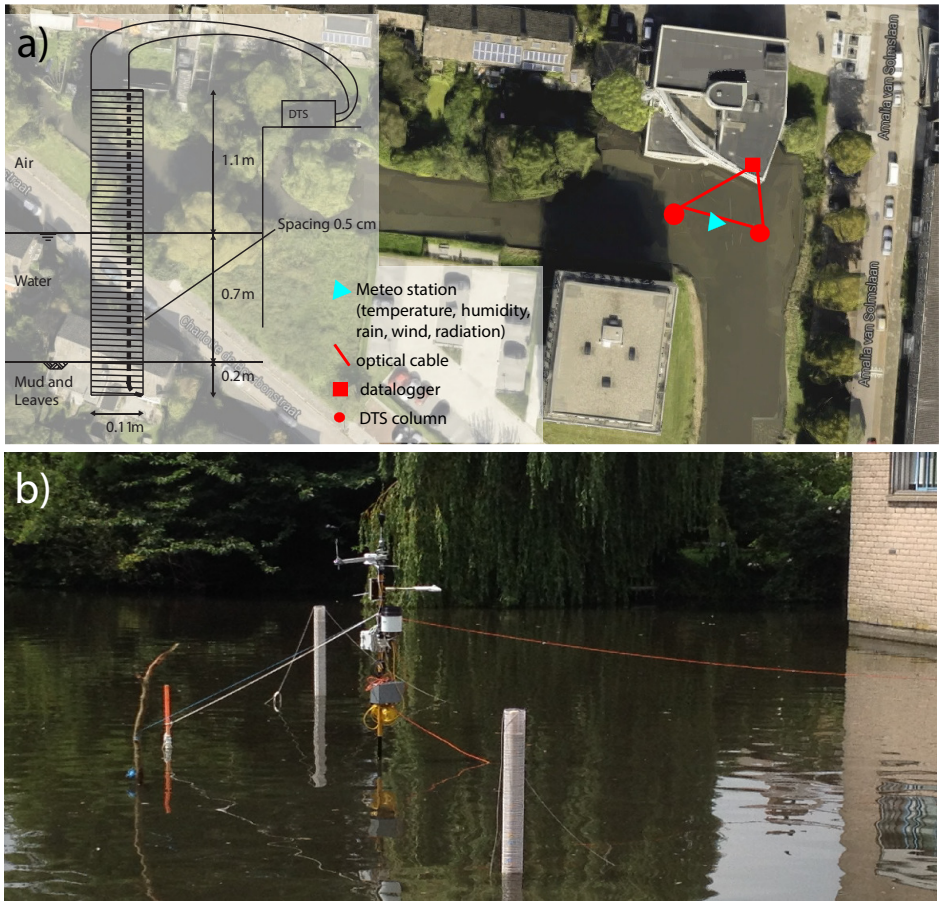

Figure 4.1: a)Positioning of measurements in an urban pond in Delft, and detailed scheme of the DTS measurement setup. b) View of the setup from the western shore of the pond. Water depth is about 0.7 m, the columns reached about 0.2 cm into the mud and leaves layer at the bottom of the pond.

subsequently derive the turbulent fluxes.

$$B = \frac{H}{E} \tag{4.1a}$$

$$B = \frac{C_p(T_{ws} - T_a)}{\lambda(q_s - q_z)} \tag{4.1b}$$

where H [Wm^{-2}] is the sensible heat, E [Wm^{-2}] is the latent heat, $C_p = 1006.43$ J kg^{-1}K^{-1} is the specific heat of air, λ is the latent heat of evaporation of water [J kg^{-1}], T_a is air temperature [C°], T_{ws} is water surface temperature [C°], q_s is saturated specific humidity at water-surface temperature [kg kg^{-1}], and q_z is specific humidity [kg kg^{-1}]. λ, q_s, and q_z were calculated for each time step.

$$\lambda = 2.501 * 10^6 - 2361 T_a \tag{4.2}$$

$$q_s = \frac{0.6108 e_{sat}}{P_{atm}} \tag{4.3}$$

$$q_z = \frac{0.6108 e_a}{P_{atm}} \tag{4.4}$$

where e_{sat} [kPa] is saturated vapour pressure, e_a [kPa] actual vapour pressure, and P_{atm} [kPa] is atmospheric pressure. e_{sat} and e_a were calculated using Tetens equation.

Additionally, water surface temperature was calculated from measured outgoing longwave radiation using Stefan-Boltzmann law:

$$Rl_{out} = \sigma \epsilon T_{ws}^4 \tag{4.5}$$

where Rl_{out} is the measured outgoing longwave radiation [Wm^{-2}], T the surface temperature [K], $\epsilon = 0.98$ [-] the emissivity of water [Wen-Yao et al. (1987)], and $\sigma = 5.67*10^{-8}$ $Wm^{-2}K^{-4}$ the Stefan-Boltzmann constant. T_{ws} was matched to the measured temperatures to precisely locate the water surface level for each time step.

The net radiation energy flux over night was calculated as the difference between incoming and outgoing longwave radiation (R_{net} = Rl_{in} - Rl_{out} [Wm^{-2}]). As Rl_{in} was always smaller than Rl_{out} above the pond at night, hence net radiation resulted in negative values. Shortwave radiation was considered, and confirmed by measurements, to be zero at night.

For this analysis, we assume closure of the energy balance between the amount of energy that was recorded as a temperature decrease over the whole water depth over night-time (Q_{water}) and the outgoing radiative (R_{net}), turbulent (H and E), and ground (G) fluxes. The overview of the different fluxes can be found in Figure 4.2.

$$-Q_{water} + R_{net} - H - E - G = 0 \tag{4.6}$$

so we define Q_{left} as

$$Q_{left} = -Q_{water} + R_{net} - G = H + E \tag{4.7}$$

for which

$$Q_{water} = \Delta T m C_p \tag{4.8}$$

where m is the mass of water and ΔT = $T_{morning}$ - $T_{evening}$. For shorter time periods (the measurements were taken with 5 minute time steps) the assumption of closure over the whole water depth becomes less reasonable. To establish hourly energy fluxes, we have used the observed temperature change for each hour of the night to calculate Q_{water} and used this in calculation of the hourly turbulent heat fluxes.

The sensible and latent heat flux can be derived from the Bowen ratio as follows:

$$E = \frac{Q_{left}}{1 + B} \tag{4.9}$$

$$H = \frac{Q_{left}}{1 + \frac{1}{B}} \tag{4.10}$$

Ground heat flux (G [Wm^{-2}]) was calculated from the slope of the temperature gradient of the lowest 10 cm using

$$G \approx K_{mud} \frac{\Delta T}{\Delta z} \tag{4.11}$$

where $K_{mud} = 2.2$ Wm^{-1}K^{-1} is the thermal conductivity of wet soil (recomended estimate for when detailed information about the soil is not available; Farouki (1981)], $\Delta z = 0.1$ m, and ΔT is a temperature difference [K].

Advection was considered irrelevant most of the time due to stagnant water conditions. Potential exceptions are two nights with heavy rainfall (07/20 and 07/28) when there was an influx of cold water and a peak in water level.

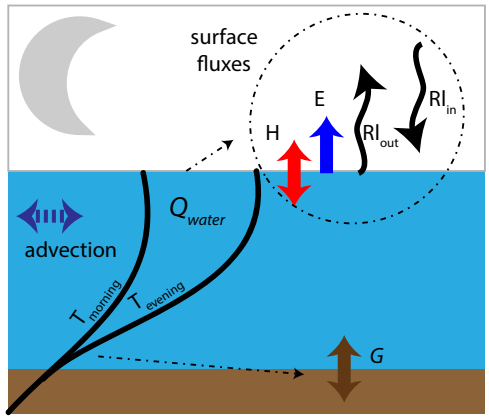

Figure 4.2: Schematic representation of all heat fluxes influencing the balance of an urban pond at night. Q_{water} represents the heat released by the pond over night as defined by integrating over the temperature change between evening ($T_{evening}$) and morning ($T_{morning}$) temperature. We define upward turbulent fluxes (E and H) as positive and downward as negative. Ground flux (G) and the net radiation are defined as positive in downward direction. This is consistent with the consensus of flux sign based on its direction.

4.3 RESULTS AND DISCUSSION

Figures 4.3a and 4.3b show the weather conditions at the measurement side. There is a gap in the dataset on 07/25 because of power failure. During the measurement period the conditions were mostly sunny with few cloudy days, and only two days with an overcast sky (07/21 and 08/06). Temperature varied between 15 and 34 °C for daytime, and 15 and 27°C for night time (Figure 4.3b). Wind speed reached highest values at night, while during the day, the conditions were often windless with average wind of 0.3 ms^{-1} (Figure 4.3a).

Figure 4.3c shows 5 minute temperature measurements taken by the DTS setup for both water and air. Recorded profiles in both set-ups were very similar A diurnal pattern is clearly visible for both air and water, although fluctuations in water temperature are not as strong. Increase in water level is visible after the two heavy rainfall events on 07/20 and 07/28.

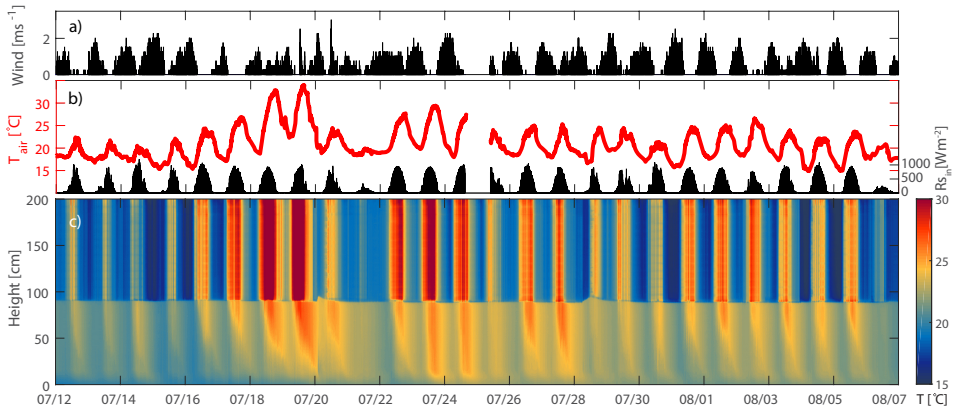

Figure 4.3: Measured variables for the whole period. a) wind speed, b) air temperature and radiation, 2 m and 1.5 m above the water surface, respectively, c) water and air temperature measured by the setup.

In order to derive the latent and sensible heat flux using equations 7 and 9, we needed to first calculate the radiative flux (R_{net}), the ground flux (G), and the net change in heat storage in the pond (Q_{water}). The resulting fluxes can be found in Figure 4.4a and 4.4b. The results in Table 4.1 show than on average 43 % of the heat is lost through radiation and 7 % is transferred downwards and stored in the muddy underlayer, leaving 50 % of the energy available for turbulent fluxes (Q_{left}).

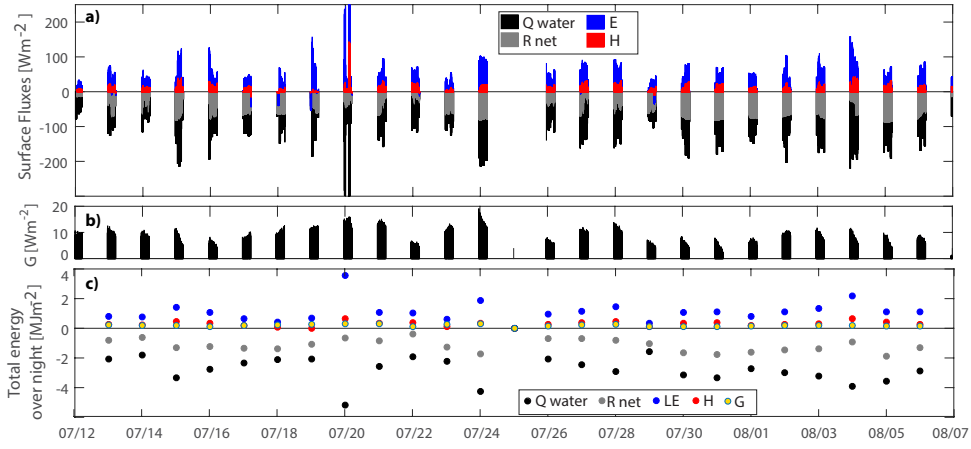

Figure 4.4: a) Fluxes at the water surface in Wm^{-2} at the night-time (23:00-05:00). E and H are positive in upward direction (from water to air), while Rl_{net} is positive in downward direction (from air to water) due to different definition of turbulent and radiative fluxes. b) Ground flux from water to the bottom of the pond (positive in downward direction). c) Sums of the different fluxes over each might in MJm^{-2}.

Second, the Bowen ratio was calculated (Figure 4.5). The nighttime values ranged form -0.07 and 0.46 with average of 0.27. The calculated values of sensible heat flux were, therefore, on average about four times smaller than latent heat flux, meaning that four

Table 4.1: Ratios of different fluxes with Q_{water} ($flux/Q_{water}$) for each day of the measurement period.

	13-jul	14-jul	15-jul	16-jul	17-jul	18-jul	19-jul	20-jul	21-jul	22-jul	23-jul	24-jul
RL	0,38	0,34	0,39	0,45	0,57	0,66	0,53	0,13	0,33	0,20	0,58	0,40
LE	0,39	0,42	0,43	0,39	0,27	0,20	0,34	0,69	0,42	0,55	0,27	0,44
H	0,12	0,13	0,13	0,12	0,08	0,04	0,01	0,12	0,13	0,20	0,05	0,08
G	0,10	0,10	0,05	0,04	0,07	0,10	0,12	0,06	0,11	0,06	0,11	0,07
	26-jul	**27-jul**	**28-jul**	**29-jul**	**30-jul**	**31-jul**	**1-aug**	**2-aug**	**3-aug**	**4-aug**	**5-aug**	**6-aug**
RL	0,34	0,28	0,27	0,66	0,52	0,53	0,59	0,48	0,43	0,23	0,53	0,46
LE	0,47	0,47	0,49	0,20	0,33	0,33	0,29	0,37	0,41	0,55	0,31	0,39
H	0,13	0,16	0,15	0,059	0,10	0,11	0,07	0,08	0,10	0,17	0,12	0,09
G	0,06	0,09	0,09	0,07	0,04	0,03	0,05	0,07	0,06	0,05	0,04	0,05

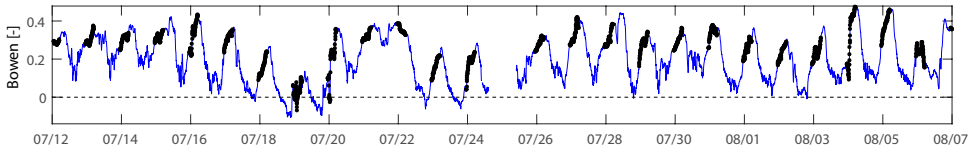

Figure 4.5: Bowen ration for the whole period. Black dots represent the nighttime values; blue are daytime values.

times more heat was used for evaporation than was used for heating the air. The results suggest that, on average, 39 % of the available energy was released by latent heat flux and only 11 % in the form of sensible heat. Day-to-day ratio of the fluxes, however, varied. Sensible heat varied between 1 % (07/19) and 20 % (07/22). Latent heat flux made up between 20 % (07/18) and 69 % (07/20) of the total thermal energy emitted.

The ratio of the turbulent and the radiative fluxes is strongly dependent on the meteorological conditions and climate of the location. For arid areas, the evaporative cooling can reach up to 57 % of the total net cooling [Ali (2007)]. Measured values of up to 69 % of latent heat compared to other fluxes suggest that the warm dry air in the urban area can create a night-time oasis effect above an urban pond.

As Q_{water} resulted from integrating the temperature change over depth, temperature changes in deeper layers (Figure 4.6 and 4.7a) of the pond provide an extra insight into the mechanism of night-time cooling of this urban pond and are vital for understanding the results presented in Figure 4.4. Both the instantaneous values of surface fluxes (Figure 4.4a), as well as the net temperature change overnight (Figure 4.4c), are dependent on the weather conditions during the previous day.

The type of profile typical for nights following a relatively cloudy or cold day is shown in Figure 4.7b. Water temperature change during these nights was gradual and equal for the whole profile. Close to the bottom of the lake, where the muddy layer begins (ca 10 - 15 cm from the bottom), the temperature was more stable and did not change much in the course of one night. The surface energy balance during such nights occasionally resulted in negative latent and sensible heat flux values for the last hour of the night (e.g. 07/29). This was caused by the assumption of energy balance closure on hourly basis and the combination of only small decrease in water temperature (Q_{water}) and longwave radiation being still relatively high.

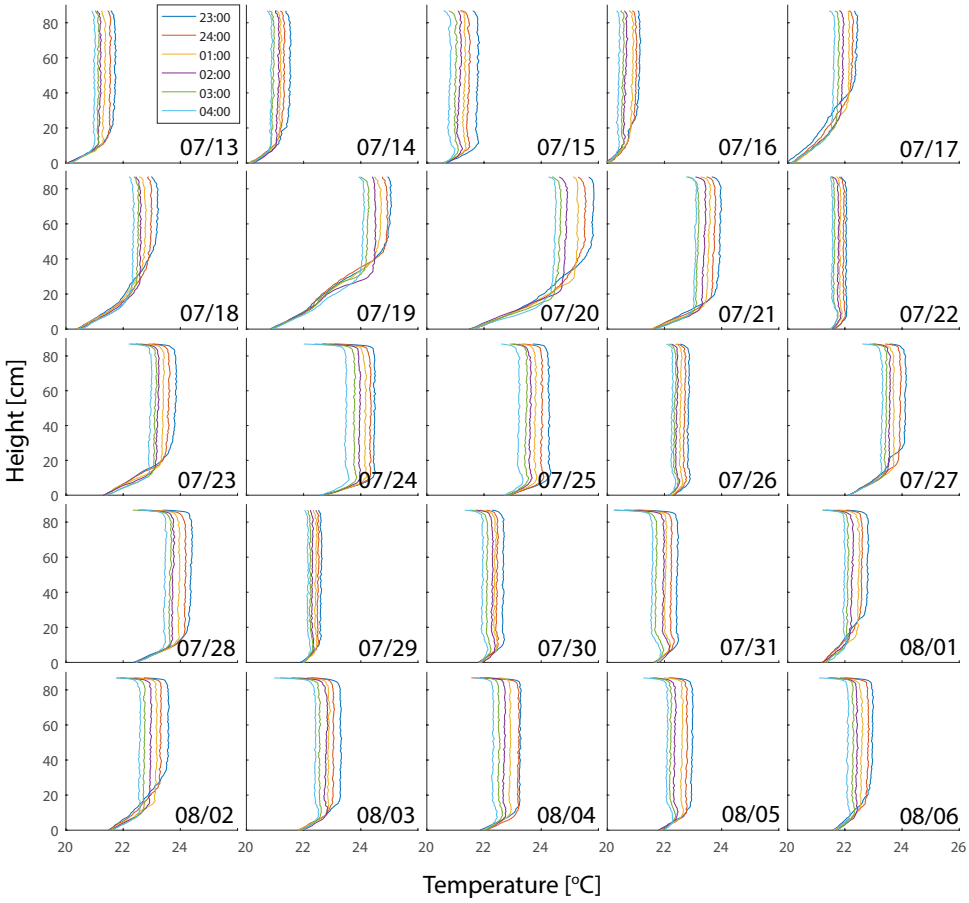

Figure 4.6: Instantaneous water temperature profiles at five different times each night of the measurement period. The night of 07/12 - 07/13 is annotated as 07/13 etc.

Second type of net temperature change profile (Figure 4.7c) usually follows warm days with a clear sky, for example 07/18 (Figure 4.3). High turbidity of the water in the pond caused that only about half of the water profile experienced increase in temperature during the day (data not shown). This resulted in a high temperature difference between the top layer (25.2 °C) and the bottom layer (20.8 °C) of the water at the beginning of the night. Energy for heating up the lower layers of water and the bed sediment was extracted from the top layer of water leaving less energy available to be released to the air. This situation is mainly visible during the first hour of the night, when the total temperature change in the water profile (Q_{water}) is close to zero, while the net longwave radiation is about -50 Wm^{-2}. As energy balance closure is assumed over each hour, the surface fluxes distribution in Figure 4.4a shows a negative sensible and latent heat flux. A similar, but more extreme, situation is visible also the following night (07/20).

The bottom 10 centimeters of the temperature profile represents the bed of the pond.

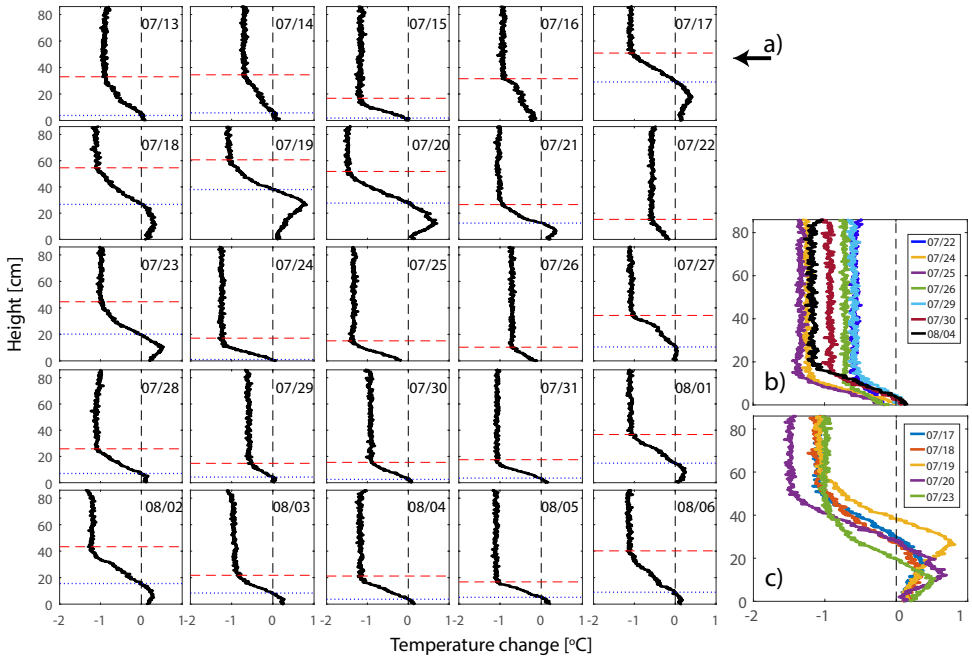

Figure 4.7: a) Change in water temperature profile ($T_{morning}$ - $T_{evening}$) for each day of the measurement period. Dashed line (red) shows location of the top well-mixed layer. Dotted line (blue) shows the depth at which the water experienced increase in temperature over the night. Subplot b) shows examples of temperature profiles representing uniform change over the whole water depth with none or small increase of the bed sediment temperature, and subplot c) shows examples of temperature profiles with net temperature increase in the lower water levels. All profiles start at the bottom of the lake (h = 0) and end at the water level (h = 86 cm).

Figure 4.6 shows that the bottom of the pond had always the lowest temperature of the whole profile. The lowest 10 cm of the profile always experienced a temperature gradient from warmer layers above, to the cold bottom of the pond. Above the lowest 10 cm was a transition layer of loose mud that functioned as a temperature buffer. This buffering is clearly visible in temperature profiles from nights following cold cloudy days (especially 07/31, Figure 4.6). In the evening of those nights, the buffer layer had a temperature similar to the water, but did not cool at the same rate, staying relatively warm compared to both the water and the bed. This difference in thermal behavior of this layer is probably caused by different composition of the mud with a high percentage of decomposing organic matter.

Uncertainty in the ground flux calculation is introduced by the choice of thermal conductivity of wet soil. 2.2 $Wm^{-1}K^{-1}$ is a value commonly used, when soil analysis is not possible [Farouki (1981)], however the values of thermal conductivity of wet soil vary between 1.5 and 2.5 $Wm^{-1}K^{-1}$ [Johansen (1977); Kersten (1949); Côté and Konrad (2005)], or even up to 6 $Wm^{-1}K^{-1}$ for saturated quartz sands [Zhang et al. (2015)]. Increasing the thermal conductivity of the mud to the highest value found in literature, will increase the ground flux by approximately factor 3. However, ground flux is likely to

stay the smallest of all components.

Situations when the calculated latent heat flux resulted in negative values very well represent the weakness of using Bowen ratio and energy balance at an hourly basis to calculate turbulent fluxes. Assuming that the heat (temperature) change over the whole depth will be the same as the sum of the outgoing fluxes is valid when considering the whole night period. On hourly basis, this method can lead to unreasonable results. Besides negative latent heat flux, the calculation can also result in extreme values. For example, at 03:05 on 07/20 the calculated latent heat flux peaked to a false 630 Wm^{-2}. This sudden bias was caused by extreme temperature drop during that hour related to influx of cold rain water. This is why this outlier was removed from the dataset used to calculate the average fluxes. A more detailed modelling of the energy fluxes in the water would be required to get better estimates of the turbulent energy fluxes for these exceptional nights.

Despite the above described weaknesses, the energy balance method provides an reasonable estimate for calculation of surface energy fluxes, certainly when integrated over the whole night instead hourly energy balances. It does not require a complex model that would calculate the fluxes under unstable atmospheric conditions. Nonetheless, due to its weaknesses, it is always necessary to take into account the whole picture. Combination of Figure 4.4a and 4.4c with the profiles in Figures 4.6 and 4.7 provides a comprehensive story about how heat leaves an urban pond at night. It is necessary to take into account all the aspects that can influence the energy balance of the pond in order to avoid misinterpretations of the data.

4.4 CONCLUSION

This paper analyzed data from a measurement campaign in a shallow urban pond in Delft, The Netherlands, in the summer of 2014 in order to assess the energy balance of such an urban surface water during hot summer nights. Previous research has shown that water bodies at night have the highest surface temperature of all the urban surfaces [Yang and Zhao (2015); Syafii et al. (2016); Theeuwes et al. (2013)], and therefore it is assumed that they act as a heating element of the city. The results of this study show that, on an average hot summer night, radiative cooling (43 %) and latent heat flux (39 %) are the predominant ways the heat escapes the water body. Sensible heat flux, which is the only one that increases the air temperature, made up to just around 11 % of all the energy released by the pond at night. The remaining 7 % was drained into the bed sediment.

Weather conditions the preceding day have a strong effect on the temperature distribution in the water column and on the cooling of the pond the night after. During warm days with high incoming solar radiation (e.g. 07/17 - 07/19), the high turbidity of the pond caused the upper layers of water to become much warmer than the water temperature near the bed. At night, this warm top layer predominantly heated the underlying water and the effect on the air was therefore minimal. Cold cloudy days resulted in smaller increases in water temperature and a more uniform temperature profile in the evening.

Lowest 10 - 15 cm of the measured profile was in the mud on the bottom of the pond. The deepest point measured in this campaign was the coldest point of the night-time

profiles for all days and the lowest 10 cm of mud always experienced a temperature gradient suggesting a heat flux from water to the bed. This ground flux was estimated to range between 0.10 MJm^{-2} and 0.32 MJm^{-2} per night but uncertainty in the thermal conductivity of the bed sediment is large.

5

How cool is Uchimizu?

Parts of this chapter have been published in Water (Solcerova et al., 2018b).

5.1 INTRODUCTION

It is well known fact that the air temperature decreases after summer rain. This is caused by several things, one of which is evaporation of the intercepted water. The energy required to evaporate the water is portioned to the latent heat flux instead of the sensible heat flux or the ground heat flux. With no moist available, the latent heat flux is zero. In this case, all net incoming radiation is transformed into sensible heat or ground heat; the high sensible heat flux yields a high air temperature and the ground heat flux retains the heat until drained via an increased air temperature. When water is applied, for example after a rain event, latent heat flux increases and sensible heat flux decreases, resulting in a lower air temperature. Consequently, evaporation of water from paved surfaces tackles heat stress in two ways: (1) it decreases the mean-radiant temperature to which the body is exposed by decreasing the surface temperature, and (2) it decreases the actual air temperature by extracting part of the energy necessary for the water to evaporate.

In the past, the Japanese water throwing tradition known as *uchimizu* has been used widely to cool urban surfaces and decrease air temperature around houses and in gardens. *Uchimizu* (combination of *uchi* for hit or throw, and *mizu* for water) is a tradition that stems from the 17th century [Poblete et al. (2012)]. However, over the last 50 years, this environmental control method lost popularity. This was mainly caused by a rapid development in technology and by socio-economic change, causing citizens to feel that traditional methods were too laborious or low class [Matsubara and Sawashima (1993)]. Nowadays, Japanese megacities such as Tokyo are aiming to revive the use of *uchimizu* to cool the city, especially during hot summer months. Citizens practicing *uchimizu* in Japanese urban areas were found to use less air-conditioning, which significantly decreased their domestic energy consumption [Matsubara and Sawashima (1993)]. Additionally, it was found that the level of outdoor comfort among citizens was higher in areas that applied *uchimizu* [Nakayoshi et al. (2015)].

The revival of *uchimizu* is promoted by Japanese authorities as a "clever way to feel cool" [Japan for Sustainability (2009); Japan Water Forum (2009)]. Also thanks to this initiative, research on this topic is becoming more frequent in Japan [Takahashi et al. (2010); Yamagata et al. (2008); Himeno et al. (2010); Harrison (2014)]. However, pavement-watering as a method to cool the ambient temperature is also popular in France [Bouvier et al. (2013); Maillard et al. (2014); Hendel et al. (2014, 2016)], and the principle is used all over the world to cool the roofs of houses [Wanphen and Nagano (2009); Naticchia et al. (2010); Meng and Hu (2005)], or for example the air temperature in railway stations in Japan [Ishii et al. (2009)].

Despite the popularity of the method, the number of published studies that have quantified the cooling effects of *uchimizu* is very limited. Most studies have only used measurements of the surface temperature, or the air temperature at a single height, as a measure of the cooling effect. Air temperature decreases between 1.5 and 2.3 °C were reported in these studies. Japanese studies report air temperature decreases of 1.5 - 3 °[Yamagata et al. (2008); Harrison (2014)] and French studies report 0.4 - 1.8 °[Bouvier et al. (2013); Hendel et al. (2016)].

Experimental work has been very important for the advancement of (urban) hydrology [van Emmerik et al. (in press)], as has also been demonstrated by previous experimental work on *uchimizu*. A few studies focused on measuring the vertical temper-

ature profile. Himeno et al. (2010) measured air temperature at four heights (0.4, 0.9, 1.5, and 1.8 m), and found that the cooling effect decreases (from 4 °C to 2 °C) with height. Slingerland (2012) measured a more detailed temperature profile in Rotterdam, The Netherlands. They concluded that an air temperature profile between 0 and 2 m above a wetted ground surface was consistently 1-2 °C lower than above a dry ground. These differences in observed air temperature profiles highlight the importance of studying reduction of air temperature decrease with increasing height above a wet surface. High-resolution air temperature profile measurements are expected to give additional insight in the above described cooling effects of *uchimizu*.

In this research, a three-dimensional setup was used to measure the air temperature within one cubic meter of air right above a wet/dry ground surface with a high spatial and temporal resolution. Several *uchimizu* experiments were performed under varying initial conditions. Objective of this chapter is to study and understand the effects of *uchimizu* under different conditions such as a varying initial ground surface temperature, shading of the pavement, and differences in the applied amount of water. Here, we provide an estimate of the cooling potential of the *uchimizu* technique as well as an explanation for the variability of its effectiveness under different initial conditions.

5.2 METHODS

5.2.1 FIELD SITE

This study presents and analyzes measurements of six experiments, with varying initial air temperature, ground surface temperature, shading, and applied amount of water. The *uchimizu* experiments were done on a paved street in an urbanized area at the Delft University of Technology campus (51.998 ° N, 4.378° E), Delft, The Netherlands. All measurements were done on 24 August 2016 between 11:24 and 17:40 local time (LT = UTC + 2). 24 August was a sunny day with a clear sky all day long. The air temperature at 2 m varied between 27.4 and 33.0 °C, relative humidity between 38.5 and 51.0 %, and wind speed between 0.1 and 0.7 m/s. Global radiation was recorded at station Rotterdam of the Royal Netherlands Meteorological Institute (KNMI), about 5.9 km from the measurement site.

Two *uchimizu* measurement locations were used during this experiment (Figure 5.1), each 3 m x 3 m. The ground surface consisted of red bricks in a 45 ° herringbone block pavement. The field site was surrounded by buildings on northern and eastern sides at distances of 6 m and 15 m from Location A, and 5 m and 5 m from Location B. An open field with trees was located in the southwest of the measurement locations. Location A was shaded by trees approximately between 14:00 and 16:00 LT. Location B was in full sunlight the whole day. In between location A and B was the reference location R. This location was uninfluenced by wetting and stayed in the sun the whole day.

Wind speed, wind gust, relative humidity, and air temperature were measured 1.5 and 2.0 m above the ground surface using a HOBO weather station (Onset Computer CO., Bourne, MA, USA), with a measurement interval of 1 min. Wet bulb temperature T_W was calculated from observed relative humidity and air temperature. This weather station was moved together with the temperature monitoring setup from location A to B and vice versa. Ground surface temperature before each *uchimizu* experiment was

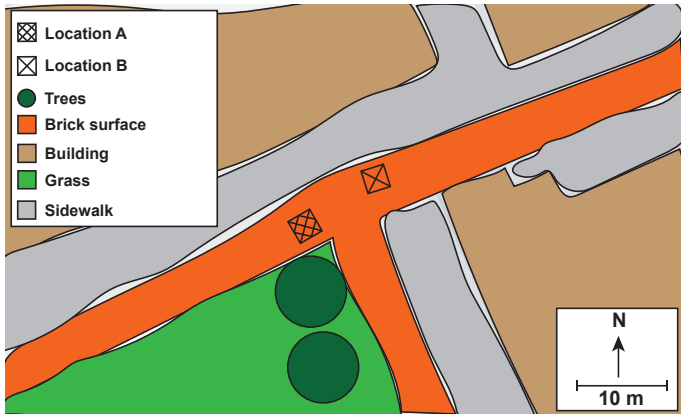

Figure 5.1: Sketched map of the field site in Delft, The Netherlands. Measurement locations are 3x3m, and are not completely to scale on the map. Reference location (R) was a location uninfluenced by application of water and remained in the sun the whole day.

measured using an infrared temperature sensor (Testo SE & Co., Lenzkirch, GR).

5.2.2 DISTRIBUTED TEMPERATURE SENSING

To study changes in the temperature distribution near the paved surface during an *uchimizu* experiment, this study used Distributed Temperature Sensing (DTS). DTS allows precise and fast temperature measurements along the length of a glass-fibre cable. This technique has, for example, been used to measure high-resolution temperature in lakes [Van Emmerik et al. (2013); Solcerova et al. (2018a)], soils [Steele-Dunne et al. (2010); Bense et al. (2016b)], streams [Westhoff et al. (2007b)], groundwater [Sebok et al. (2013b)], and atmosphere [Euser et al. (2014); De Jong et al. (2015)]. A more detailed description of DTS can be found in [Selker et al. (2006)] and [Tyler et al. (2009)].

DTS allows temperature measurements with sub-centimeter vertical measurement resolution by wrapping fiber-optic cables around a coil or other construction [Van Emmerik et al. (2013)]. However, as cables are often attached to the construction, this can introduce a significant error in observed air temperature values [Hilgersom et al. (2016b)]. The measurement setup used in this study [Hilgersom et al. (2016a)] reduced this effect by spanning cables across the construction without a physical contact between the cable and the construction anywhere in the region of interest for the temperature measurements (Figure 5.2).

The temperature monitoring setup consisted of a cage construction with 80 vertical bars, spanning a space of 1 m^3 (1 m x 1 m x 1 m). Two bend-proof white-colored fibre-optic cables (AFL, part number SR0015161001) with lengths of 1143 and 1243 m and diameter of 1.6 mm were spanned within the cage, resulting in more than 34,000 sampling points. The cables were unequally vertically spaced, with 3 mm spacing in the lowest 120 mm of the setup, 15 mm spacing between 120 and 200 mm, 35 mm spacing between 200 and 500 mm, and 80 to 200 mm spacing in the upper 500 mm. The cables were connected to the four channels of an Ultima-S DTS device (Silixa Ltd., Lon-

Figure 5.2: Measurement setup, consisting of the cage construction ($1m^3$) during the experiments.

don, UK) with a sampling resolution of 12.5 cm and a time interval of 1 minute with a 2 s integration time for each channel. More details about the used setup can be found in [Hilgersom et al. (2016a)]. Double-ended calibration was used [Van De Giesen et al. (2012b)] to achieve high precision monitoring results.

5.2.3 EXPERIMENTS

Six *uchimizu* experiments were done, with the aim of studying the influence of varying initial ground surface temperatures, shading, and applied amount of water on the cooling effect. An overview of conducted experiments is presented in Table 5.1.

Table 5.1: Details of the six experiments, with starting time, location, sun or shaded, water applied, surface temperature before water application T_g, and links to videos showing vertical evolution of temperature during each experiment.

Exp.	Time	Loc.	Sun/ Shade	Water applied	T_g [°C]	Link to video
1	11:24	A	sun	1 mm	37.5 ± 1.4	https://youtu.be/SwwEf8-BNxw
2	13:21	B	sun	1 mm	40.6 ± 1.1	https://youtu.be/9oVsFIpk5Yg
3	14:33	A	shade	1 mm	36.9 ± 4.8	https://youtu.be/bI__iyApdKo
4	15:29	B	sun	2 mm	42.6 ± 1.3	https://youtu.be/8WDEklxFj2U
5	16:23	A	sun	2 mm	47.7 ± 0.9	https://youtu.be/5sS6C13elTY
6	17:00	B	sun	> 5 mm	41.3 ± 1.9	https://youtu.be/k8ID4dLhDxY

Before each measurement, the temperature monitoring setup was placed at the reference location, and the ground surface temperature was measured at nine places within the 9 m^2 area of the experimental location (A or B). The values presented in Table 5.1 are averages of these measurements and their standard deviation. As can be seen, a wide

variety of initial temperatures is covered by the six experiments. Standard deviation of the ground temperature before the third experiment is relatively high, because the surface was shaded by a tree, and therefore the ground temperature varied depending on the instantaneous position of the shade patches.

Water was applied through pouring and evenly distributed over the whole 9 m^2 of the experimental location. This took on average 1.0 to 2.5 minutes. Immediately after application of water, the temperature monitoring setup was positioned in the middle of the wet area to monitor the cooling effect of the evaporating water. To prevent water from running off from this space, a 5 mm threshold was applied around the measurement area. An experiment was ended only when the ground surface was dry again, based on visual inspection. Each time a new *uchimizu* experiment started, the weather station was repositioned to the location of this experiment.

To investigate the influence of water on the cooling rate and change in temperatures, different depths of water were applied: 1 mm (9 liters), 2 mm (18 liters), and until the whole area experienced continuous surface runoff (i.e., the amount of water was much higher than the 5 mm threshold surrounding the experimental location). Three experiments were done on location A, and three experiments on location B (Figure 5.1 and Table 5.1). One of the experiments on location A was done on a shaded surface, to study the influence of shade. Before the beginning of this experiment, the setup was not placed on the reference location R, but close to the measurement location, to ensure the measurements before and after *uchimizu* were both taken in the shade of the tree.

5.2.4 ENERGY BALANCE ANALYSIS

To understand the mechanism behind the varying initial conditions of the experiments, simple heat transfer balance calculations were done. The intent of this analysis is not to predict the precise magnitude of the decrease in air temperature, but to assess the potential effect of initial ground surface temperature on the cooling effect *uchimizu* has on air temperature.

The total energy (E_{tot} [kJ/kg]) available to cool the ground (E_G) and the air (E_A) was calculated as the sum of energy necessary for increasing the water temperature to the observed temperature of the ground before the start of the experiment (see Table 5.1 for each experiment) and energy necessary to evaporate the water.

$$E_{tot} = E_G + E_A \tag{5.1a}$$

$$E_{tot} = m_{water} * Cp_{water} * \Delta T + m_{water} * L \tag{5.1b}$$

$$E_G = m_{brick} * Cp_{clay} * (T_g - T_W) \tag{5.1c}$$

where m_{water} [kg] is the mass of applied water, Cp_{water} = 4.2 kJ $kg^{-1}K^{-1}$) is specific heat of water, $\Delta\ T$ [K] is the temperature difference between the initial pavement temperature and the tap water (15 °C) used for the experiment, and L = 2257 kJ/kg is the latent heat of evaporation. Furthermore, m_{brick} [kg] is the mass of the brick pavement cooled by the applied amount of water, Cp_{clay} = 1.381 kJ $kg^{-1}K^{-1}$, T_g [K] is the measured ground temperature, and T_W [K] is the wet bulb temperature.

To simplify the calculation, we assumed that the clay bricks are cooled first because of their order-of-magnitude higher thermal conductivity (k_{clay} = 0.48 W $m^{-1}K^{-1}$) com-

pared to air (k_{air} = 0.03 W m^{-1}K^{-1}). We also assumed that the bricks were cooled uniformly in both vertical and horizontal direction. Energy necessary to cool the brick pavement to wet bulb temperature (E_G) and the total energy (E_{tot}) were, therefore, calculated first and subtracted to find out how much was left to cool the air (E_A). When the energy available for cooling the air was known, change in air temperature ($\Delta\ T_{air}$) could be calculated using

$$\Delta T_{air} = \frac{E_{tot} - E_G}{m_{air} * Cp_{air}} \tag{5.2}$$

The air temperature change was then divided by this "ventilation coefficient" (C_v [-]) to simulate the exchange of the air in the measured area (A = 1 m^2).

$$C_v = U_{gust} * \frac{E_A}{k_{air} * A * \Delta T_{air}} \tag{5.3}$$

Where U_{gust} [m/s] is measured gust speed.

All variables in equations 1 - 3 were known with exception of the mass of the clay bricks necessary to calculate E_G. Density (ρ) of clay is 1746 kg/m^3, so with known volume (V) the mass can be calculated using m = V/ρ. However, to what depth the bricks were cooled by the *uchimizu* experiment was not measured. Therefore, a range between 0.1 and 50 mm (thickness of the bricks) was prescribed and temperature changes were calculated for each "heat infiltration depth" for the clay bricks, as well as for the air. Figure 5.3a) shows how much cooling reached the air ($\Delta\ T_{air}$) after a given portion of the brick was cooled down to wet bulb temperature by 1 mm of water.

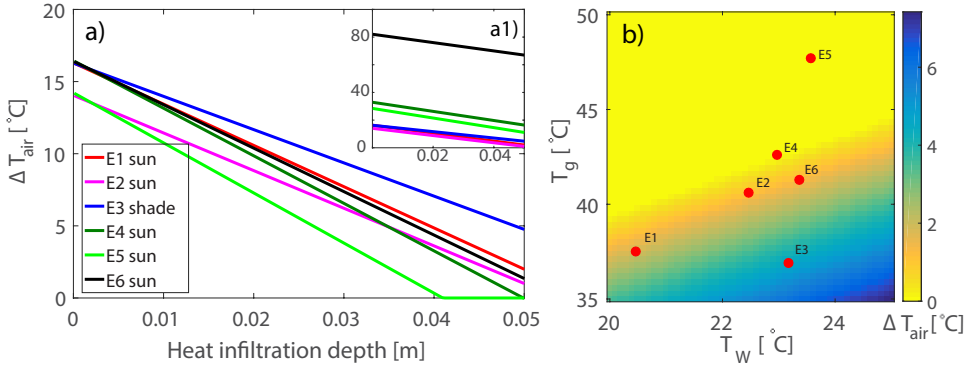

Figure 5.3: Analysis of influence of a) heat-infiltration depth, and b) wet bulb temperature (T_W) and ground temperature before beginning of the experiment (T_g) on the cooling power of *uchimizu* ($\Delta\ T_a$). Subplot a) uses measured values of T_g, T_W, and gust speed at the beginning of each experiment, and 1 mm of water. Subplot a1) shows the same analysis with actual amounts of water used in each experiment. Subplot b) has prescribed gust speed of 2.41 m/s (average gust speed), 50 mm of heat infiltration depth, and applied amount of water of 1 mm. Red dots in subplot b) show the combination of T_g and T_W for each experiment.

Assuming that the ground was cooled to wet bulb temperature, the energy supplied by the ground, and consequently the amount of energy that was needed to be supplied by the air, was dependent on the difference between the wet bulb temperature and the

temperature of the ground. The higher the difference T_g-T_W, the more energy was supplied by the ground and less cooling was left for the air. Figure 5.3b) shows the influence of combination of various wet bulb temperatures (T_W) and ground surface temperatures (T_g) on the air temperature change ($\Delta\ T_{air}$) resulting from application of 1 mm of water, and assuming the whole brick was cooled (50 mm). Red dots represent the measured combination of T_g and T_W at the start of each of our experiment.

Although the energy balance calculation using 1 mm of water resulted in numbers similar to those measured by previous studies [Kano et al. (2004); Harrison (2014); Yamagata et al. (2008); Slingerland (2012)], the calculated cooling effect for 2 mm and 5 mm of water was unrealistically strong (Figure 5.3a1)). When 2 mm of water was used, the calculation predicted cooling between 11 and 32 °C, and for 5 mm the difference reached 66 to 80 °C according to the used energy balance calculation. For three reasons such a simplified energy balance approach is no longer applicable when more water is applied: (1) No additional energy entered the system. In reality, energy was constantly being added in the form of incoming solar radiation which resulted in increasing temperature. (2) All the energy was extracted from the 1 m^2 of bricks and the 1 m^3 of air above. This assumption was partly addressed by introducing the ventilation coefficient (Equation 3) which simulates the exchange of the 1 m^3 of air used in the calculation. (3) All the water evaporated. It is, however, realistic to assume that a certain amount of water infiltrated and did not contribute to the cooling. Five, or even two, millimeters of water on brick pavement by far exceeds the wetting loss of a brick pavement [Van de Ven (1990)]. Hence, infiltration losses will occur. The only effect of this extra water is cooling of the brick according to equation 1b.

5.2.5 OVERVIEW OF DATA ANALYSIS METHODS

Measurements taken during the six experiments on 24 August 2016 were analyzed from several perspectives. To simplify the representation of the 3D results, averages of horizontal layers were used. First, the general horizontal profile is discussed. Vertical profiles for the reference location and profiles after application of water were compared. Effect of incoming solar radiation on the temperature measurements was quantified, as well as the effect of the applied water on relative humidity of the air. Four aspects of the cooling properties of *uchimizu* were looked into with more detail: the effect of the amount of water applied, the effect of shade, the effect of initial ground temperature, and the general spatial variability in the 3D measurements.

5.3 RESULTS

5.3.1 ENERGY BALANCE ANALYSIS

The energy balance analysis provided a simplified insight into some of the physical drivers such as initial ground surface temperature effect on evaporative cooling. The calculations suggest that there might be no cooling effect for experiment 5 and strong cooling after the third experiment. Experiments 1, 2, 4 and 6 are expected to have similar results with cooling effect between 0 and 2 °C. Slingerland (2012) showed that a high amount of water might have a larger influence on the near ground temperatures than 1 mm of water, which suggests that experiment 6 might result in different vertical cooling profile

than the other experiments.

5.3.2 GENERAL FINDINGS

Figure 5.4 presents recordings for the whole day, i.e. horizontal averages of temperature measured by the setup for each 1-minute time step (Figure 5.4d and e) in relation with instantaneous weather conditions (Figure 5.4a,b and c). Solid vertical lines show the times when water distribution was finished and the setup and meteorological station repositioned to a new location. This time is considered as the beginning of each new *uchimizu* experiment. Dashed vertical lines in subplots 5.4d and 5.4e show the times when the setup was repositioned from a measurement location to the uninfluenced reference location. Since the meteorological station was not repositioned to the reference location and stayed at the original location until the beginning of a new experiment when it was moved to a new location, the dashed lines are not present in subplots 5.4a and 5.4c. No vertical lines can be found in subplot 5.4b, because the radiation measurements were taken from the KNMI weather station in Rotterdam. Finally, in 5.4e red vertical lines depict times when the application of water began. Distributing the water equally over the 9 m^2 location took around about 1 - 2 minutes.

Figure 5.4e shows average temperature profiles of several layers in the cube, with focus on the lowest three layers (13, 16, and 19 mm above the ground). For more detail, please see the cross-sections of the measurement setup for each time step of each event. Links to videos created from these cross-sections are provided in Table 5.1, and can be also downloaded from https://doi.org/10.5281/zenodo.182395 Solcerova et al. (2016).

Temperature measured from 200 mm up showed, in general, very small differences among the layers. This suggests that the air above this level was already relatively well mixed by turbulence. When the setup was positioned on the reference location the temperature decreased with height. The application of water took around one minute, and the effect of *uchimizu* is immediately visible in the dataset from the moment the application of water started, as the reference location was in proximity of the measurement location and the cooling effect stretched beyond the boundary of the measurement location. After re-positioning of the setup above the a wet surface, the vertical profile changed. The cooling effect was strongest for the 13 mm layer, followed by 16 mm layer, followed by above laying layers.

A pocket of warm air formed above the cold layer close to the ground almost immediately after application of water. Highest temperatures were measured between 30 and 80 mm (see videos from Table 5.1 for more detailed view). This pocket persisted until the end of the experiment.

The measured effect of the added water on relative humidity (RH) was negligible. The biggest increase in RH was measured 1.5 m above the ground right after the last experiment (added water amount over 5 mm) and reached only 2.3%. Fluctuations of several percentage points were also measured above the dry reference position.

5.3.3 EFFECT OF APPLIED WATER AMOUNT

To simplify the presentation of the data, we focus mostly on the seven chosen layers in Figure 5.4e) and the temperature differences before and after *uchimizu*. Figure 5.5

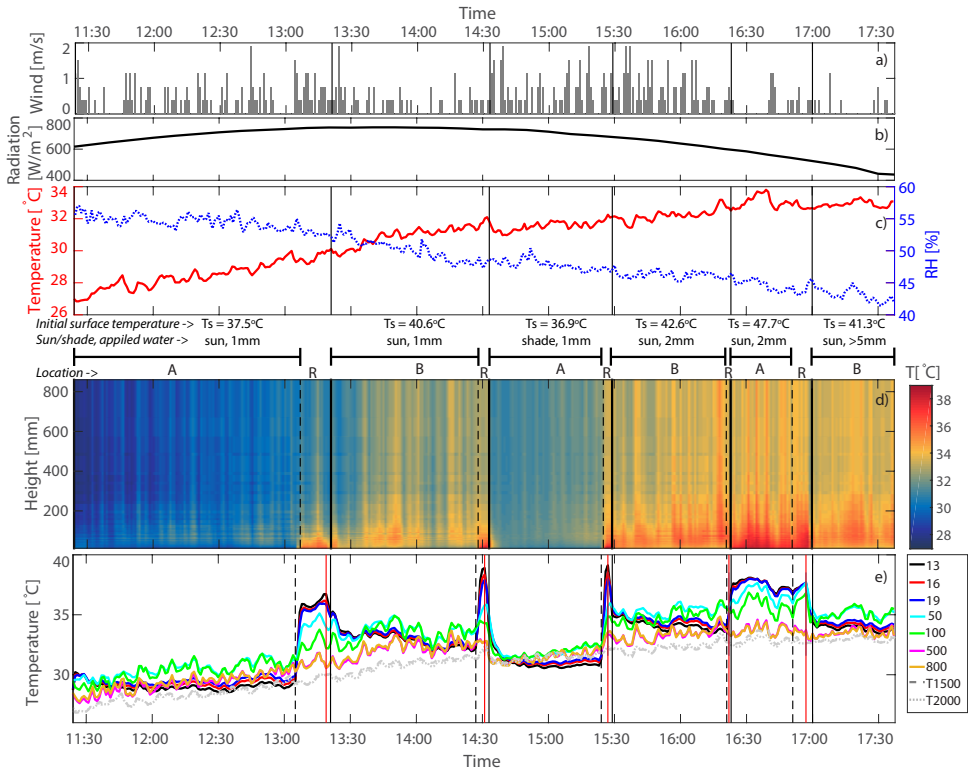

Figure 5.4: Measured a) wind speed, b) incoming radiation, and c) temperature and relative humidity 2 m above the ground. Horizontal averages of temperatures in time for d) all the layers of the setup, and e) 9 chosen layers of the setup and 2 temperature sensors (T1500 and T2000 for 1.5 m and 2 m above the ground, respectively). Vertical dashed lines show times when the setup was moved from its original location (A or B) to the reference location (R). Red vertical lines (only in e)) show times when the wetting of the surface started. Black vertical lines show the times when the setup was repositioned on the wet location. The weather station was always repositioned directly from location A to B and vice versa at times indicated by the black vertical lines.

presents the difference between horizontal profile measured at the reference location before the *uchimizu* and the measurement location after *uchimizu* (T_{after}-T_{before}). The temperature difference profiles shown in the diagram are at times when the cooling effect of *uchimizu* reached its maximum.

The first three experiments were done with 1 mm of water. The third experiment was conducted in the shade and, will be therefore discussed separately. The first experiment took place in the morning, when initial ground temperature and global radiation were relatively low, resulting in only very weak cooling (-0.7 °C) close to the ground. The second experiment repeated the conditions of the first experiment, but now on location B, and resulted in a stronger cooling effect, especially near the ground. Near-surface cooling reached -2.9 °C, while higher layers of air experienced cooling of only about -0.3 °C on average. Measured ground surface temperature before the first and second exper-

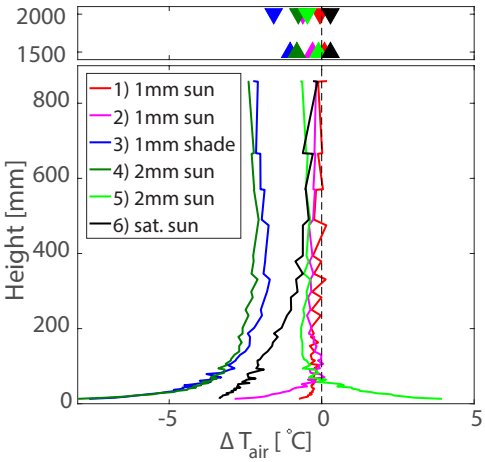

Figure 5.5: Temperature differences for average value of each layer before and after the *uchimizu* (T_{after}-T_{before}). Chosen times are different for each experiment and represent the maximum temperature drop, i.e. difference between maximum temperature before the *uchimizu* and minimum temperature after: For E1) T_{t+6}-T_{t+1}, E2) T_{t+3}-T_{t-2}, E3) T_{t+6}-T_{t-2}, E4) T_{t+8}-T_{t-2}, E5) T_{t+2}-T_{t-2}, E6) T_{t+7}-T_{t-3}, where t represents the time of *uchimizu* and numbers minutes. Triangles on the top show temperature change measured by the meteo-station 1.5 and 2 m above the ground.

5

iment were 37.5 °C and 40.6 °C, respectively. After the water application, the ground surface temperature was not measured, however the air temperature measured by the setup 13 mm above the ground reached after *uchimizu* were 30.2 °C and 35.0 °C for first and second experiment, respectively.

Double the amount of water (2 mm) was used in the fourth and the fifth experiment. The temperature difference profile of the fourth experiment was very similar to the profile described in the second experiment. However, the cooling effect was stronger. Eight minutes after application of water, temperature close to the ground dropped 8 °C compared to the situation before *uchimizu*. Higher up, the cooling reached -2.2 °C on average. In contrast to that, the fifth experiment showed almost no cooling effect. Zero cooling effect after the fifth experiment was predicted by the energy balance analysis due to the high T_g-T_W difference.

Figure 5.5 also shows increase in near-surface temperature by 4 °C for the fifth experiment, which was not expected. The measured increase in the near-surface temperature at the start of the fifth experiment might be explained by a large underestimation of T_{before}. The initial ground temperature on location A at the start of experiment 5 was 47.7 °C before the water was applied. Moreover, the setup was not located at the reference location for more than two minutes. This might not have been sufficient for the setup to reach equilibrium. Spruit et al. (2016) showed that the response time of DTS to shock changes in temperature can be up to 1 minute.

The fifth experiment cooled the pavement to approximately 38 °C but did not result in a colder layer of air close to the ground surface. As shown in Figure 5.4d, the lower layers of air continue to be the warmest all the time during experiment 5, while the temperature profile inverts at least partly during all other experiments. A contributing factor

for the creation of such a profile may have been the low wind speed during this experiment as it often dropped to 0 m/s (see Figure 5.4a).

During the sixth experiment, water was applied until continuous runoff from the area appeared. Vertical distribution of temperature change during the last experiment differs from the previous ones, especially in the lower layers. Temperature change of the lowest layer was only a decrease of 3.4 °C, which is 4.6 °C weaker cooling than after the fourth experiment. However, the rapid decrease in cooling effect on the following layers was not present after this last experiment. For the first 100 mm the temperature change decreased only by ~ 0.5 °C. The uniform cooling typical for higher layers was reached only after ~ 400 mm. The wind speed during this experiment was again very low and might have, similarly to the previous experiment, contributed to a different vertical temperature profile.

5.3.4 EFFECT OF SHADE

The third experiment was performed in the shade of a tree, and 1 mm of water was applied. Initial temperature of the pavement was only 36 °C. Compared to other experiments, *uchimizu* performed in the shade showed the strongest cooling effect on air temperature. The strongest cooling was measured close to the ground with -6.5 °C temperature drop within the first two minutes, and reached its maximum -8.3 °C at 14:48. For the third experiment, Figure 5.4e shows immediate response of all the measured layers to *uchimizu*.

Based on the lower T_s-T_W difference, the energy balance analysis predicted this experiment to have the strongest cooling effect. This was mainly due to the lower T_s compared to other experiments. In general, shade decreases the amount of shortwave radiation that reaches the ground, which consequently leads to lower ground temperature compared to sun exposed location, but it also leads to lower amount of energy available in the system.

The results suggest that shade might increase the air cooling effect of *uchimizu*. Shashua-Bar et al. (2009) measured an amplified cooling effect in the shade of trees for grassy areas. The study, however, also reported an increase in temperature if the shade was provided by a mesh. Our experiment in combination with the energy balance of Equation 1 shows that indeed a better cooling performance is to be expected if the pavement is shaded.

5.3.5 EFFECT OF INITIAL GROUND TEMPERATURE

The effect of initial ground temperature was predicted by the energy balance analysis to play an important role in the cooling efficiency of *uchimizu*. The results show that, indeed, the experiment with the lowest ground temperature (experiment 3) resulted in the highest cooling and vice versa. However, if the initial ground temperature was the only driving force, the first experiment should have resulted in almost as strong a cooling effect as the third experiment. The initial ground temperatures of these two experiments differ only by 0.6 °C. Nonetheless, the results of the first experiment showed very weak cooling effect, as predicted and visualized in Figure 5.3b, due to the low wet bulb temperature. Similarly, the fourth experiment was done on a relatively warm surface (T_s = 42.6 °C) and resulted, as expected, in strong cooling comparable to the experiment per-

formed in the shade.

5.3.6 LOCAL VARIABILITY

Using the high-resolution temperature monitoring method above a wet surface during a hot summer day resulted in several interesting insights into the cooling effect of *uchimizu*, such as a vertical profile of rising turbulent eddies. Figure 5.6 allows a more detailed examination of the cooling effect of *uchimizu* for the fourth experiment (2 mm of water applied over a sun exposed location) than the average-value profile shown in Figure 5.5 (dark green line). Compared to the previous figures, Figure 5.6 shows the absolute instantaneous values of that particular cross-section, not the averages over the whole layer (as in, for example, Figure 5.4d)).

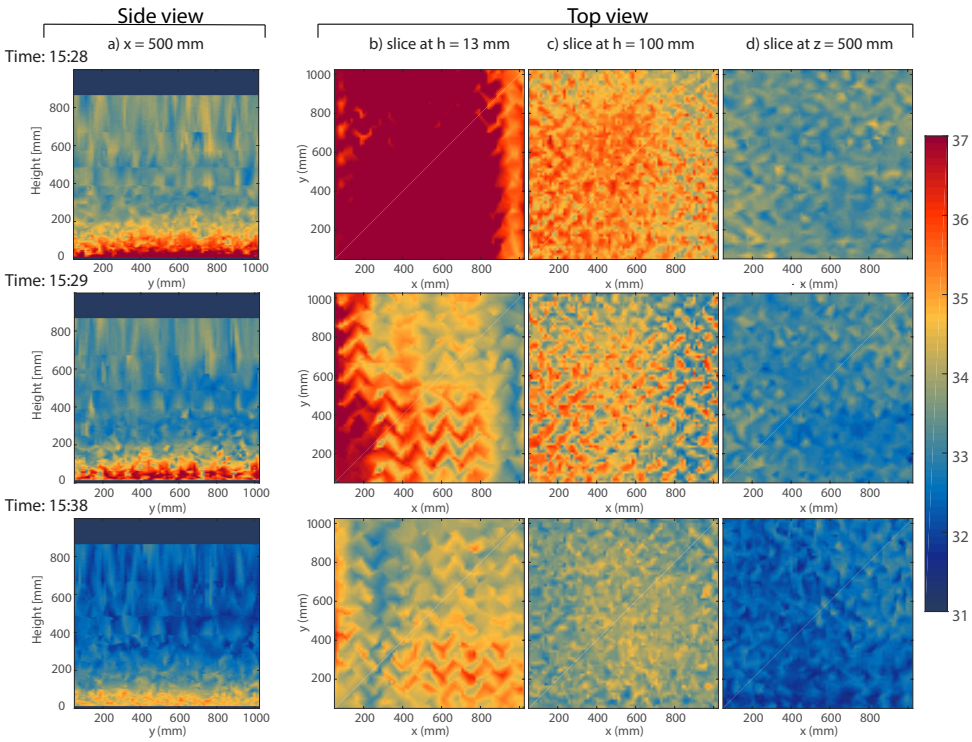

Figure 5.6: Vertical and horizontal profiles for the fourth experiment measured right before the *uchimizu* (15:28), right after (15:29), and 9 minutes after (15:38). Subplots in column a) show vertical cross-sections through the middle of the setup (x = 500 mm), and subplots in columns b), c), and d) show horizontal cross-sections at height h = 13 mm, h = 100 mm, and h = 500 mm, respectively.

Figure 5.6a shows three vertical cross-sections through the middle of the setup (x = 500 mm) for the fourth experiment. The top left subplot depicts the situation just before the water was applied, which means that the setup was at the reference location, and the two subplots below show situation 1 and 9 minutes after the *uchimizu*. Especially in the lowest 200 mm of air, where the measurement resolution was highest, creation of

turbulence (eddies) can be observed. The spatial variability of the rising warm air was very well revealed by the fine resolution of the setup.

Figures 5.6b-d show the horizontal spatial variability of the temperature distribution before and after the fourth *uchimizu* experiment. The spatial variability originated primarily from the shape of the pavement. The herringbone pattern, with warm bricks and colder interstices, was clearly visible in the data. This influence could even be seen 500 mm above the ground (Figure 5.6d). Detailed vertical and horizontal cross-sections of the instantaneous temperature also provided an insight in the effect of insolation and shading. Figure 5.6b, especially at the time = 15:29, suggests that the side of the setup where x = 0 was more exposed to sun than the side where x = 1000. This localized temperature increase is however only visible for the lowest layers of the set up and might partly be an artifact of unevenly heated pavement.

5.4 DISCUSSION

5.4.1 DISCUSSION OF ENERGY BALANCE ANALYSIS

Monitoring results of the six *uchimizu* experiments were analyzed from different perspectives. Using simplification of the system to a basic energy balance proved to be helpful in understanding the sensitivity to different variables, such as the wet bulb temperature or the ground surface temperature. As shown by Figure 5.3b, the energy balance analysis predicted low-to-no cooling effects for the fifth experiment and strongest cooling effect for the third experiment. This was indeed what the measurement results showed. However, the energy balance analysis predicted more cooling when more water was applied. This was not confirmed by the measurements. Most likely explanation for this overestimation of the cooling effect for water amounts greater than 1 mm is infiltration of part the water. With recorded infiltration rates of at least 10 mm/hr for similar brick pavements, a significant part of the applied water can infiltrate in the joints between the bricks [Van Dam and Van de Ven (1984)] and is no longer available for evaporative cooling.

In our energy balance model, the dynamic properties of the atmosphere were represented simplistically. To include the effect of air exchange by wind the ventilation coefficient was used to relate the amount of energy to cool the air E_A with the air temperature decrease ΔT_{air}. Similarly, the decrease in turbulence due to the transition of the temperature of the bricks from being warmer than the air to being colder than the air, as well as the effect of entrainment and vertical wind, was not taken into account in the calculation. Instead, we continued to use the observed U_{gust} in Equation 3.

When it comes to the paving material, it was assumed that the whole brick had the same temperature as the temperature measured on the surface and that the cooling was homogeneous throughout the whole volume of the brick. In reality, it is likely that the temperature of the brick gradually changed from the surface towards deeper layers, but this difference was not monitored and not included in the energy balance approach. Instead, the cooling could be seen more as a process starting on the surface, where the water was applied, and proceeding deeper into the brick. This simplification introduced in our energy balance analysis likely led to an overestimation of energy necessary to cool the ground.

The type of pavement seems to play an important role in the cooling effect of *uchimizu*. The simple energy balance analysis revealed the importance of density and heat capacity of the paving material. Equation 1c shows a direct proportionality between heat capacity and energy necessary to cool the pavement. The same equation then hints at inverse proportionality between density and energy (m = V/ρ). Surface with higher density and lower heat capacity, such as for example asphalt ($\rho \approx 2000$ kg/m^3, Cp $\approx$ 0.95 kJ/(kg*K)), might require less energy for cooling than clay bricks.

5.4.2 DISCUSSION OF THE EXPERIMENTAL SETUP

The construction of the setup was specially designed to capture variation in temperature with very fine spatial resolution. However, the dense cable spacing in the set-up and the vertical bars of the walls of the cube may have led to undesired effects, such as reduced ventilation inside and at the bottom of the construction. Although the ventilation was not restricted totally, the chosen setup might to a certain extent limit the effective area of cooling to that directly above the wetted ground surface. The influence of the grid is expected to be small, since the relative volume of the optical fibre over the complete setup is only 0.4 %. In the bottom 10 cm, the percentage is a bit higher at 2 %. However, the cable nets could induce small-scale convection cells by the physical tendency to diffuse the temperature interface [Hilgersom et al. (2016a)].

Similarly, the grid of the "walls" of the cube provided shading for the area under and behind the construction causing differences in influence of radiation along the vertical axis of the setup. As can be seen by studying the films, this influence was relatively small. Also in the recordings shown in Figure 5.6 Top view h = 13 mm, a colder strip due to the shading is visible at x > 800 mm.

Effect of solar radiation on the temperature monitoring setup is visible from Figure 5.4e. As there was a very small vertical variation in the temperature measured by the setup above ~ 200 mm, the highest layer of the setup (yellow line in Figure 5.4e) should have similar temperature to the air temperature measured at 1.5 m by the sensors with radiation shields (gray lines in Figure 5.4e). However, measurements taken by the shielded sensors collected up to 2 °C lower temperatures than the highest layers of the setup. This difference disappeared when the setup was in the shade (14:33-15:23). Differences between the measurements of the highest layer (859 mm) and the 1.5 m temperature sensor (T_{859}-T_{T1500}) for each time step are shown in Figure 5.7. Effect of radiation on the recorded temperatures was around 1 °C on average when positioned in the sun, and close to zero for measurements in shade (-0.02 °C). Later in the afternoon (after 16:20) the effect of direct insolation on the white fibre optic cable decreased again, probably as a consequence of lower incoming solar radiation. This is in agreement with research done by [Sigmund et al. (2016)]. They have found that the effect of radiation on DTS can reach up to 2.8 °C when the values of incoming shortwave radiation are high. Although, [De Jong et al. (2015)] showed smaller effects of solar radiation - 0.4 °C on average for 1.6 mm white cable, the same one as used in our *uchimizu* measurements, we observe an effect of up to about 1.0 to 1.5 °C.

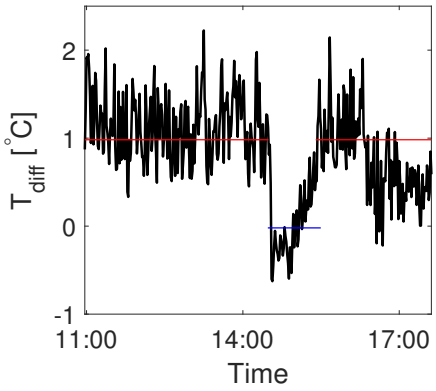

Figure 5.7: Difference between temperature measured by the setup at 859mm and reference temperature at 1500mm (T_{859}-T_{T1500}). Red and blue lines show average values for all time steps when the setup was positioned in sun and in shade, respectively.

5.4.3 DISCUSSION OF THE MEASUREMENT RESULTS

The amount of water applied did not show a clear relation with the cooling effect. Applying 1 mm of water resulted in relatively weak cooling effect, with strongest cooling near the ground. Strong cooling effect recorded after the fourth experiment, using 2 mm of water, might suggest that double the amount of water leads to more cooling. However, the following experiment with 2 mm of water resulted in almost no cooling and even an increase in temperature near the ground. The last experiment, when the surface was fully saturated by water, resulted in a slightly different profile than all previous experiments. It is possible that the amount of water influenced the thickness of the lower air-layer that was experiencing stronger cooling than the higher well-mixed air. The measured differences for small (1 - 2 mm) and large (>5 mm) amounts of water correspond with the preliminary research done by Slingerland (2012).

Previous studies done by Kano et al. (2004); Harrison (2014); Yamagata et al. (2008) reported temperature decreases between 1.5 and 2.3 °C measured at one point 2 m above the ground, and a more detailed profile done by Himeno et al. (2010) showed a cooling effect decreasing from 4 °C at 0.4 m above the ground to 2 °C at 1.8 m above the ground. Similar values were measured in our experiment, but with much higher resolution. While Himeno et al. (2010) measured the effect on four levels, the setup used in this research consisted of 53 horizontal layers. Similarly, the dense measurement grid in each of these layers allowed for detailed observation of spatial variability in temperature caused by the unevenly heated pavement underneath.

Average values for each horizontal layer, Figure 5.5, showed a typical profile of strong cooling close to the ground followed by constant cooling higher up. Air above 200 mm experienced similar cooling for all measured horizontal layers. Nonetheless, even with stronger cooling close to the ground, the lowest layer of air (under 200 mm in Figure 5.6 Side view) stayed warmer than the air above. The homogeneous temperature of air above 200 mm is inconsistent with the measurements of Himeno et al. (2010), which showed

variations among the measured levels. This difference might have been caused by using average values of a horizontal layer vs. using point measurements. Figure 5.6 Top view shows variation of up to 1 °C for the higher layers of air (100 and 500 mm), and up to 3 °C for the layer closest to the ground. For this reason, we recommend averaging several measurement points at one level as a better estimation of the temperature change.

Uchimizu showed a promising potential for mitigating the UHI at a local scale by decreasing both air and ground temperature. Decreasing the ground temperature lowers the mean radiant temperature (MRT) and consequently increases human comfort. Another factor influencing human comfort is relative humidity (RH). Higher RH has generally a negative impact on human comfort. The effect of *uchimizu* on RH was measured to be negligible (2.3%) in the climate of The Netherlands, but implications of increasing the RH should be considered for more humid climates. Human comfort is influenced by a broad scale of factors and was not explicitly studied in this research.

The brick pavement showed a distinct change in colour the moment all water had disappeared from the brick. This was the moment each experiment was stopped as further cooling was not expected. As visible from Figure 5.4e temperatures at h = 13 mm were constant by the end of each experiment – and temperatures at h = 100 were already running up. As expected, results suggested that at the end of each experiment the near-surface temperature was still lower at the experimental location than at the reference location. The conclusion that the cooling stops the moment the pavement is dry seems to be valid. Although it is not the scope of the current paper, it would be interesting to continue monitoring after the moment the pavement runs dry to proof this and to see how quickly temperature starts to increase again.

5.4.4 OUTLOOK

Limitations and uncertainties described above showed the need for further research. It was assumed that all the water evaporated. However, further research is needed to assess how much infiltrates and how much evaporates. Simultaneous measurements of a profile of areas with and without *uchimizu* might provide more accurate quantification of the cooling effect. Alternatively, application of *uchimizu* on a plot of artificial street surface on a small scale can also provide an estimate of how much water infiltrates.

A second setup measuring simultaneously above a dry surface would also contribute to another important aspect, the duration of the cooling effect. Information about the time when the cooled surface and air warmed up again to a temperature of an uninfluenced area cannot be precisely derived from measurements of a single setup. However, the results of this research suggest that the effect lasts longer than one hour. As visible from Figure 5.4e), the reference location was always warmer than the measurement location, even after a long measuring period (e.g. 13:20-14:20).

More measurements are also necessary to fully understand the potential of shade and initial ground temperature on *uchimizu* practices. Results of this study suggest that shade might enhance the cooling effect of *uchimizu*. Similarly, lower ground temperature can be beneficial for cooling by *uchimizu*, since less energy is extracted from the ground and more from the air. Such effect, however, is only confirmed for the warmest and coldest initial ground temperature measured in our experiment.

This research specifically focused on the temperature change within the 1 m^3 of air

closest to the ground. Further research should extend to areas around and above this 1 m^3. Further research is also needed for deeper understanding of the effect of evaporation in general and *uchimizu* in particular on UHI at the city level. The temperature decreases measured in this research showed potential for local cooling. However, if *uchimizu* should be used over a whole city, more research needs to be done to come to a reliable estimate of the decrease of temperature and the amount of water that would be necessary to achieve this decrease. This water demand is the reason why this topic is also interesting from a water management point of view.

5.5 CONCLUSION

This research focused on quantifying the cooling effect of the traditional Japanese water throwing tradition of *uchimizu* on air temperature in an urban environment. The measurements show a decrease in air temperature up to 1.6 °C at 2 m height, and up to 8 °C for near-ground temperature. Strongest cooling was measured for the experiment performed in the shade. Stronger cooling effects were also predicted for lower initial ground temperatures, especially in combination with high wet bulb temperatures. Results of the third and fifth experiment agree with this hypothesized effect of initial ground temperature, nonetheless the remaining experiments do not show this relationship. For an applied amount of water of 1 mm and 2 mm, there is no clear difference in cooling effect.

We further conclude that use of high resolution temperature monitoring setups, such as the one used in this research, can potentially lead to significant improvements in understanding of atmospheric processes at a micro-scale. Thanks to the dense measurement grid we are able to capture the vertical distribution of temperature over time in high detail. The fine resolution is even able to capture the rising turbulent eddies created by the heated surface.

Overall, this study sheds a promising new light on a traditional cooling method. This simple water throwing method has a potential to decrease temperatures in impervious and paved parts of urban areas by using a limited amount of water. Besides its cooling effect, *uchimizu* practice is also an opportunity to activate awareness among citizens, and stimulate citizen participation in solving heat stress problems and cooling energy saving. *Uchimizu* is a local technique with proven local effects. Application at city scale as an UHI mitigation strategy is beyond the scope of this study but could provide interesting new insights on urban climate control and water resources management.

6

DO GREEN ROOFS COOL THE AIR?

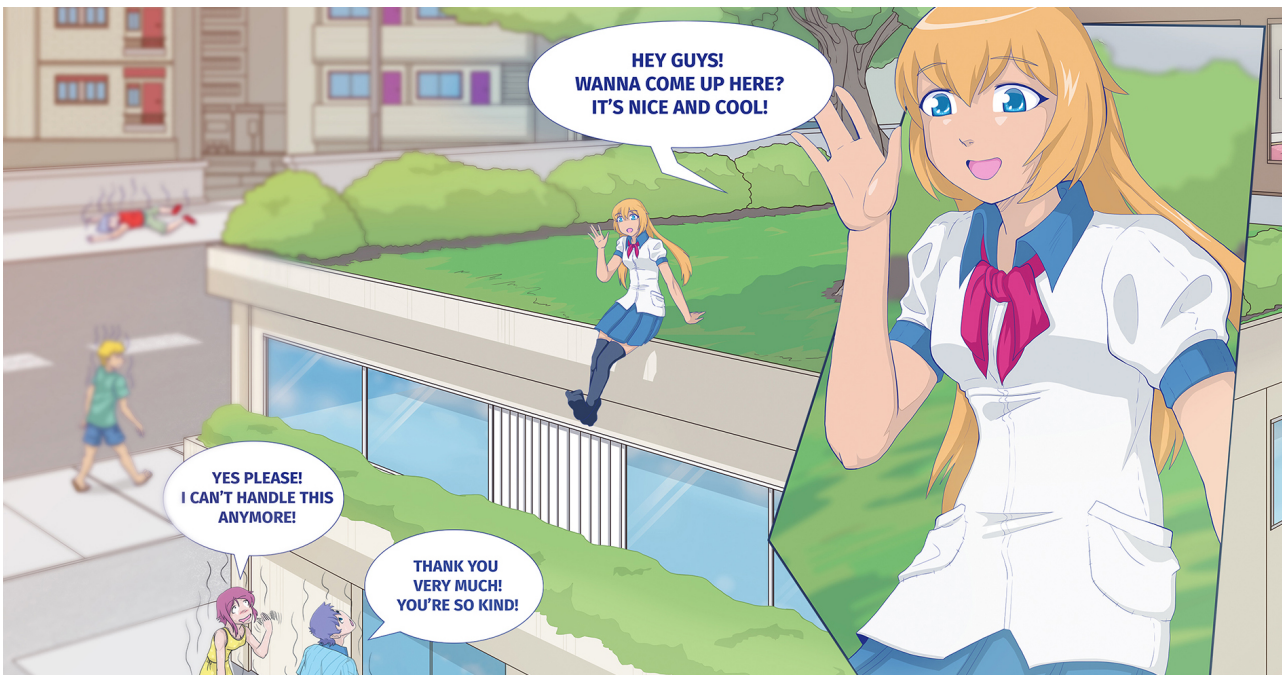

Parts of this chapter have been published in Building and Environment [(Solcerova et al., 2017).

6.1 INTRODUCTION

Increasing the vegetated fraction in a city has shown to be an effective way to decrease urban temperatures [Susca et al. (2011); Qiu et al. (2013)]. Green roofs are suggested as one of the possible ways to achieve this [Santamouris (2014); Gaffin et al. (2006); Takebayashi and Moriyama (2007)]. Implementing green roofs is popular due to their versatile effects and functions, such as roof gardens [Wong et al. (2003)], isolation [Jaffal et al. (2012)], or runoff peak delay [Stovin (2010)]. The thermal effects of green roofs on the urban environment are another widely used argument to promote their implementation [Alexandri and Jones (2008)].

Literature focused on temperature measurements of green roofs generally covers two topics: (1) Cooling effect of green roofs on indoor environment and its use as insulation layer and (2) Effect on roof surface temperature. Many studies showed potential benefits of green roofs for the indoor environment of the building, such as energy savings [Castleton et al. (2010)] or reduction of indoor temperatures by several degrees [Kumar and Kaushik (2005)]. This is closely connected to green roofs' ability to work as insulator and temperature buffer and decrease high surface temperatures [Wong et al. (2007)],as well as low winter temperatures [Teemusk and Mander (2010)].

When it comes to the effect of green roofs on outdoor temperature, most modelling studies agree that green roofs have the potential to decrease UHI [Scherba et al. (2011); Alexandri and Jones (2008); Virk et al. (2015)]. Those results are supported by several measurement studies [Klein and Coffman (2015); Peng and Jim (2015); Heusinger and Weber (2015); MacIvor et al. (2016)]. Additionally, Peng and Jim (2015) also showed a slight warming effect of green roofs during winter months.

However, measurement studies focusing primarily on effects of green roofs on outdoor temperature are relatively scarce. Berardi et al. (2014) summarized the literature about green roofs. From the large number of articles presented in that review, only three dealt with outdoor air temperature measurements [Speak et al. (2013); Susca et al. (2011); Lazzarin et al. (2005)]. Another highly cited review article [Oberndorfer et al. (2007)] discusses the ecosystem services of green roofs. From 61 references only one [Bass and Baskaran (2003)] focused on urban heat island mitigation.

Some studies discuss possible negative effects of green roofs. Jim (2015) showed that sedum covered green roofs might under tropical conditions increase the air-conditioning energy consumption in apartments below. Contrary to that, MacIvor et al. (2016) promote sedum for its cooling properties as a good choice for temperate continental climates. Previous studies also suggested that green roofs need a certain level of maintenance, because vegetation damage can reduce the desired cooling effects [Speak et al. (2013)], and the temperature of the bare substrate can easily run higher than surface temperature of a bare roof [Wong et al. (2007)].

Research presented in this chapter is based on monitoring results from an extensive, sedum-covered green roof in Utrecht and provides an analysis of these observations. We aim to provide additional insight in thermal behavior of sedum-covered green roofs in a temperate climate, and to contribute to understanding of the role of soil moisture in the cooling effect of green roofs. We also aim to clarify how thermal behavior of a green roof changes under extreme conditions, and compare the effects of a dry green roof to a well prospering green roof, and white gravel roof.

Table 6.1: Sensors' specifications

Variable	Sensor manufacturer and type	Accuracy
Air temperature	EKOPOWER thermometer TS 21	<0.1°C
Soil temperature	EKOPOWER thermometer TS 21	<0.1°C
Soil moisture	ECH_2O EC-20	<0.04 $m^3 m^{-3}$
Rainfall	EKOPOWER rain collector 7852M	<0.2 mm
Runoff	STS pressure transmitter ATM/N	<0.5%
Wind speed	EKOPOWER anemometer MAX40	<0.1 ms^{-1}
Solar radiation	EKOPOWER solar rad. sensor 6450	< 3% (0° to ±70° zenith angle) ±10% (±85° zenith angle)

6.2 METHODS

6.2.1 MONITORING SITE

The study site is located in Utrecht, The Netherlands (52°5′ N, 5°7′ E). The climate is a moderate sea climate with summer starting in June and ending mid-late September.

We examined seven green roofs installed on a rooftop of a one-story school building two of which were examined in depth (GR4 and GR7); they are considered, and proved by comparison, to be representative of the other ones (Figure 6.1). Additionally, those two roofs had preinstalled soil moisture sensors, and therefore provided more information for the analysis. All roofs were installed in 2010 and did not receive routine maintenance. All green roofs were 7 m long and 3.5 m wide, with exception of GR2 which had dimensions 7 x 7.5 m. Part of the installation was also a conventional white gravel (WG) roof which was used as a baseline for comparison (8.5 x 8 m).

The construction of each green roof was as follows. A membrane separated the rooftop from the green roof, above which lied a drainage layer (ca. 2 cm) and a cloth layer (0.3 cm). On top was a substrate layer with vegetation. The combined depth of root zone and substrate layer was approx. 3.5 cm. The vegetation on all the green roofs was a mixture of six sedum species(*S. floriferum "Weihenstephaner gold", S. album "Coral carpet", S. reflexum, S. spurium "Fuldaglut", S. sexangulare, S. album superbum*) and was considered stabilized. As visible from Figure 6.1a), the percentual representation of the sedum species was different for each roof.

During the monitoring period (2010 - 2015), a small meteorological station was installed on the roof including an air temperature sensor 2m above rooftop level, solar radiation, wind speed, and rainfall. Each roof had two additional temperature sensors positioned 15 cm (T15) and 30 cm (T30) above the ground in the center of each green roof, and one temperature sensor positioned 2 cm under the surface inside the substrate layer or gravel layer (Ts). Runoff was measured from each roof separately [Stomph et al. (2002)]. Soil moisture sensors were placed in GR4 and GR7 2.5 cm under the substrate surface. All data were recorded at 5 minute intervals. The accuracy of the sensors, as well as the manufacturer and sensor type, can be found in Table 6.1 Calibration of the sensors was done before installation and the green roofs, as well as the devices, were regularly checked.

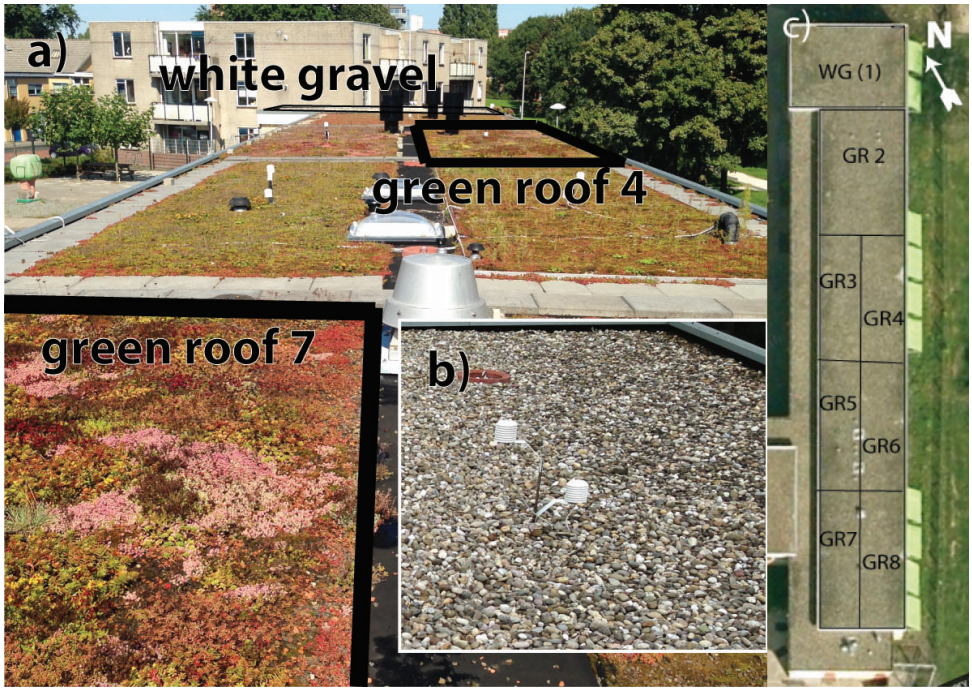

Figure 6.1: Green roofs in Utrecht on 03-09-2014. a) plant cover and positioning of GR4, GR7, and WG with respect to each other, and position of temperature sensors b) white gravel roof with temperature sensors, and c) layout of the fields on the roof.

6.2.2 INFLUENCE OF SOIL MOISTURE

Influence of initial soil moisture on the thermal performance of green roofs was studied using the 2014 dataset. Two six-day periods in July were chosen for the analysis, further referred to as "cloudy" and "clear sky". First period, 12-17 July was considered as a cloudy period with average daytime solar radiation of 212.5 Wm^{-2}. 15 July was an exception and was relatively sunny (average radiation 351.5Wm^{-2}). Second period, 22-27 July, was considered relatively sunny with average solar radiation of 328.8 Wm^{-2}. It should be noted that the incoming long-wave radiation was not measured. The cloudy and the clear sky periods were only based on the day time measurements of the short wave radiation and therefore nights may or may not be cloudy.

Weather conditions during the examined periods is shown in Figure 6.2. A rainy week before 12 July caused a relatively high soil moisture level (0.18 $m^3 m^{-3}$ in GR7) at the beginning of the examined period. Soil moisture then decreased continuously until it reached zero value on 19 July. After a heavy rain on 21 July the soil moisture increased again to 0.21 $m^3 m^{-3}$. The highest value of soil moisture measured in July reached 0.22 $m^3 m^{-3}$ (GR7). Two short rain events (14 and 26 July) with precipitation around 0.2 mm did not cause any change in soil moisture, probably because all the water was intercepted by the vegetation. Effects of the differences in soil moisture conditions on observed temperature are discussed in section 3.1.

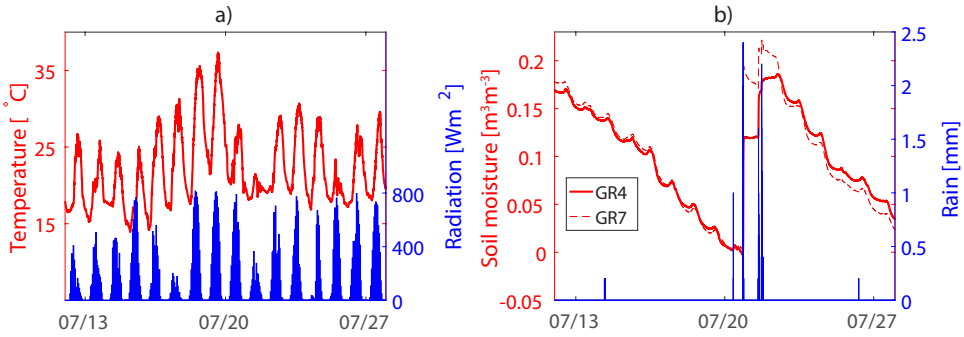

Figure 6.2: a)Air temperature 2 m above the roof and incoming shortwave radiation, and b) soil moisture and rain during the study period.

6.2.3 PROSPERING VS. DRY GREEN ROOF

In August 2012 several of the green roofs dried out. This was due to relatively dry and warm spring and summer with higher than average temperatures. Already in the end of April, temperature occasionally reached 30°C. In order to stimulate the growth, the roofs were fertilized and irrigated in early autumn 2012. No additional plants were added, so we can assume that the mixture of the sedum species was similar for both years (2012 and 2013). With the exception of this singular intervention, all green roofs were not fertilized or irrigated again during the study period. Figure 6.3 shows the difference in appearance between a dry and a well prospering green roof.

To evaluate the thermal behavior of a wilted and a dried out green roof, a comparison was made between 15-31 August 2012 and 15-31 August 2013. Those two periods were chosen because of their similar weather patterns. They were both relatively sunny/warm months with small amounts of rainfall and few rainstorms. Average 2 m temperature was 1°C higher in 2012 than in 2013 (19.0 vs. 20.1°C). Correspondingly, the surface temperature of the gravel was also 1°C warmer in 2012. Soil moisture showed higher variability during the dry year (values between 0 and 0.28 $m^3 m^{-3}$) than during the well prospering year (values between 0 and 0.18 $m^3 m^{-3}$).

Although both selected seasons had similar weather patterns, a day-to-day variability was still visible. We dealt with this variability in weather conditions in three ways: (1) we chose the same 15 days of the two years to minimize the influence of different sunrise and sunset times. (2) we only looked at the differences between the green roof and the white gravel roof temperature. No analysis was done with absolute values of the temperature measurements. The assumption was that even though the instantaneous temperature varied in time, the difference in the instantaneous temperature measured above two spots, within proximity as not to experience different weather conditions, was dependent on the differences in the local conditions, such as albedo, exposure to radiation, proximity to source of evaporation, etc. Lastly (3), we averaged the differences for each hour of the day over the whole 15 day period for both 2012 and 2013. This way, we were able to analyze the diurnal pattern with smaller influences of a day-to-day or minute-to-minute variability.

The performance of a dry and a well prospering green roofs compared to a conven-

Figure 6.3: Well prospering (top) and dry (bottom) green roof.

tional white gravel roof was analyzed using data from the same two green roofs (GR4 and GR7) used to analyze influence of soil moisture (sections 2.1 and 3.1).

6.3 RESULTS

6.3.1 INFLUENCE OF SOIL MOISTURE

In general, some similarities were found in the behavior of the soil and the air temperature in and above the green roofs and the white gravel roof independently on the initial soil moisture. Clearly, all the day time temperatures were higher than the night time temperatures. Further, all roofs indicated a vertical pattern of Ts_{max}>$T15_{max}$>$T30_{max}$ in terms of daily maximum temperature despite the difference in a soil moisture content. Soil temperature of the white gravel roof was always the lowest measured temperature at night and the highest during the day. Measured for Ts and $T15$ for white gravel and GR4 are shown in Figure 6.4.

Despite the similarities, the studied green roofs showed differences in their thermal performance depending on the soil moisture and the incoming solar radiation. Differ-

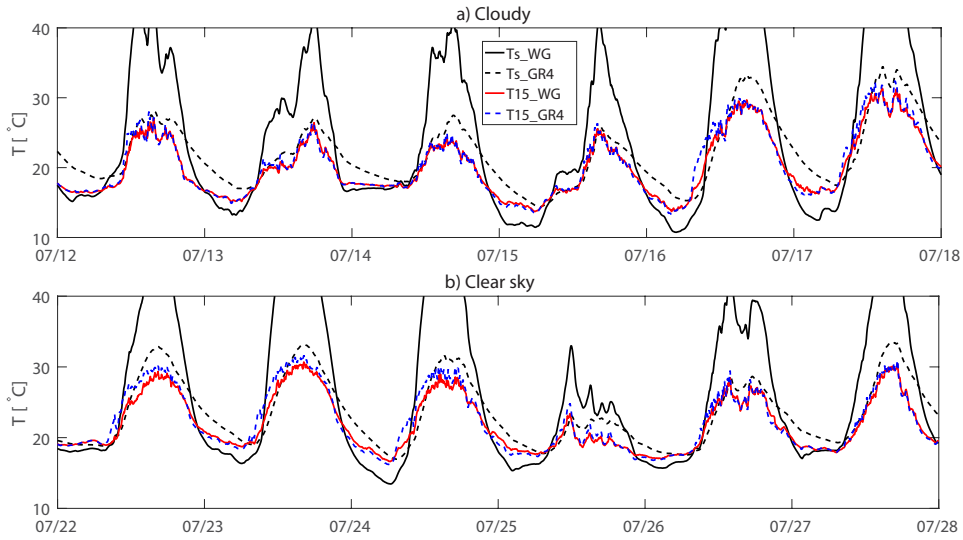

Figure 6.4: Measured values of soil temperature (Ts) and temperature 15 cm above the roof (T15) for green roof (GR4) and white gravel roof (WG) for the two examined periods. Maximum values of Ts_WG reached 56°C (17 July) and are not shown in the figure.

ences between green roofs and the white gravel roof (T_{dif} = T_{GR} - T_{WG}) were calculated for all the time steps between 00:00 and 06:00 for the night, and 7:30 and 21:30 for the day. These differences were then summed up to one number that represents the cooling power of the green roof during the whole day/night (Figure 6.5). If divided by the number of measurements (72 for night and 168 for day for the 5 min time-step) we would get the mean cooling effect. Graphs showing mean values and standard deviations of the differences can be found in the appendix (Figure IV).

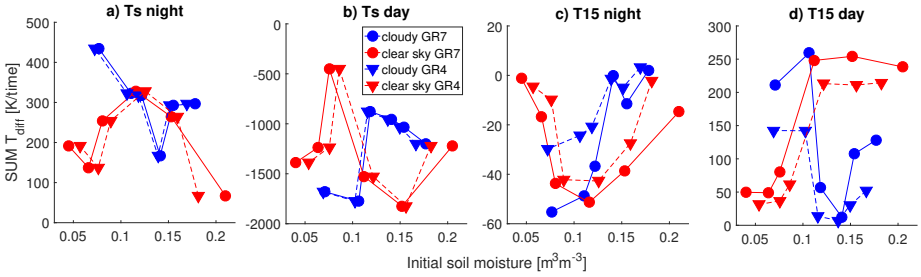

Figure 6.5: Influence of the initial soil moisture on the temperature change. Each point represents the sum of the temperature differences (T_{dif} = T_{GR} - T_{WG}) for the whole night/day with respect to initial soil moisture. Please note, the vertical scale is different for each figure.).

Sum of the differences between soil temperature of the green roofs and the white gravel roof is shown in Figure 6.5a) and b). To analyze the thermal behavior of the green roof, the data points can be separated into periods with relatively high soil moisture

(HSM), and with relatively low soil moisture (LSM), with a tipping point around 0.12 $m^3 m^{-3}$.

Differences in soil temperatures (Ts_{dif}) showed opposite behavior for the clear sky and the cloudy scenarios. At night, low soil moisture showed to be beneficial under clear sky conditions, while under cloudy conditions green roofs exhibited relatively high differences between green roofs and the white gravel. Interestingly, the same situation was found for high soil moisture. Average soil moisture, with values around 0.12 $m^3 m^{-3}$, resulted in relatively low values of Ts_{dif} under cloudy conditions and vice versa.

Differences in air temperatures 15 cm above the roof ($T15_{dif}$, Figure 6.5c) and d)) were generally negative at night and positive during the day, unlike Ts_{dif}. During clear sky nights, $T15_{dif}$ mirrored the concave behavior of Ts_{dif} for the same period. At 15 cm above the ground, the green roofs showed strongest cooling for the medium levels of the soil moisture. Both HSM and LSM, on the other hand, resulted in near zero cooling. High soil moisture levels were similarly non-beneficial during cloudy nights. $T15_{dif}$ showed average cooling lower than 0.2°C for all three HSM days. For cloudy conditions, the cooling effect for 15 cm measurements got stronger with dropping soil moisture. The lowest soil moisture level analyzed during a cloudy night reached only 0.07 $m^3 m^{-3}$. Due to the lack of lower soil moisture measurements we can not be sure that the overall dynamics were not the same as for the clear sky, but then just shifted.

During a daytime, $T15_{dif}$ showed opposite behavior under cloudy and clear sky conditions. During sunny days, HSM resulted in larger positive differences between green roof and white gravel than LSM. For cloudy days the differences reached only up to 0.7 °C on average. For LSM, the air above the green roofs was during cloudy days warmer than above white gravel. On the other hand, $T15_{dif}$ showed values close to zero on sunny days. Interestingly, the thermal behavior changed abruptly around the values of 0.12 $m^3 m^{-3}$ for both cloudy and clear sky conditions, as if a wilting point was reached.

$T30_{dif}$ showed a similar pattern as $T30_{dif}$, however, the sums reached ca. three times lower values (results not shown). During a day, the sum of the differences stayed positive for all examined days. At night, $T30_{dif}$ showed average values between -0.2 and 0.2°C with highest positive values during cloudy nights with LSM and strongest cooling for average moisture and clear sky.

Net effect can be calculated by summing up the day time and night time temperature differences. For $T15_{dif}$ the total sum reached values between 0 and 120 °C/24hrs. This shows that the net effect of this sedum covered green roof was warming the outdoor environment. Net temperature of the soil was colder than of the white gravel, despite higher temperatures at night.

6.3.2 PROSPERING VS. DRY GREEN ROOF

Results from 2012 showed effects of the unmaintained green roof that, due to unfavorable weather conditions, wilted and died. We compared observed temperature differences (T_{dif} = T_{GR} - T_{WG}) from August 2012 to August 2013. Figure 6.6 shows averages of temperature difference between green roof and white gravel roof for each hour of the day, starting with midnight, for the three measured levels. Extra figures containing median values and percentiles (Figure I and II), average absolute values (Figure III), and a table with P-values of Kolmogorov–Smirnov test (Table I) can be found in the appendix.

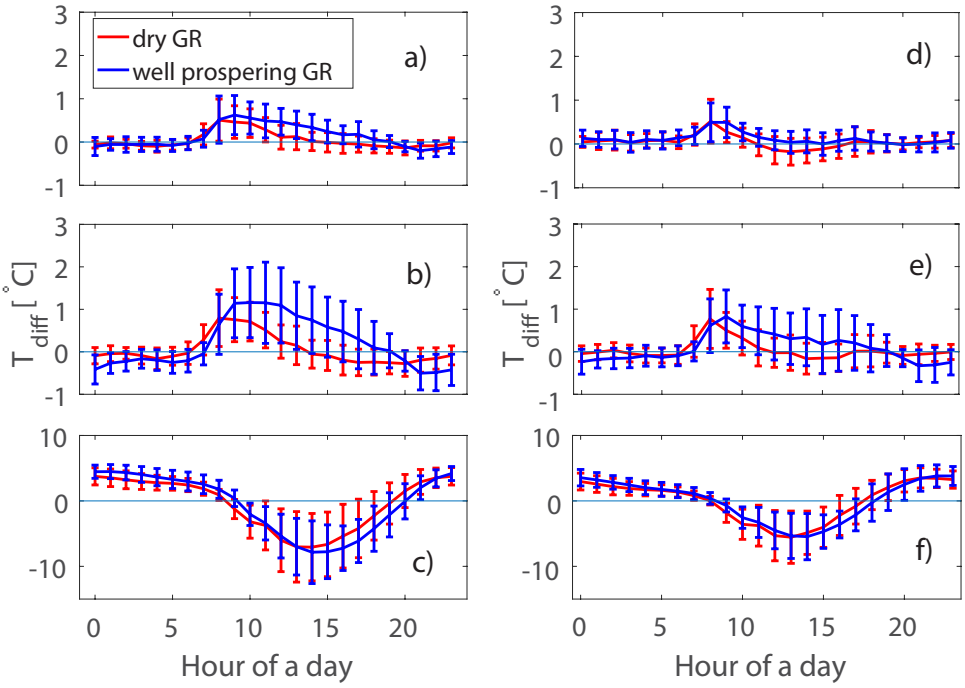

Figure 6.6: Averages and standard deviations for each hour of the day for temperature difference (T_GR - T_WG) 30 cm above the roof surface (a) and (d), 15 cm above the roof surface (b) and (e), and in the soil (c) and (f) for well prospering green roof (blue, Aug 2013) and dried out green roof (red, Aug 2012). Left column (a,b,and c) represents measurements for GR4 and right column (d,e,and f) for GR7.

Figures 6.6a) and d) show the diurnal pattern 30 cm above dry (red) and well prospering (blue) green roofs. At this level above the roofs, there was hardly any temperature difference between green roof and white gravel (T_{dif}), especially for the dry green roofs. At this level, well prospering GR4 still showed a slight warming effect during the day with highest average value reaching 0.5 °C in the morning. This morning peak was also slightly visible in the data from the dry year. For the rest of the day and night, average hourly value of T_{dif} at $T30$ stayed under ±0.2°C.

The diurnal pattern of T_{dif} 15 cm above roof surface (Figure 6.6b) and e) differed between both years. While dry green roofs showed very small differences with white gravel at night, well prospering green roofs showed temperatures lower than white gravel. This cooling was mostly between 0°C and 0.5°C. During the day (8:00-19:00), T_{dif} of the well prospering green roofs reached positive values, meaning the green roof was warmer than the white gravel. Around 19:00, average T_{dif} dropped to 0°C and the cooling effect of well prospering green roofs was again visible after sunset. A positive peak in T_{dif} during morning hours above dry green roof had an earlier onset, but also diminished faster. Around noon, dry green roofs seemed to already have a similar temperature as the white gravel and during the afternoon (14:00-17:00) dry green roofs were even slightly colder than white gravel.

Diurnal pattern of T_{dif} of the soil temperature (Figure 6.6c) and f) was almost identical for the well prospering and the dry green roofs. Small differences were visible in magnitude of the cooling and warming effect of the two scenarios and between the two green roofs. During morning and early afternoon we observed an upward shift in values of the well prospering green roof compared to the dry green roof. This shift was equalized around noon (12:00-14:00). During the afternoon and early evening (14:00-21:00), the well prospering green roof was colder than the dry green roof (differences up to 1°C). Although the nocturnal cooling effect of the green roof was reduced when the vegetation wilted, the dry layer of substrate with dead vegetation on top had a lower surface temperature than the white gravel roof.

6.4 DISCUSSION

The largest differences in temperature were measured in the soil between extensive sedum-covered green roofs and white gravel. This corresponds with previous research indicating that green roofs have a lower temperature than traditional white gravel roofs [Sonne (2006); Wong et al. (2003); Alexandri and Jones (2007)]. However, surfaces of the green roofs were not colder during the entire 24 hour period. At night they were generally slightly warmer than the conventional roof. This also corresponds with previous research [Heusinger and Weber (2015); Coutts et al. (2013); Jelínková et al. (2015)]

Data from air temperature measurements suggest that sedum covered green roofs may not always have the cooling effect on the urban environment during daytime, as some modeling studies have predicted [Li et al. (2014)]. On the contrary, we measured a warming effect of the green roof predominantly during the daytime in comparison to the white gravel roof. The green roofs were especially warm during morning hours when the soil was still warmer or had a similar temperature as the white gravel. With the sun shining on the roof, a lower albedo of the green roofs, together with the special metabolism of sedum, is likely to have caused the air above the green roofs to warm up more than above the white gravel.

Sedum is a CAM (Crassulacean acid metabolism) genus and its species are often used on green roofs in temperate climates, because of their high resistant to drought [Nagase and Dunnett (2010); Kircher (2002); Monterusso et al. (2005)]. CAM plants transpire at night, while during daytime are stomata of CAM plants closed to prevent water loss [Ranson and Thomas (1960)]. Thanks to this mechanism, CAM plants are relatively drought resistant, but they do not transpire and consequently decrease the air temperature during daytime, but at night.

The cooling effect of green roofs on the surrounding environment is mostly evident at night. Although the cooling reaches relatively low values (average 0.5°C), it has been repeatedly measured for situations with optimal soil moisture conditions. The nocturnal cooling effect is lost when the green roofs are dry (yr. 2012), because the plants can no longer transpire. Under the conditions of our testing site, conditions limiting the cooling effect are high soil moisture levels (above 0.12 $m^3 m^{-3}$) combined with cloudy sky. Presence of clouds at night generally increases the incoming long-wave radiation, which decreases the radiative cooling.

The effect of a different initial soil moisture content is visible in both the air and the soil temperature. The tipping point observed around 0.12 $m^3 m^{-3}$ can be the result of

the low moisture pressure in the substrate (pF < 4.2) or the result of plant physiological properties of sedum. As the pF curve of the substrate is unknown, it was not possible to establish why this tipping point occurs.

Higher air temperatures 15 cm above green roofs, compared to 15 cm above white gravel, during the day time are probably caused by lower albedo values and different roughness lengths. The sedum mixture growing on these roofs had mostly a reddish color with bright yellow flowers (albedo 7%). Overall, the green roofs are significantly darker than the predominantly white and gray stones of the gravel. The height of the sedum plants is not uniform, with some of them reaching up to 8 cm during bloom. This height could increase the roughness length of the green roof and hinder the ventilation of the air layer closest to the surface.

Measurements 15 cm above the dry green roofs show some interesting results, i.a. in the afternoon. We can only speculate, why is the air above the dry green roofs colder than above the white gravel in the afternoon. This may have been caused partly by evaporation from the soil. After rainfall, part of the moisture is trapped in the substrate and the drainage layer of the green roof, and evaporates later. For the rest of the day and night, the air temperature above the dry green roof is very close to the temperature above the white gravel. This means that the green roof not only looses its nocturnal cooling effect when the vegetation is dry, but also has a slight heating effect during daytime. Decrease in the nighttime cooling caused by the damaged vegetation was also described by Speak et al. (2013) in Manchester, UK.

Measurements 30 cm above the roof surface show a similar pattern for all years and roof types. It is postulated that at this height, the air layer is already relatively well mixed and the measurements are influenced more by the air advected from the surroundings than by the roof cover type. Although measurements at this height do not provide many interesting insights into the variability of green roof behavior with respect to soil moisture, influence of the roof cover at this level is still evident as, for example, in the morning peak in T_{dif} at $T30$ described in section 3.2.

Similarities in T_{dif} 30 cm above roof top during both measured years, for the well prospering and the dry green roof analysis, support our methodology regarding the variability in weather conditions. Assuming measurements 30 cm above the roof top are mostly influenced by surrounding areas and general weather patterns, minimal differences between T_{dif} in 2012 and 2013 suggest that the influence of diurnal temperature variability is small.

Several possible challenges need to be taken into account. Our analysis is based on comparing different days and years. When we compare several days with different initial soil moisture level, instantaneous weather conditions may still influence the result. Although the data are separated over two scenarios according to incoming radiation and normalized for air temperature differences, wind speed and relative humidity might also play a role in the thermal behavior of green roofs. Similarly, the results for dry vs. well prospering green roofs can still be influenced by a different number of sun hours (116.6 for given period in 2012 and 107.3 in 2013 [KNMI (2016)]), different amount and distribution of precipitation, and slightly different sedum development and composition.

As mentioned in the Methods section, there are inter-field variations in vegetation coverage. These differences in plant composition may affect soil temperature, surface

temperature, and, consequently, air temperature above the green roof. Since there is only one measurement location per green roof, the variations are not measured. However, the variability is partly represented in the differences between GR4 and GR7. It is visible from Figures 6.5 and 6.6 that both roofs exhibit slightly different magnitudes in terms of the cooling/warming effect. Nonetheless, the general pattern of the temperature differences, or their sums, stay the same for both examined green roofs. Similarly, although data for GR2, GR3, GR5, GR6, and GR8 are not shown in this article, the general pattern of diurnal behavior and temperature differences with white gravel were consistent for all the monitored roofs.

Further research is needed in order to fully understand the influence of spatial variability of vegetation. Several measurement points equally distributed over each green roof can contribute to the understanding of the complex system of unmaintained sedum-covered green roofs. Additionally, the effect of surrounding areas on the measurements should be studied more in depth. Although the measurement points were positioned in the middle of the field in order to minimize the effect of surrounding areas, the results suggest that measurements 30 cm above the ground experience strong influence of surrounding areas.

6.5 CONCLUSION

We examined the influence of sedum-covered green roofs on the air temperature 15 and 30 cm above the green roofs. Two green roofs were compared with a conventional white gravel roof under different soil moisture scenarios, and under extreme water stress. Our results support other studies showing that, under normal conditions, the sedum-covered green roof exhibits a slight warming effect on its surrounding during the day, and cools down the immediate environment at night. The nighttime cooling effect was, however, weaker than daytime warming, which resulted in a net warming effect of the green roof on the surrounding environment over the whole 24 hour period.

Under the conditions of our site, the cooling effect of extensive green roofs on the outdoor environment, as often claimed in landscaping literature, was not confirmed for day time as compared to a white gravel roof, and was shown to be limited at night time. This was most likely because of the predominantly CAM type plants growing on the monitored green roofs. Consequently, CAM plants, more specifically sedum, might not be the best choice for a green roof, when aiming to mitigate higher daytime air temperatures during a summer. Further research is needed in order to better understand the influence of spatial variability of green roofs on air temperature.

Our research further suggests that availability of water in the substrate plays an important role in the cooling behavior of the vegetation. The effect of soil moisture showed different patterns for cloudy and sunny days. These patterns need to be further verified over longer periods and including more detailed analysis of meteorological variables.

7

Conclusion and Recommendations

A je to!

Ancient Czech proverb

This thesis provides new insights into the role of water in the cooling effect of several blue-green climate adaptation facilities in urban area. An extensive literature review revealed the need for deeper understanding of how several blue-green climate adaptations measures perform when it comes to cooling. We have tested the cooling performance of a sedum covered extensive green roof, an urban pond, and intercepted water on paved surfaces. Additionally, we presented several ways of using Distributed Temperature Sensing for detailed temperature measurements in an urban environment, both in water and in air.

7.1 URBAN POND

Urban water is considered to be a heating element at night. We have investigated the nighttime behaviour of an urban pond in Delft. Those measurements provided insight into the ways an urban pond releases its stored energy at night. The daytime behaviour of air-water interface showed an unexpected temperature anomaly, which was present during almost all daytime measurement points.

A detailed DTS setup allowed for a 2 mm vertical resolution measurements of air and water temperature in an urban pond in Delft. As expected, the water temperature was gradually increasing during daytime, and part of the stored heat was then released during the following night. Our measurements show that the majority of the released heat escapes in the form of longwave radiation and latent heat flux, hence does not influence the air temperature. On average, only about 11 % of the energy escaped in the form of sensible heat. This is contrary to the generally accepted view that open water has a strong heating effect on nighttime air temperatures in urban environment.

Weather conditions on the preceding day have a strong effect on cooling of different water depths the night after. While cold cloudy days are followed by homogeneous cooling through the whole depth of the pond, after warm sunny days the heat is still being transferred from top layers to the deeper layers of water, resulting in net increase in temperature close to the bottom of the pond. These results showed a need for further research on the effect of turbidity on the energy balance of an urban pond over its depth. It is likely, that for less turbid ponds this distinction between cloudy-days and sunny-days behaviour would be less apparent.

The muddy bed-layer of the pond exhibits slightly different behaviour. During the monitoring period, the lowest 10 cm of mud always experienced a temperature gradient from the warmer water above to the colder bottom. This ground flux of thermal energy from water to the mud was estimated to range between 0.1 MJm^{-2} and 0.3 MJm^{-2} per night but uncertainty in the thermal conductivity of the bed sediment is large.

Daytime measurements of air-water interface revealed an existence of a temperature drop in the water close to the water surface. This temperature anomaly is present during most of the daytime and disappears at night. Similar behaviour was also measured in lake Kinneret (Israel) and lake Binaba (Ghana). Analysis of data collected from all three locations confirmed that the measured temperature drop could be attributed to a so-called skin effect. Our data suggest that the skin effect of fresh water bodies is predominantly a daytime phenomenon and only occurs during low to zero wind speeds. Our measurements show skin thicknesses up to 3 cm, which is considerably higher than acclaimed maximum thickens of 1 mm previously found in literature.

Existence of a colder layer of water on top of warm water creates instability. Our measurements, as well as calculation of energy balance of the cold layer, showed that the layer will empty periodically every hour. Further research is needed in order to understand this temperature anomaly. As evaporation rate and other heat and radiative fluxes are strongly dependent on surface temperature, understanding the processes that happen around the air-water interface is crucial for proper estimation of these fluxes.

As the daytime air temperature measurements inevitably experienced effect of solar radiation, we used part of the data to quantify the effect solar radiation has on the resulting measurements. Since the optical fibre was wrapped around a PVC tube, the measurements were influenced not only by the radiation heating up the cable itself, but also by the temperature of the construction. The effect of radiation on the cable itself was previously found to be around 0.2 °C [De Jong et al. (2015)]. Our results show that using PVC auxiliary constructions can cause temperature measurement deviations up to 0.5 °C. This can be even higher for other set-ups and/or conditions. Interestingly, we recorded a clear hysteresis pattern in the radiation effect on temperature measurements. This is probably caused by slow warming-up of the PVC in the morning, which cools the cable, and a heat-retention by the PVC in the afternoon, which slightly warms up the cable during early evening hours.

7.2 INTERCEPTED WATER

Second area of investigation was the cooling effect of intercepted water that is on paved surface on air temperature. Wetting the streets and roofs is becoming a more and more popular way of decreasing both indoor - in case of application on roof - and outdoor - in case of application on streets - temperature. In Japan, the tradition of spreading water around houses and temples in order to settle dust and decrease ambiant air temperature is called uchimizu (= "throwing water").

The cooling effect of uchimizu was measured under the climatic conditions of Delft, The Netherlands, during a hot summer day. A complex DTS setup was used also for our uchimizu research. We employed a 1 m^3 (1 x 1 x 1 m) 3D monitoring set up of more than 34,000 temperature sampling points. The measurements show an immediate effect on air temperature with cooling up to 1.6 °C at 2 m height, and up to 8 °C for near-ground temperature. We showed that initial ground temperature in combination with wet bulb temperature has an effect on the final cooling of air. The strongest cooling was measured for the experiment with lowest initial surface temperature and a relatively high wet bulb temperature. This measurement was performed in the shade of a tree. Increase in air humidity might hinder the decrease of perceived temperature, however, for our case, the peak increase in humidity was only around 2.5 %. Unfortunately, research and weather conditions allowed for only one day of experimenting. More measurements are necessary to fully understand the relationship between cooling effect of intercepted water and shade.

The uchimizu method offers a possibility of citizen participation in mitigation of extreme temperatures. This has two important advantages compared to more complex UHI mitigation methods such as urban ponds, or parks: (1) It is relatively easy for everyone to practice this method and apply the cooling wherever and whenever needed. And (2) the energy to evaporate the applied water is taken from both the ground and the air,

resulting in decrease of both air and surface temperature. Lower surface temperature leads to lower radiative temperature, hence leads to higher thermal comfort. Nonetheless, the area of effect of uchimizu and similar techniques on human comfort still needs to be investigated in more depth.

Use of the 1 m^3 DTS setup allowed for observation of creation and rise of small turbulent eddies in the lowest 1 m of atmospheric boundary layer right above the paved surface. Such measurements, although beyond the scope of this thesis, open up possibilities for observation of the dynamics of small scale atmospheric processes.

7.3 GREEN ROOF

Green roofs are generally promoted as a way to manage rain water, but also for their positive effect on urban climate. Most popular and widely applied are sedum-covered extensive green roofs. We have investigated several extensive sedum-covered green roofs in Utrecht, The Netherlands, and their thermal performance under different soil moisture scenarios and under extreme water stress. Air temperature measurements were taken 15 and 30 cm above the roof, and also soil temperature was measured in the layer of growing medium.

Contrary to the general believe, the net effect of a well-watered green roof, as compared to a traditional white gravel roof, was a slight *increase* in air temperature during summer. When examining the diurnal cycle in the behaviour of the studied green roofs, a distinct pattern was discovered. During daytime, green roofs exhibit a slight warming effect on their surrounding while at night the effect is opposite, and sedum-covered green roofs provide some cooling. The recorded nighttime cooling effect is, however, weaker than the daytime warming.

As expected, availability of water in the substrate plays an important role in the cooling behavior of the vegetation. The effect of a different initial soil moisture content is visible in both the air and the soil temperature. This effect is different for sunny and cloudy days, and might even be opposite depending on the weather. Under extreme conditions, when the green roof is almost entirely wilted, the nighttime cooling stops entirely and the green roof influences the air temperature in almost the same way as a white gravel roof. Our results also suggest that there is a threshold value of soil moisture, around which the effect of green roof on air temperature undergoes a step change from high to low cooling or other way round, depending on the weather conditions. For the tested green roofs, this value was $\sim 0.12\ m^3 m^{-3}$. The existence of a threshold might help with optimizing the soil moisture on green roofs to a value for which the nighttime cooling effect is relatively strong and the daytime heating relatively low. Interestingly, the ability of green roof to buffer soil temperature stays intact, even when the plants are dead.

Results from our green roofs investigation suggest that temperature measured 0.3 m above the green roof surface is already strongly influenced by the surroundings, hence that the influence of the green roof on ambient air temperature in the surrounding is very limited. The vertical profile of thermal effect of a green roof should be studied more extensively with relation to wind speed and soil type and moisture content, actual evaporation, and vegetation type to quantify the cooling effect of other types of green roof.

7.4 FUTURE RESEARCH

As is common in science, every answered question raises us several other issues. This thesis addressed a few questions about how water is involved in urban cooling and only addressed a few aspects influencing the cooling effect. Performance of many other blue-green solutions still needs to be investigated. The cooling effect of urban vegetation on street level needs to be investigated in a way that allows for extrapolation of results to other locations. Performance of urban trees, green walls, and other types of vegetation needs to be linked to measurable variables such as air temperature and humidity, exposure to solar radiation, wind speed, proximity to buildings, etc. When it comes to urban pond, its daytime behaviour should be studied in more detail as well. The daytime cooling effect provided by urban pond is causes by two effects: evaporation and heat storage. The ratio of those two effects is not well understood. For example, how is the heat absorption by (urban) surface water influenced by the turbidity and what is the effect on daytime evaporation?

7.5 GENERAL CONCLUSION

Results of this thesis show how important it is to properly understand the leading mechanisms behind cooling efficiency of water in climate adaptation solutions. Almost every chapter (except Chapter 2) of this thesis demonstrates in some way that the general opinion about some blue-green solution is different from reality. An extensive green roof did not significantly contribute to cooling of ambient temperature, and even had a slight warming effect during daytime. Urban pond at night, indeed, radiated an extensive amount of heat energy, but majority of this heat was released in the form of longwave radiation and latent heat flux and did not influence air temperature. Water poured on a hot pavement does not always decrease the air temperature, since the ground might be so hot that all the necessary energy to evaporate the water is simply supplied by the pavement.

It is an opinion of the author that understanding the processes driving the cooling effect of water in different adaptation solutions on urban environment is the way forward in the field of urban climate. Nowadays, the scientific field of urban climate suffers from everything-is-a-case-study bias. If measurements are done in Delft, The Netherlands, it is extremely difficult to extrapolate the results to other places with other climates, but even for different neighbourhoods of the same city. Urban climate is so vastly complex that air temperature can change by several degrees within the same street. Understanding of what influences this temperature change (or any other variable), how the different influencing factors are connected, and what can be neglected and what not, is the only way to up-scale the knowledge from a case study to potential world-wide contribution.

REFERENCES

Albers, R., Bosch, P., Blocken, B., van den Dobbelsteen, A., van Hove, L., Spit, T., van de Ven, F., van Hooff, T., and Rovers, V.: Overview of challenges and achievements in the climate adaptation of cities and in the Climate Proof Cities program, Building and Environment, 83, 1 – 10, special Issue: Climate adaptation in cities, 2015.

Alexandri, E. and Jones, P.: Developing a one-dimensional heat and mass transfer algorithm for describing the effect of green roofs on the built environment: Comparison with experimental results, Building and Environment, 42, 2835 – 2849, 2007.

Alexandri, E. and Jones, P.: Temperature decreases in an urban canyon due to green walls and green roofs in diverse climates, Building and Environment, 43, 480 – 493, 2008.

Ali, A. H. H.: Passive cooling of water at night in uninsulated open tank in hot arid areas, Energy Conversion and Management, 48, 93 – 100, 2007.

Allen, D., Olive, V., Arthur, S., and Haynes, H.: Urban sediment transport through an established vegetated swale: Long term treatment efficiencies and deposition, Water (Switzerland), 7, 1046–1067, 2015.

Aparicio Medrano, E.: Urban Surface water as energy source and collector, master thesis, Delft University of Technology, 2008.

Armson, D., Stringer, P., and Ennos, A. R.: The effect of tree shade and grass on surface and globe temperatures in an urban area, Urban Forestry and Urban Greening, 11, 245–255, 2012.

Baccini, M., Biggeri, A., Accetta, G., Kosatsky, T., Katsouyanni, K., Analitis, A., Anderson, H. R., Bisanti, L., D'ippoliti, D., Danova, J., et al.: Heat effects on mortality in 15 European cities, Epidemiology, 19, 711–719, 2008.

Baird, G. and Field, C.: Thermal comfort conditions in sustainable buildings–Results of a worldwide survey of users' perceptions, Renewable Energy, 49, 44–47, 2013.

Barlow, J. F.: Progress in observing and modelling the urban boundary layer, Urban Climate, 10, 216–240, 2014.

Barr, A. G., King, K., Gillespie, T., Den Hartog, G., and Neumann, H.: A comparison of Bowen ratio and eddy correlation sensible and latent heat flux measurements above deciduous forest, Boundary-Layer Meteorology, 71, 21–41, 1994.

Bass, B. and Baskaran, B.: Evaluating Rooftop and Vertical Gardens as an Adaptation Strategy for Urban Areas. National Research Council, Institute for Research in Construction, Montreal, Ontario, 2003.

Bense, V., Read, T., and Verhoef, A.: Using distributed temperature sensing to monitor field scale dynamics of ground surface temperature and related substrate heat flux, Agricultural and Forest Meteorology, 220, 207–215, 2016a.

Bense, V., Read, T., and Verhoef, A.: Using distributed temperature sensing to monitor field scale dynamics of ground surface temperature and related substrate heat flux, Agricultural and Forest Meteorology, 220, 207–215, 2016b.

Berardi, U., GhaffarianHoseini, A., and GhaffarianHoseini, A.: State-of-the-art analysis of the environmental benefits of green roofs, Applied Energy, 115, 411 – 428, 2014.

Bidleman, T. and Olney, C.: Chlorinated hydrocarbons in the Sargasso Sea atmosphere and surface water, Science, 183, 516–518, URL https://www.scopus.com/inward/record.uri?eid=2-s2.0-0016387173&partnerID=40&md5=a409781bf8246d1e516ac94bb4a16474, 1974.

Bouvier, M., Brunner, A., and Aimé, F.: Nighttime watering streets and induced effects on the surrounding refreshment in case of hot weather. The city of Paris experimentations, Tech. Sci. Méthodes, 12, 43–55, 2013.

Bowen, I. S.: The ratio of heat losses by conduction and by evaporation from any water surface, Physical review, 27, 779, 1926.

Bowler, D. E., Buyung-Ali, L., Knight, T. M., and Pullin, A. S.: Urban greening to cool towns and cities: A systematic review of the empirical evidence, Landscape and Urban Planning, 97, 147–155, 2010.

Bush, S. E., Pataki, D. E., Hultine, K. R., West, A. G., Sperry, J. S., and Ehleringer, J. R.: Wood anatomy constrains stomatal responses to atmospheric vapor pressure deficit in irrigated, urban trees, Oecologia, 156, 13–20, doi:10.1007/s00442-008-0966-5, 2008.

Cao, X., Onishi, A., Chen, J., and Imura, H.: Quantifying the cool island intensity of urban parks using ASTER and IKONOS data, Landscape and Urban Planning, 96, 224–231, 2010.

Castleton, H., Stovin, V., Beck, S., and Davison, J.: Green roofs; building energy savings and the potential for retrofit, Energy and Buildings, 42, 1582 – 1591, 2010.

Changnon, S. A., Kunkel, K. E., and Reinke, B. C.: Impacts and responses to the 1995 heat wave: a call to action, Bulletin of the American Meteorological society, 77, 1497–1506, 1996.

Chen, Y. and Wong, N. H.: Thermal benefits of city parks, Energy and Buildings, 38, 105–120, 2006.

Ciocca, F., Lunati, I., Van de Giesen, N., and Parlange, M. B.: Heated optical fiber for distributed soil-moisture measurements: A lysimeter experiment, Vadose Zone Journal, 11, 2012.

Côté, J. and Konrad, J.-M.: A generalized thermal conductivity model for soils and construction materials, Canadian Geotechnical Journal, 42, 443–458, 2005.

Coutts, A. M., Tapper, N. J., Beringer, J., Loughnan, M., and Demuzere, M.: Watering our cities: The capacity for Water Sensitive Urban Design to support urban cooling and improve human thermal comfort in the Australian context, Progress in Physical Geography, 37, 2–28, 2012.

Coutts, A. M., Daly, E., Beringer, J., and Tapper, N. J.: Assessing practical measures to reduce urban heat: Green and cool roofs, Building and Environment, 70, 266–276, 2013.

CPC-Consortium: Eindreport Climate Proof Cities 2010-2014, 2014.

de Graaf, R., van de Ven, F., Miltenburg, I., van Bert, E., van de Winckel, L., and van Wijk, G.: Exploring the technical and economic feasibility of using the urban water system as a sustainable energy source, Thermal Science, 12, 35–50, 2008.

De Jong, S., Slingerland, J., and Van de Giesen, N.: Fiber optic distributed temperature sensing for the determination of air temperature, Atmospheric Measurement Techniques, 8, 335–339, 2015.

Djongyang, N., Tchinda, R., and Njomo, D.: Thermal comfort: A review paper, Renewable and Sustainable Energy Reviews, 14, 2626–2640, 2010.

Duan, F., Thompson, I., and Ward, C.: Statistical rate theory determination of water properties below the triple point, The Journal of Physical Chemistry B, 112, 8605–8613, 2008.

Edinger, J. E., Brady, D. K., and Geyer, J. C.: Heat exchange and transport in the environment. Report No. 14, Tech. rep., Johns Hopkins Univ., Baltimore, MD (USA). Dept. of Geography and Environmental Engineering, 1974.

Elbers, J., Moors, E. J., and Jacobs, C.: Gemeten actuele verdamping voor twaalf locaties in Nederland, 2010-36, Stowa, 2010.

Euser, T., Luxemburg, W., Everson, C., Mengistu, M., Clulow, A., and Bastiaanssen, W.: A new method to measure Bowen ratios using high-resolution vertical dry and wet bulb temperature profiles, Hydrology and Earth System Sciences, 18, 2014, 2014.

Fairall, C., Bradley, E. F., Godfrey, J., Wick, G., Edson, J. B., and Young, G.: Cool-skin and warm-layer effects on sea surface temperature, J. Geophys. Res, 101, 1295–1308, 1996.

Farouki, O. T.: Thermal properties of soils, Tech. rep., DTIC Document, 1981.

Frontczak, M. and Wargocki, P.: Literature survey on how different factors influence human comfort in indoor environments, Building and Environment, 46, 922–937, 2011.

Furumai, H.: Rainwater and reclaimed wastewater for sustainable urban water use, Physics and Chemistry of the Earth, Parts A/B/C, 33, 340 – 346, integrated Water Resources Management in a Changing World, 2008.

Gabor, P. and Jombach, S.: The relation between the biological activity and the land surface temperature in Budapest, Applied Ecology and Environmental Research, 7, 241–251, 2010.

Gaffin, S., Rosenzweig, C., Parshall, L., Hillel, D., Eichenbaum-Pikser, J., Greenbaum, A., Blake, R., Beattie, D., and Berghage, R.: Quantifying evaporative cooling from green roofs and comparison to other land surfaces, in: Fourth Annual Greening Rooftops for Sustainable Communities Conference, Awards and Trade Show, pp. 11–12, 2006.

Gago, E. J., Roldan, J., Pacheco-Torres, R., and Ordonez, J.: The city and urban heat islands: A review of strategies to mitigate adverse effects, Renewable and Sustainable Energy Reviews, 25, 749–758, 2013.

Grassl, H.: The dependence of the measured cool skin of the ocean on wind stress and total heat flux, Boundary-Layer Meteorology, 10, 465–474, 1976.

Halper, E. B., Scott, C. A., and Yool, S. R.: Correlating Vegetation, Water Use, and Surface Temperature in a Semiarid City: A Multiscale Analysis of the Impacts of Irrigation by Single-Family Residences, Geographical Analysis, 44, 235–257, 2012.

Hardy, J.: The sea surface microlayer: Biology, chemistry and anthropogenic enrichment, Progress in Oceanography, 11, 307 – 328, 1982.

Harrison, B.: Non-greenification Techniques for Mitigating the Heat Island Effect in Tokyo, CJPSCS/JJPC, 22, 57–63, 2014.

Hathway, E. A. and Sharples, S.: The interaction of rivers and urban form in mitigating the Urban Heat Island effect: A UK case study, Building and Environment, 58, 14–22, 2012.

Hausner, M. B., Suárez, F., Glander, K. E., Giesen, N. v. d., Selker, J. S., and Tyler, S. W.: Calibrating single-ended fiber-optic Raman spectra distributed temperature sensing data, Sensors, 11, 10 859–10 879, 2011.

Hendel, M., Colombert, M., Diab, Y., and Royon, L.: Improving a pavement-watering method on the basis of pavement surface temperature measurements, Urban Climate, 10, Part 1, 189 – 200, 2014.

Hendel, M., Gutierrez, P., Colombert, M., Diab, Y., and Royon, L.: Measuring the effects of urban heat island mitigation techniques in the field: Application to the case of pavement-watering in Paris, Urban Climate, 16, 43 – 58, 2016.

Henderson-Sellers, B.: Calculating the surface energy balance for lake and reservoir modeling: A review, Reviews of Geophysics, 24, 625–649, 1986.

Hester, E. T. and Bauman, K. S.: Stream and Retention Pond Thermal Response to Heated Summer Runoff From Urban Impervious Surfaces, Journal of the American Water Resources Association, 49, 328–342, 2013.

Heusinger, J. and Weber, S.: Comparative microclimate and dewfall measurements at an urban green roof versus bitumen roof, Building and Environment, 92, 713–723, 2015.

Heusinkveld, B., van Hove, B., and Jacobs, C.: Ruimtelijke analyse van het stadsklimaat in Rotterdam., Report, Wageningen Universiteit en Research centre, 2011.

Hicks, B. B.: A procedure for the formulation of bulk transfer coefficients over water, Boundary-Layer Meteorology, 8, 515–524, 1975.

Hien, W. N. and Jusuf, S. K.: Air temperature distribution and the influence of sky view factor in a green singapore estate, Journal of Urban Planning and Development, 136, 261–272, 2010.

Hilgersom, K., van de Giesen, N., de Louw, P., and Zijlema, M.: Three-dimensional dense distributed temperature sensing for measuring layered thermohaline systems, Water Resources Research, 52, 6656–6670, 2016a.

Hilgersom, K., Van Emmerik, T., Solcerova, A., Berghuijs, W., Selker, J., and Van de Giesen, N.: Practical considerations for enhanced-resolution coil-wrapped Distributed Temperature Sensing, Geoscientific Instrumentation, Methods and Data Systems, 2016, 2016b.

Hilgersom, K., Zijlema, M., and van de Giesen, N.: An axisymmetric non-hydrostatic model for double-diffusive water systems, Geoscientific Model Development Discussions, 2017, 2017.

Himeno, S., Takahashi, R., Asakura, A., Koike, K., and Fujita, S.: Using Snow Melting Pipes to Verify the Water Sprinkling s Effect over a Wide Area, NOVATECH 2010, 2010.

Hisatake, K., Tanaka, S., and Aizawa, Y.: Evaporation rate of water in a vessel, Journal of Applied Physics, 73, 7395–7401, 1993.

Höppe, P.: The physiological equivalent temperature–a universal index for the biometeorological assessment of the thermal environment, International journal of Biometeorology, 43, 71–75, 1999.

Howard, L.: The Climate of London: Deduced from Meteorological Observations Made at Different Places in the Neighbourhood of the Metropolis. In Two Volumes, v. 2, W.Phillips, 1820.

Huang, G. and Cadenasso, M.: People, landscape, and urban heat island: dynamics among neighborhood social conditions, land cover and surface temperatures, Landscape ecology, 31, 2507–2515, 2016.

Ishii, T., Tsujimoto, M., Yoon, G., and Okumiya, M.: Cooling system with water mist sprayers for mitigation of heat-island, in: Proceedings of the Seventh International Conference on Urban Climate, Yokohama, Japan, vol. 29, 2009.

Jacobs, A. F. G., Jetten, T. H., Lucassen, D. C., Heusinkveld, B. G., and Nieveen, J. P.: Diurnal temperature fluctuations in a natural shallow water body, Agricultural and Forest Meteorology, 88, 269–277, 1997.

Jaffal, I., Ouldboukhitine, S.-E., and Belarbi, R.: A comprehensive study of the impact of green roofs on building energy performance, Renewable Energy, 43, 157 – 164, 2012.

Jansen, J., Stive, P., Van De Giesen, N., Tyler, S. W., Steele-Dunne, S., and Williamson, L.: Estimating soil heat flux using Distributed Temperature Sensing, IAHS Publ, 343, 20, 2011.

Japan for Sustainability: The Mission Uchimizu Campaign as Social Design, http://www.japanfs.org/en/news/archives/news_id029260.html, accessed: 11-11-2016, 2009.

Japan Water Forum: Mission Uchimizu, http://www.waterforum.jp/eng/uchimizu/, accessed: 11-11-2016, 2009.

Jelínková, V., Dohnal, M., Picek, T., et al.: A green roof segment for monitoring the hydrological and thermal behaviour of anthropogenic soil systems, Soil Water Res, 10, 262–270, 2015.

Jenerette, G. D., Harlan, S. L., Buyantuev, A., Stefanov, W. L., Declet-Barreto, J., Ruddell, B. L., Myint, S. W., Kaplan, S., and Li, X.: Micro-scale urban surface temperatures are related to land-cover features and residential heat related health impacts in Phoenix, AZ USA, Landscape ecology, 31, 745–760, 2016.

Jessup, A. and Branch, R.: Integrated ocean skin and bulk temperature measurements using the calibrated infrared in situ measurement system (CIRIMS) and through-hull ports, Journal of Atmospheric and Oceanic Technology, 25, 579–597, 2008.

Jim, C.: Assessing climate-adaptation effect of extensive tropical green roofs in cities, Landscape and Urban Planning, 138, 54–70, 2015.

Johansen, O.: Thermal conductivity of soils, Tech. rep., DTIC Document, 1977.

Kang, H.-J., Yoo, J.-M., Jeong, M.-J., and Won, Y.-I.: Uncertainties of satellite-derived surface skin temperatures in the polar oceans: MODIS, AIRS/AMSU, and AIRS only, Atmospheric Measurement Techniques, 8, 4025–4041, 2015.

Kano, M., Tebakari, T., Kinouchi, T., Shigeyuki, S., and Yamada, T.: Social Experiment of Watering and Numerical Verification, Proceedings of Hydraulic Engineering, 48, 193–198, 2004.

Kersten, M. S.: Laboratory research for the determination of the thermal properties of soils., Tech. rep., DTIC Document, 1949.

Kircher, W.: Annuals and Sedum-cuttings in seed-mixtures for extensive roof gardens, in: International Conference on Urban Horticulture 643, pp. 301–303, 2002.

Kleerekoper, L., van Esch, M., and Salcedo, T.: How to make a city climate-proof, addressing the urban heat island effect, Resources, Conservation and Recycling, 64, 30–38, 2012.

Klein, P. M. and Coffman, R.: Establishment and performance of an experimental green roof under extreme climatic conditions, Science of The Total Environment, 512–513, 82 – 93, 2015.

KNMI: ZonurenCalculator.nl, URL http://www.zonurencalculator.nl/sun_hours_calculation, this website is initiative of MinderGas.nl and uses data from KNMI. Accessed: 01-03-2016, 2016.

Kumar, R. and Kaushik, S.: Performance evaluation of green roof and shading for thermal protection of buildings, Building and Environment, 40, 1505 – 1511, 2005.

Lazzarin, R. M., Castellotti, F., and Busato, F.: Experimental measurements and numerical modelling of a green roof, Energy and Buildings, 37, 1260 – 1267, 2005.

Lee, H.-Y.: An application of NOAA AVHRR thermal data to the study of urban heat islands, Atmospheric Environment. Part B. Urban Atmosphere, 27, 1–13, 1993.

Leroy, M.-C., Portet-Koltalo, F., Legras, M., Lederf, F., Moncond'huy, V., Polaert, I., and Marcotte, S.: Performance of vegetated swales for improving road runoff quality in a moderate traffic urban area, Science of the Total Environment, 566-567, 113–121, 2016.

Li, D., Bou-Zeid, E., and Oppenheimer, M.: The effectiveness of cool and green roofs as urban heat island mitigation strategies, Environmental Research Letters, 9, 055 002, 2014.

Li, J., Li, Y., and Li, Y.: SWMM-based evaluation of the effect of rain gardens on urbanized areas, Environmental Earth Sciences, 75, 1–14, 2016.

Liao, K.-H., Deng, S., and Tan, P. Y.: Blue-Green Infrastructure: New Frontier for Sustainable Urban Stormwater Management, in: Greening Cities, pp. 203–226, Springer, 2017.

MacIvor, J. S., Margolis, L., Perotto, M., and Drake, J. A.: Air temperature cooling by extensive green roofs in Toronto Canada, Ecological Engineering, 95, 36 – 42, 2016.

Maillard, P., David, F., Dechesne, M., Bailly, J.-B., and Lesueur, E.: Characterization of the Urban Heat Island and evaluation of a road humidification mitigation solution in the district of La Part-Dieu, Lyon (France), Tech. Sci. Méthodes, 6, e35, 2014.

Manteghi, G., bin Limit, H., and Remaz, D.: Water Bodies an Urban Microclimate: A Review, Modern Applied Science, 9, 1, 2015.

Martin, E. H.: Effectiveness of an urban runoff detention pond-wetlands system, Journal of Environmental Engineering, 114, 810–827, 1988.

Matsubara, N. and Sawashima, T.: The actual conditions of practising traditional methods of environmental control and utilization of air conditioners by the residents of detached houses in kyoto during summer, Journal of Thermal Biology, 18, 577–582, 1993.

McPherson, E. G., Herrington, L. P., and Heisler, G. M.: Impacts of vegetation on residential heating and cooling, Energy and Buildings, 12, 41–51, 1988.

Meierdiercks, K. L., Smith, J. A., Baeck, M. L., and Miller, A. J.: Analyses of urban drainage network structure and its impact on hydrologic response, Journal of the American Water Resources Association, 46, 932–943, 2010.

Meng, Q. and Hu, W.: Roof cooling effect with humid porous medium, Energy and Buildings, 37, 1 – 9, 2005.

Minnett, P. J., Smith, M., and Ward, B.: Measurements of the oceanic thermal skin effect, Deep Sea Research Part II: Topical Studies in Oceanography, 58, 861–868, 2011.

Monterusso, M. A., Rowe, D. B., and Rugh, C. L.: Establishment and persistence of Sedum spp. and native taxa for green roof applications, HortScience, 40, 391–396, 2005.

Nagase, A. and Dunnett, N.: Drought tolerance in different vegetation types for extensive green roofs: effects of watering and diversity, Landscape and Urban Planning, 97, 318–327, 2010.

Nakayoshi, M., Kanda, M., Shi, R., and de Dear, R.: Outdoor thermal physiology along human pathways: a study using a wearable measurement system, International journal of biometeorology, 59, 503–515, 2015.

Nasar, J. L. and Li, M.: Landscape mirror: the attractiveness of reflecting water, Landscape and Urban Planning, 66, 233 – 238, 2004.

Naticchia, B., D'Orazio, M., Carbonari, A., and Persico, I.: Energy performance evaluation of a novel evaporative cooling technique, Energy and Buildings, 42, 1926 – 1938, 2010.

Neilson, B. T., Hatch, C. E., Ban, H., and Tyler, S. W.: Solar radiative heating of fiber-optic cables used to monitor temperatures in water, Water Resources Research, 46, 2010.

Nordbo, A., Launiainen, S., Mammarella, I., Leppäranta, M., Huotari, J., Ojala, A., and Vesala, T.: Long-term energy flux measurements and energy balance over a small boreal lake using eddy covariance technique, Journal of Geophysical Research: Atmospheres, 116, 2011.

Oberndorfer, E., Lundholm, J., Bass, B., Coffman, R., Doshi, H., Dunnett, N., Gaffin, S., Köhler, M., Liu, K., and Rowe, B.: Green roofs as urban ecosystems: Ecological structures, functions, and services, BioScience, 57, 823–833, 2007.

Oke, T. R.: The energetic basis of the urban heat island, Quarterly Journal of the Royal Meteorological Society, 108, 1–24, 1982.

Oke, T. R.: The micrometeorology of the urban forest, Philosophical Transactions - Royal Society of London, B, 324, 335–349, 1989.

Oke, T. R., Johnson, G. T., Steyn, D. G., and Watson, I. D.: Simulation of surface urban heat islands under 'ideal' conditions at night part 2: Diagnosis of causation, Boundary-Layer Meteorology, 56, 339–358, 1991.

Olah, A. B.: The possibilities of decreasing the urban heat Island, Applied Ecology and Environmental Research, 10, 173–183, 2012.

Oldroyd, H. J., Higgins, C., Huwald, H., Selker, J., and Parlange, M.: Thermal diffusivity of seasonal snow determined from temperature profiles, Advances in water resources, 55, 121–130, 2013.

Oleson, K., Bonan, G., and Feddema, J.: Effects of white roofs on urban temperature in a global climate model, Geophysical Research Letters, 37, doi:10.1029/2009GL042194, 2010.

Oswald, E. M., Rood, R. B., Zhang, K., Gronlund, C. J., O'Neill, M. S., White-Newsome, J. L., Brines, S. J., and Brown, D. G.: An investigation into the spatial variability of near-surface air temperatures in the Detroit, Michigan, Metropolitan Region, Journal of Applied Meteorology and Climatology, 51, 1290–1304, 2012.

Paravantis, J., Santamouris, M., Cartalis, C., Efthymiou, C., and Kontoulis, N.: Mortality Associated with High Ambient Temperatures, Heatwaves, and the Urban Heat Island in Athens, Greece, Sustainability, 9, 2017.

Patz, J. A., Campbell-Lendrum, D., Holloway, T., and Foley, J. A.: Impact of regional climate change on human health, Nature, 438, 310–317, 2005.

Peng, L. L. and Jim, C.: Seasonal and diurnal thermal performance of a subtropical extensive green roof: The impacts of background weather parameters, Sustainability, 7, 11 098–11 113, 2015.

Peng, R. D., Bobb, J. F., Tebaldi, C., McDaniel, L., Bell, M. L., and Dominici, F.: Toward a quantitative estimate of future heat wave mortality under global climate change, Environ Health Perspect, 119, 701–6, 2011.

Peri, G., Rizzo, G., Scaccianoce, G., and Sorrentino, G.: Role of green coverings in mitigating heat island effects: An analysis of physical models, in: green roof, inside, vol. 261-262, pp. 251–256, 2013.

Perkins, S. E., Alexander, L. V., and Nairn, J. R.: Increasing frequency, intensity and duration of observed global heatwaves and warm spells, Geophysical Research Letters, 39, l20714, 2012.

Peters, E. B., Hiller, R. V., and McFadden, J. P.: Seasonal contributions of vegetation types to suburban evapotranspiration, Journal of Geophysical Research G: Biogeosciences, 116, 2011.

Pisello, A.: State of the art on the development of cool coatings for buildings and cities, Solar Energy, 144, 660–680, 2017.

Poblete, P., Moor, D., Wada, Y., Iha, K., and Okayasu, N.: Japan Ecological Footprint Report 2012, Tech. rep., WWF, 2012.

Psiloglou, B. and Kambezidis, H.: Estimation of the ground albedo for the Athens area, Greece, Journal of Atmospheric and Solar-Terrestrial Physics, 71, 943–954, 2009.

Qiu, G. Y., Li, H. Y., Zhang, Q. T., Chen, W., Liang, X. J., and Li, X. Z.: Effects of Evapotranspiration on Mitigation of Urban Temperature by Vegetation and Urban Agriculture, Journal of Integrative Agriculture, 12, 1307–1315, 2013.

Ranson, S. L. and Thomas, M.: Crassulacean acid metabolism, Annual Review of Plant Physiology, 11, 81–110, 1960.

Ridley, I. K., Lawrence, S. P., Llewellyn-Jones, D. T., Parkes, I. M., Yokoyama, R., Tanba, S., and Oikawa, S.: Use of ATSR-measured ocean skin temperatures in ocean and atmosphere models, ESA SP, pp. 1317–1321, 1997.

Rinner, C. and Hussain, M.: Toronto's Urban Heat Island - Exploring the Relationship between Land Use and Surface Temperature, Remote Sensing, 3, 1251–1265, 2011.

Romeijn, L.: Monitoring albedo of urban surfaces under wet and dry conditions, bachelor thesis, Delft University of Technology, 2014.

Rozos, E., Makropoulos, C., and Maksimović, v.: Rethinking urban areas: An example of an integrated blue-green approach, Water Science and Technology: Water Supply, 13, 1534–1542, doi:10.2166/ws.2013.140, 2013.

Rupp, R., Vásquez, N., and Lamberts, R.: A review of human thermal comfort in the built environment, Energy and Buildings, 105, 178–205, 2015.

Rutgers: Remote Sensing of Earth Radiation Budget, http://marine.rutgers.edu/cool/education/class/yuri/albedo.gif, accessed: 2015-01-15, 1998.

Ryu, Y.-H. and Baik, J.-J.: Quantitative Analysis of Factors Contributing to Urban Heat Island Intensity, Journal of Applied Meteorology and Climatology, 51, 842–854, 2012.

Saaroni, H. and Ziv, B.: The impact of a small lake on heat stress in a Mediterranean urban park: the case of Tel Aviv, Israel, Int J Biometeorol, 47, 156–65, 2003.

Salamanca, F., Martilli, A., and Yagüe, C.: A numerical study of the Urban Heat Island over Madrid during the DESIREX (2008) campaign with WRF and an evaluation of simple mitigation strategies, International Journal of Climatology, 32, 2372–2386, 2012.

Saneinejad, S., Moonen, P., and Carmeliet, J.: Comparative assessment of various heat island mitigation measures, Building and Environment, 73, 162–170, 2014.

Santamouris, M.: Cooling the cities – A review of reflective and green roof mitigation technologies to fight heat island and improve comfort in urban environments, Solar Energy, 103, 682 – 703, 2014.

Saunders, P. M.: The temperature at the ocean-air interface, Journal of the atmospheric sciences, 24, 269–273, 1967.

Scherba, A., Sailor, D. J., Rosenstiel, T. N., and Wamser, C. C.: Modeling impacts of roof reflectivity, integrated photovoltaic panels and green roof systems on sensible heat flux into the urban environment, Building and Environment, 46, 2542 – 2551, 2011.

Schluessel, P., Emery, W. J., Grassl, H., and Mammen, T.: On the bulk-skin temperature difference and its impact on satellite remote sensing of sea surface temperature, Journal of Geophysical Research: Oceans, 95, 13 341–13 356, 1990.

Sebok, E., Duque, C., Kazmierczak, J., Engesgaard, P., Nilsson, B., Karan, S., and Frandsen, M.: High-resolution distributed temperature sensing to detect seasonal groundwater discharge into Lake Væng, Denmark, Water Resources Research, 49, 5355–5368, 2013a.

Sebok, E., Duque, C., Kazmierczak, J., Engesgaard, P., Nilsson, B., Karan, S., and Frandsen, M.: High-resolution distributed temperature sensing to detect seasonal groundwater discharge into Lake Væng, Denmark, Water Resources Research, 49, 5355–5368, 2013b.

Selker, J. S., Thevenaz, L., Huwald, H., Mallet, A., Luxemburg, W., Van De Giesen, N., Stejskal, M., Zeman, J., Westhoff, M., and Parlange, M. B.: Distributed fiber-optic temperature sensing for hydrologic systems, Water Resources Research, 42, 2006.

Shashua-Bar, L., Pearlmutter, D., and Erell, E.: The cooling efficiency of urban landscape strategies in a hot dry climate, Landscape and Urban Planning, 92, 179–186, 2009.

Shishegar, N.: The impact of green areas on mitigating urban heat island effect: A review, International Journal of Environmental Sustainability, 9, 119–130, 2014.

Sigmund, A., Pfister, L., Sayde, C., and Thomas, C. K.: Quantitative analysis of the radiation error for aerial coiled fiber-optic Distributed Temperature Sensing deployments using reinforcing fabric as support structure, Atmospheric Measurement Techniques Discussions, 2016, 1–26, 2016.

Slingerland, J.: Mitigation of the urban heat island effect by using water and vegetation., Master thesis, Delft University of Technology, 2012.

Solcerova, A., van Emmerik, T., and Hilgersom, K.: Uchimizu, doi:10.5281/zenodo.168469, URL https://doi.org/10.5281/zenodo.182395, 2016.

Solcerova, A., van de Ven, F., Wang, M., Rijsdijk, M., and van de Giesen, N.: Do green roofs cool the air?, Building and Environment, 111, 249–255, 2017.

Solcerova, A., Emmerik, T. v., Ven, F. v. d., Selker, J., and Giesen, N. v. d.: Skin Effect of Fresh Water Measured Using Distributed Temperature Sensing, Water, 10, 2018a.

Solcerova, A., van Emmerik, T., Hilgersom, K., van de Ven, F., and van de Giesen, N.: Uchimizu: A Cool(ing) Tradition to Locally Decrease Air Temperature, Water, 10, 741, 2018b.

Solcerova, A., van de Ven, F., and van de Giesen, N.: Nighttime cooling of an urban pond, Frontiers: Hydrosphere, submitted.

Sonne, J.: Evaluating green roof energy performance, ASHRAE Journal, 48, 59, 2006.

Speak, A., Rothwell, J., Lindley, S., and Smith, C.: Reduction of the urban cooling effects of an intensive green roof due to vegetation damage, Urban Climate, 3, 40 – 55, 2013.

Spruit, R., van Tol, F., Broere, W., Doornenbal, P., and Hopman, V.: Distributed Temperature Sensing applied during diaphragm wall construction, Canadian Geotechnical Journal, 2016.

Steele-Dunne, S., Rutten, M., Krzeminska, D., Hausner, M., Tyler, S., Selker, J., Bogaard, T., and Van de Giesen, N.: Feasibility of soil moisture estimation using passive distributed temperature sensing, Water Resources Research, 46, 2010.

Steeneveld, G. J., Koopmans, S., Heusinkveld, B. G., and Theeuwes, N. E.: Refreshing the role of open water surfaces on mitigating the maximum urban heat island effect, Landscape and Urban Planning, 121, 92–96, 2014.

Stomph, T., De Ridder, N., and Van de Giesen, N.: A flowmeter for low discharges of laboratory flumes, Transactions of the ASAE, 45, 345, 2002.

Stovin, V.: The potential of green roofs to manage Urban Stormwater, Water and Environment Journal, 24, 192–199, 2010.

Suárez, F., Aravena, J., Hausner, M., Childress, A., and Tyler, S.: Assessment of a vertical high-resolution distributed-temperature-sensing system in a shallow thermohaline environment, Hydrology and Earth System Sciences, 15, 1081, 2011.

Sun, R., Chen, A., Chen, L., and Lü, Y.: Cooling effects of wetlands in an urban region: The case of Beijing, Ecological Indicators, 20, 57–64, 2012.

Susca, T., Gaffin, S., and Dell'Osso, G.: Positive effects of vegetation: Urban heat island and green roofs, Environmental Pollution, 159, 2119 – 2126, 2011.

Suter, I., Čedo Maksimović, and van Reeuwijk, M.: A neighbourhood-scale estimate for the cooling potential of green roofs, Urban Climate, 20, 33 – 45, 2017.

Syafii, N. I., Ichinose, M., Wong, N. H., Kumakura, E., Jusuf, S. K., and Chigusa, K.: Experimental Study on the Influence of Urban Water Body on Thermal Environment at Outdoor Scale Model, Procedia Engineering, 169, 191 – 198, 2016.

Takahashi, R., Asakura, A., Koike, K., Himeno, S., and Fujita, S.: Using snow melting pipes to verify the water sprinkling's effect over a wide area, NOVATECH 2010, 10, 2010.

Takebayashi, H. and Moriyama, M.: Surface heat budget on green roof and high reflection roof for mitigation of urban heat island, Building and Environment, 42, 2971 – 2979, 2007.

Taleghani, M.: Outdoor thermal comfort by different heat mitigation strategies- A review, Renewable and Sustainable Energy Reviews, 2017.

Tan, J., Zheng, Y., Song, G., Kalkstein, L., Kalkstein, A., and Tang, X.: Heat wave impacts on mortality in Shanghai, 1998 and 2003, International Journal of Biometeorology, 51, 193–200, 2007.

Tang, S., Luo, W., Jia, Z., Li, S., Wu, Y., and Zhou, M.: Effect of rain gardens on storm runoff reduction, Shuikexue Jinzhan/Advances in Water Science, 26, 787–794, 2015.

Tanny, J., Cohen, S., Assouline, S., Lange, F., Grava, A., Berger, D., Teltch, B., and Parlange, M.: Evaporation from a small water reservoir: Direct measurements and estimates, Journal of Hydrology, 351, 218–229, 2008.

Teemusk, A. and Mander, Ü.: Temperature regime of planted roofs compared with conventional roofing systems, Ecological Engineering, 36, 91–95, 2010.

Theeuwes, N. E., Solcerova, A., and Steeneveld, G. J.: Modeling the influence of open water surfaces on the summertime temperature and thermal comfort in the city, Journal of Geophysical Research: Atmospheres, 118, 8881–8896, 2013.

Thomas, C. K., Kennedy, A. M., Selker, J. S., Moretti, A., Schroth, M. H., Smoot, A. R., Tufillaro, N. B., and Zeeman, M. J.: High-resolution fibre-optic temperature sensing: A new tool to study the two-dimensional structure of atmospheric surface-layer flow, Boundary-layer meteorology, 142, 177–192, 2012.

Tyler, S. W., Selker, J. S., Hausner, M. B., Hatch, C. E., Torgersen, T., Thodal, C. E., and Schladow, S. G.: Environmental temperature sensing using Raman spectra DTS fiber-optic methods, Water Resources Research, 45, 2009.

Van Dam, C. and Van de Ven, F.: Infiltration in Pavement. In: Balmer, P. e.a.(ed), Proc. of the Third Int. Conf. on Urban Storm Drainage, 1984.

Van De Giesen, N., Steele-Dunne, S. C., Jansen, J., Hoes, O., Hausner, M. B., Tyler, S., and Selker, J.: Double-ended calibration of fiber-optic Raman spectra distributed temperature sensing data, Sensors, 12, 5471–5485, 2012a.

Van De Giesen, N., Steele-Dunne, S. C., Jansen, J., Hoes, O., Hausner, M. B., Tyler, S., and Selker, J.: Double-ended calibration of fiber-optic Raman spectra distributed temperature sensing data, Sensors, 12, 5471–5485, 2012b.

Van de Ven, F.: Water balances of urban areas, in: Hydrological Processes and Water Management in Urban Areas, pp. 21–32, IAHS, 1990.

Van Emmerik, T., Rimmer, A., Lechinsky, Y., Wenker, K., Nussboim, S., and Van de Giesen, N.: Measuring heat balance residual at lake surface using Distributed Temperature Sensing, Limnol. Oceanogr.: Methods, 11, 79–90, 2013.

van Emmerik, T., Popp, A., Solcerova, A., Müller, H., and Hut, R.: Reporting negative results to stimulate experimental hydrology, Hydrological Sciences Journal, in press.

van Hove, L., Jacobs, C., Heusinkveld, B., Elbers, J., van Driel, B., and Holtslag, A.: Temporal and spatial variability of urban heat island and thermal comfort within the Rotterdam agglomeration, Building and Environment, 83, 91 – 103, special Issue: Climate adaptation in cities, 2015.

Vercauteren, N., Huwald, H., Bou-Zeid, E., Selker, J. S., Lemmin, U., Parlange, M. B., and Lunati, I.: Evolution of superficial lake water temperature profile under diurnal radiative forcing, Water resources research, 47, 2011.

Verhagen, F., Spek, T., Witte, F., Voortman, B., Moors, E., and Querner, E.: Begrijpen we het watersysteem., Stromingen, 20, 5–19, 2014.

Virk, G., Jansz, A., Mavrogianni, A., Mylona, A., Stocker, J., and Davies, M.: Microclimatic effects of green and cool roofs in London and their impacts on energy use for a typical office building, Energy and Buildings, 88, 214–228, 2015.

Vogt, T., Schneider, P., Hahn-Woernle, L., and Cirpka, O. A.: Estimation of seepage rates in a losing stream by means of fiber-optic high-resolution vertical temperature profiling, Journal of Hydrology, 380, 154–164, 2010.

Völker, S., Baumeister, H., Classen, T., Hornberg, C., and Kistemann, T.: Evidence for the temperature-mitigating capacity of urban blue space - A health geographic perspective, Erdkunde, 67, 355–371, 2013.

Voskamp, I. and Van de Ven, F.: Planning support system for climate adaptation: Composing effective sets of blue-green measures to reduce urban vulnerability to extreme weather events, Building and Environment, 83, 159 – 167, special Issue: Climate adaptation in cities, 2015.

Wang, Y. and Akbari, H.: The effects of street tree planting on Urban Heat Island mitigation in Montreal, Sustainable Cities and Society, 27, 122–128, 2016.

Wang, Z., Lu, J., Xie, L., and Chen, S.: Study on heat island effect of Chongqing in summer, vol. 2, pp. 588–593, 2011.

Wanphen, S. and Nagano, K.: Experimental study of the performance of porous materials to moderate the roof surface temperature by its evaporative cooling effect, Building and Environment, 44, 338 – 351, 2009.

Ward, B. and Minnett, P. J.: An autonomous profiler for near surface temperature measurements, Gas Transfer at Water Surfaces, pp. 167–172, 2002.

Wen-Yao, L., Field, R., Gantt, R., and Klemas, V.: Measurement of the surface emissivity of turbid waters, Remote Sensing of Environment, 21, 97 – 109, 1987.

Westhoff, M., Savenije, H., Luxemburg, W., Stelling, G., Van de Giesen, N., Selker, J., Pfister, L., and Uhlenbrook, S.: A distributed stream temperature model using high resolution temperature observations, Hydrology and Earth System Sciences, 11, 1469–1480, 2007a.

Westhoff, M., Savenije, H., Luxemburg, W., Stelling, G., Van de Giesen, N., Selker, J., Pfister, L., and Uhlenbrook, S.: A distributed stream temperature model using high resolution temperature observations, 2007b.

Wilson, R. C., Hook, S. J., Schneider, P., and Schladow, S. G.: Skin and bulk temperature difference at Lake Tahoe: A case study on lake skin effect, Journal of Geophysical Research: Atmospheres, 118, 2013.

Wong, N., Tan, P., and Chen, Y.: Study of thermal performance of extensive rooftop greenery systems in the tropical climate, Building and Environment, 42, 25 – 54, 2007.

Wong, N. H., Chen, Y., Ong, C. L., and Sia, A.: Investigation of thermal benefits of rooftop garden in the tropical environment, Building and Environment, 38, 261 – 270, 2003.

Woodcock, A. H. and Stommel, H.: Temperatures Observed Near the Surface of a Fresh-Water Pond at Night., Journal of Atmospheric Sciences, 4, 102–103, 1947.

Wu, J.-H., Tang, C.-S., Shi, B., Gao, L., Jiang, H.-T., and Daniels, J.: Effect of ground covers on soil temperature in urban and rural areas, Environmental and Engineering Geoscience, 20, 225–237, 2014.

Xu, J., Wei, Q., Huang, X., Zhu, X., and Li, G.: Evaluation of human thermal comfort near urban waterbody during summer, Building and Environment, 45, 1072–1080, 2010.

Yamagata, H., Nasu, M., Yoshizawa, M., Miyamoto, A., and Minamiyama, M.: Heat island mitigation using water retentive pavement sprinkled with reclaimed wastewater, Water science and technology, 57, 763–771, 2008.

Yamashita, S., Sekine, K., and Shoda, M.: On relationships between heat island and sky view factor in the cities of Tama River basin, Japan, Atmospheric Environment - Part A General Topics, 20, 681–686, 1986.

Yang, X. and Zhao, L.: Diurnal thermal behavior of pavements, vegetation, and water pond in a hot-humid city, Buildings, 6, 2015.

Zhang, N., Yu, X., Pradhan, A., and Puppala, A. J.: Thermal conductivity of quartz sands by thermo-time domain reflectometry probe and model prediction, Journal of Materials in Civil Engineering, 27, 04015 059, 2015.

Zhang, X., Hu, L., Bian, X., Zhao, B., Chai, F., and Sun, X.: The most economical irrigation amount and evapotranspiration of the turfgrasses in Beijing City, China, Agricultural Water Management, 89, 98–104, 2007.

Zhou, D., Zhao, S., Liu, S., Zhang, L., and Zhu, C.: Surface urban heat island in China's 32 major cities: Spatial patterns and drivers, Remote sensing of environment, 152, 51–61, 2014.

Zölch, T., Maderspacher, J., Wamsler, C., and Pauleit, S.: Using green infrastructure for urban climate-proofing: An evaluation of heat mitigation measures at the micro-scale, Urban Forestry and Urban Greening, 20, 305–316, 2016.

APPENDIX

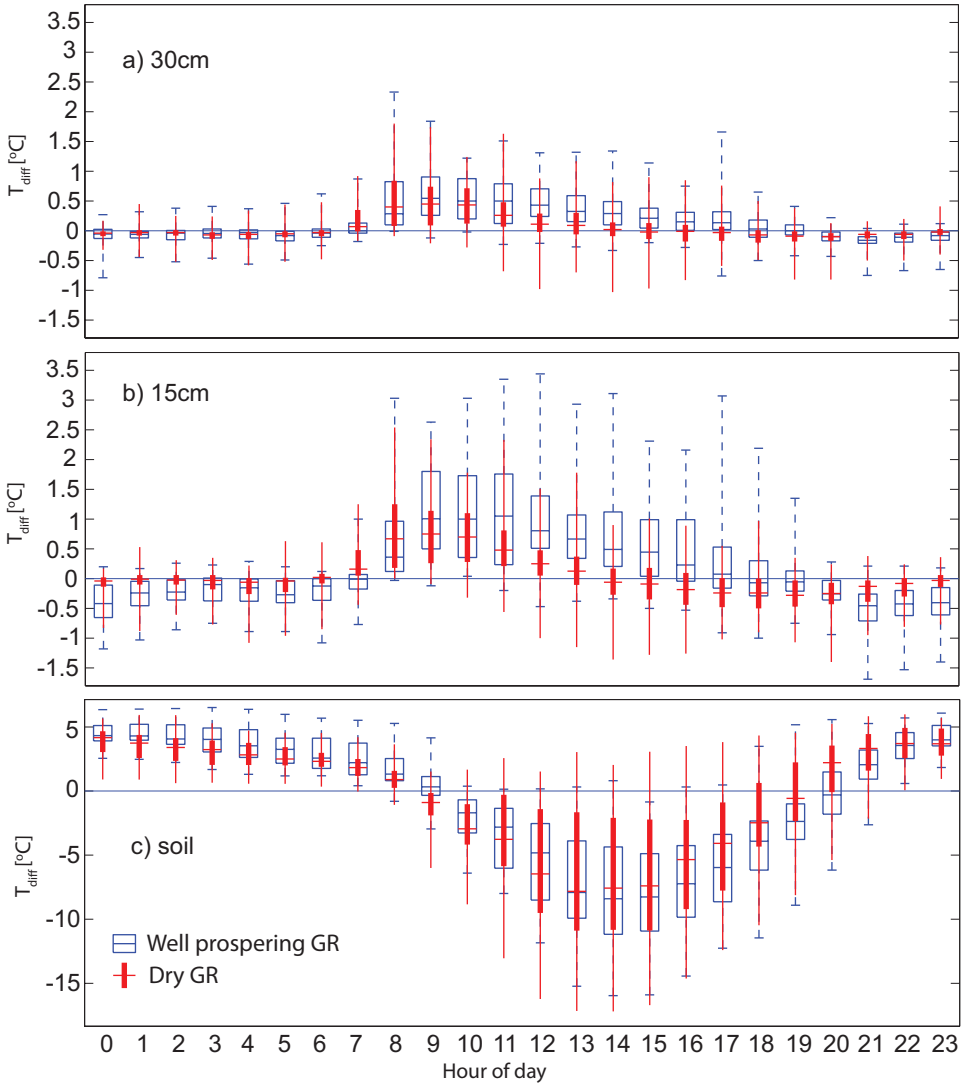

Figure I: Averages for each hour of a day for temperature difference (T_GR4 - T_WG) 30 cm above the roof surface (a), 15 cm above the roof surface (b) and in the soil (c) for well prospering GR (blue boxes, 2013) and dried out GR (red bars, 2012). On each box or bar, the central mark is the median, and the edges of the box or the spread of the bar are the 25th and 75th percentiles. Whiskers represent extreme values excluding outliers.

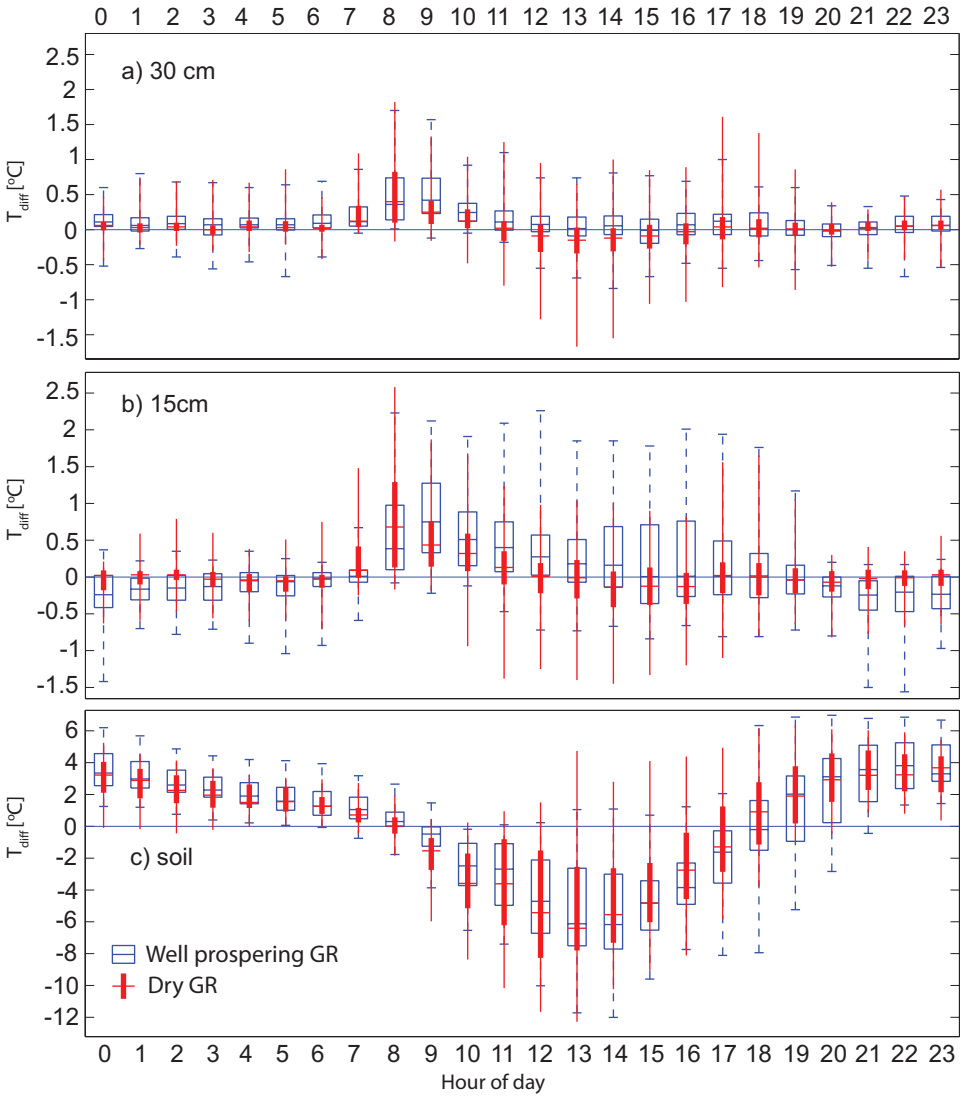

Figure II: Averages for each hour of a day for temperature difference (T_GR7 - T_WG) 30 cm above the roof surface (a), 15 cm above the roof surface (b) and in the soil (c) for well prospering green roof (blue boxes, 2013) and dried out green roof (red bars, 2012). On each box or bar, the central mark is the median, and the edges of the box or the spread of the bar are the 25th and 75th percentiles. Whiskers represent extreme values excluding outliers.

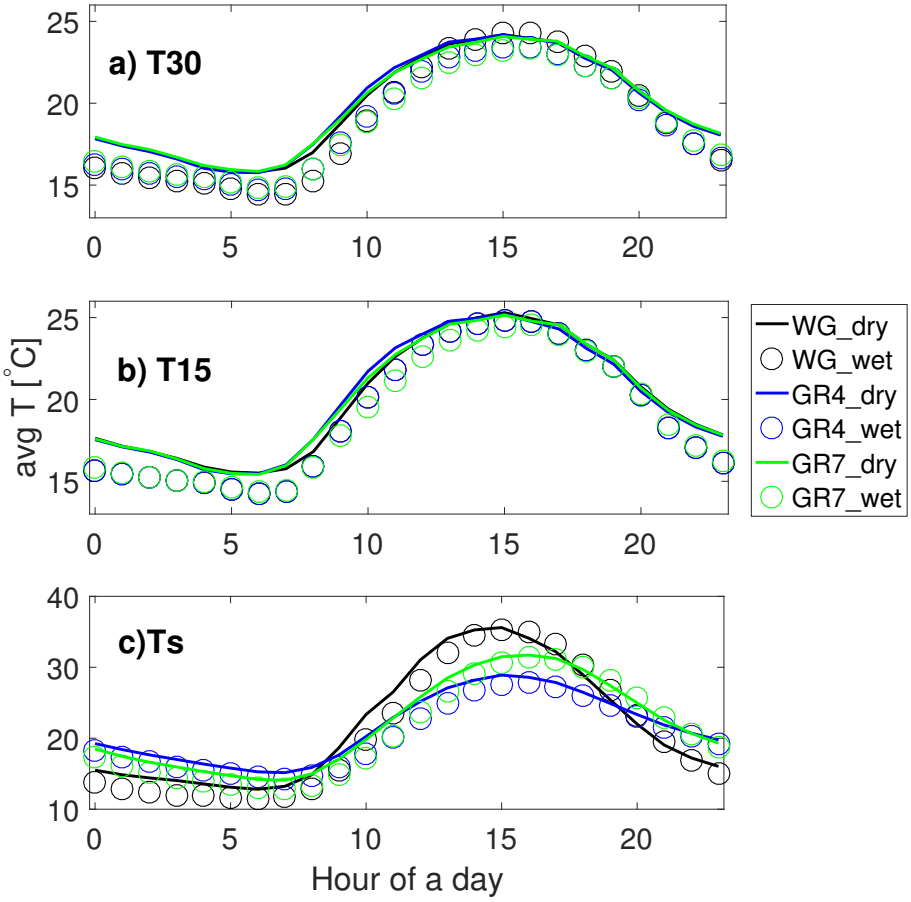

Figure III: Averages for each hour of the day for all the measured temperatures for 30 cm above the roof surface (a), 15 cm above the roof surface (b) and in the soil (c) for well prospering GR (circles, 2013) and dried out GR (lines, 2012). Note that average 2 m temperature was 1°C higher in 2012 than in 2013 (19.0 vs. 20.1°C). Correspondingly, the surface temperature of the gravel was also 1°C warmer in 2012. For this reason we only include the temperature differences in the main text.

Table I: P-values for Kolmogorov–Smirnov test comparing T_{dif} for well prospering GR with T_{dif} for dried GR for each hour of a day, as shown in Figures 6, 7 and 8. Two data sets with P-value below 0.05 are generally considered significantly independent. The lower the P-value the higher the statistical significance of rejecting the hypothesis that both data sets (dry and well prospering year) are drawn from the same overall dataset.

	Ts_GR4	**T15_GR4**	**T30_GR4**	**Ts_GR7**	**T15_GR7**	**T30_GR7**
0	$1.3\ 10^{-3}$	$3.8\ 10^{-13}$	0.02	$3.9\ 10^{-3}$	$1.6\ 10^{-6}$	$3.9\ 10^{-3}$
1	$3.5\ 10^{-6}$	$4.0\ 10^{-9}$	0.04	$1.3\ 10^{-3}$	$1.0\ 10^{-8}$	$6.5\ 10^{-3}$
2	$1.6\ 10^{-6}$	$3.5\ 10^{-12}$	0.04	$6.0\ 10^{-5}$	$1.4\ 10^{-7}$	$3.9\ 10^{-3}$
3	$1.6\ 10^{-6}$	0.01	0.01	$1.3\ 10^{-3}$	$4.1\ 10^{-4}$	$7.3\ 10^{-6}$
4	$4.1\ 10^{-4}$	0.04	0.01	0.03	0.53	$3.9\ 10^{-3}$
5	0.02	$3.1\ 10^{-5}$	0.04	0.06	0.24	0.09
6	0.03	$1.6\ 10^{-6}$	0.65	0.32	0.42	$6.0\ 10^{-8}$
7	$7.5\ 10^{-4}$	$6.0\ 10^{-10}$	$2.3\ 10^{-3}$	0.02	$4.1\ 10^{-4}$	0.88
8	$1.2\ 10^{-4}$	0.04	0.65	0.01	0.13	0.42
9	$2.2\ 10^{-10}$	$1.3\ 10^{-3}$	0.04	$6.0\ 10^{-8}$	$1.3\ 10^{-3}$	$1.6\ 10^{-6}$
10	$1.3\ 10^{-3}$	$1.4\ 10^{-7}$	0.04	$2.3\ 10^{-3}$	$1.2\ 10^{-4}$	$1.3\ 10^{-3}$
11	0.02	$8.2\ 10^{-9}$	$2.7\ 10^{-5}$	0.08	$2.7\ 10^{-5}$	$5.4\ 10^{-5}$
12	0.09	$1.2\ 10^{-13}$	$1.0\ 10^{-11}$	0.09	$7.3\ 10^{-6}$	$1.0\ 10^{-8}$
13	0.42	$3.5\ 10^{-12}$	$6.0\ 10^{-8}$	0.65	$2.3\ 10^{-3}$	$1.6\ 10^{-6}$
14	0.24	$3.6\ 10^{-15}$	$3.9\ 10^{-14}$	0.17	$2.5\ 10^{-8}$	$3.2\ 10^{-7}$
15	0.09	$8.2\ 10^{-11}$	$1.0\ 10^{-8}$	0.13	$4.1\ 10^{-4}$	0.03
16	0.03	$2.8\ 10^{-10}$	$4.0\ 10^{-6}$	0.03	$8.3\ 10^{-6}$	$8.1\ 10^{-4}$
17	$2.1\ 10^{-3}$	$3.2\ 10^{-8}$	$6.3\ 10^{-12}$	$3.5\ 10^{-3}$	$5.7\ 10^{-3}$	0.11
18	$2.1\ 10^{-3}$	$3.8\ 10^{-4}$	$3.1\ 10^{-5}$	0.07	0.27	0.15
19	$2.1\ 10^{-4}$	$1.7\ 10^{-6}$	$3.7\ 10^{-6}$	$2.1\ 10^{-3}$	0.20	0.57
20	$3.8\ 10^{-7}$	0.46	0.69	0.01	0.05	0.12
21	$5.9\ 10^{-5}$	$7.6\ 10^{-13}$	$1.8\ 10^{-11}$	0.05	$3.2\ 10^{-8}$	0.36
22	0.20	$8.8\ 10^{-10}$	$3.5\ 10^{-3}$	$9.0\ 10^{-3}$	$3.7\ 10^{-6}$	0.27
23	$5.7\ 10^{-3}$	$7.6\ 10^{-13}$	$3.2\ 10^{-8}$	$1.2\ 10^{-3}$	$5.5\ 10^{-9}$	0.03

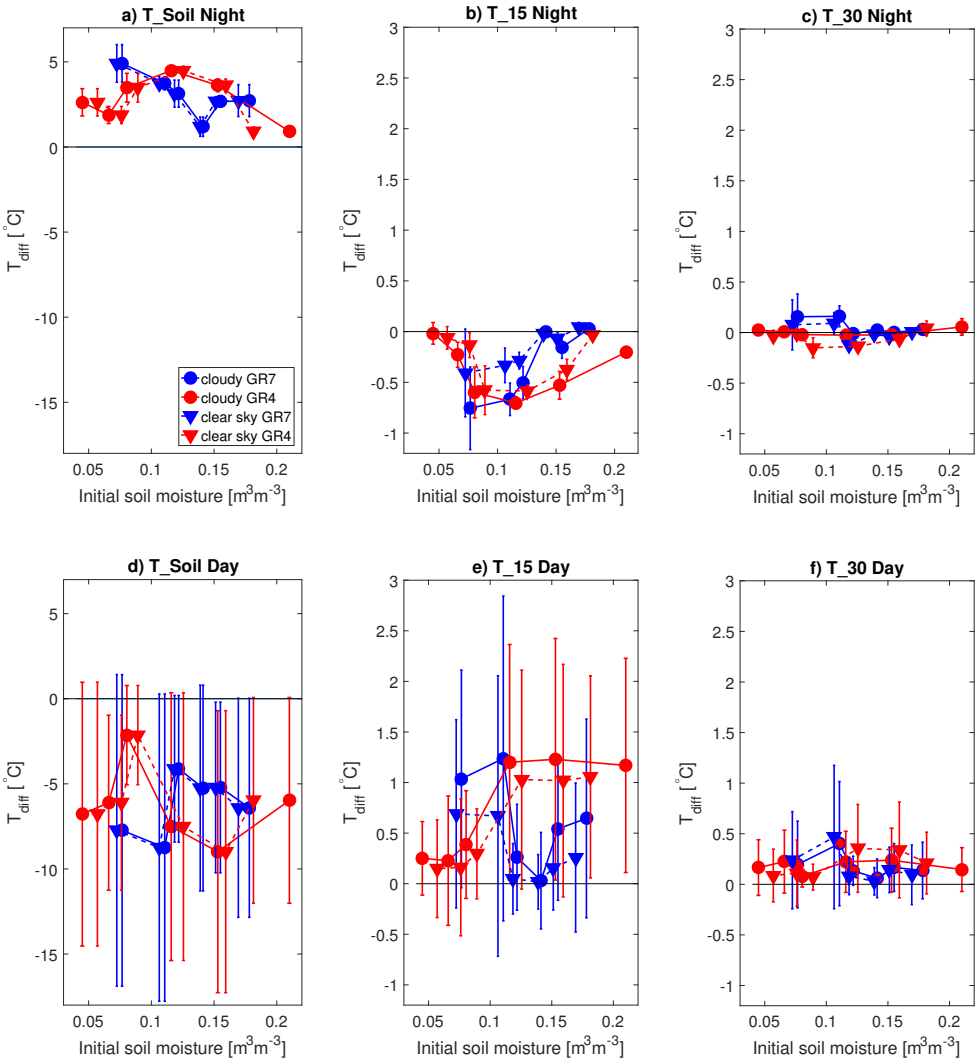

Figure IV: Influence of soil moisture on temperature change. Each point represent the mean temperature difference (T_{dif} = T_{GR} - T_{WG}) for the whole night/day with respect to initial soil moisture. Error bars show the standard deviation. Note the different scales for soil temperatures and air temperatures.

ACKNOWLEDGEMENTS

There. Done. Finally.

After five years at TU Delft I am saying good bye. Good bye and thank you! Thank you, all you people without whom this could not have been done, and people without whom this would not be done; simply because I would loose my focus, my enthusiasm, my will to go on.

Originally, I considered to just write a very short acknowledgement chapter: "*To whom it might concern: Thank you!*". But no, for once I'll put aside my natural urge to be concise and praise the heroes of my academic life publicly.

First on the list are undoubtedly Frans van de Ven and Nick van de Giesen, my supervisor / co-promotor and my promotor. I value your input and your guidance! I distinctly remember that during the interview I had while applying for this position, I mentioned I don't like frequent supervision; that I like to work on my own. Now, at the end of my journey I feel lucky for the perfect balance of supervision and independence we found over the years. I feel that the research I have done is *mine*. I was not controlled and pushed in certain direction, but left to make my decisions and find my ways while carefully guided through the difficult moments. When I needed help, it was always there and for that I am grateful. Thank you!

This PhD could never even start without the financial support of Climate KIC, and more specifically, the Blue Green Dream project. Thanks to the BGD project I have met many interesting people and shared innovative research ideas. Climate KIC then provided not only the necessary financial support, but also the opportunity to travel and get inspired by meeting young entrepreneurs in the field of sustainable development.

I would like to thank the committee members for investing their time into reading my thesis and participating in the discussion.

I want to thank my co-authors for contributing significantly to this dissertation.

To Michiel Rijsdijk for providing all the data for the green roof research, the access to the site, and the idea to do this in a first place.

To Mengyu Wang for being a great student and doing a wonderful job analyzing the green roof data.

To John Selker for helping me figure out the whole surface energy balance of that thin layer of water on the op of the pond. It was our discussion that finally made me realize the direction of the "skin paper".

To Koen for ...so much. Thank you for showing me how DTS works, for teaching me how to use Ultima and for what are all the settings. Thank you for teaching me how to splice cables, and showing me how tight I can wrap them before it becomes a problem. Thanks for all the MatLab scripts that I could use as a base for my analysis. Thank you for

the possibility to use your measurement setup (and helping me with it), without which the Uchimizu research would never happen. Thank you for coauthoring three papers with me. You have been a great help and a good friend!

To Tim for writing almost all the introductions to almost all my papers. I hate that stuff and you are great at it!

And of course, once more, thanks to Nick and Frans.

Thanks all the other people who helped with the research. Thank you everyone, who helped with the field work. Thank you all for helping me when I had a question. Thanks for all the help with measurement equipment.

I would like to also thank Gordon Godshalk. Gordon, the short lesson you gave me about scientific writing left a deep impression and helped me organize my thoughts more than any course I took before. Thank you.

Big thanks to the secretaries, Betty, Lydia, Luz, and Petra. Without your help with administration and the-small-every-day-stuff-I-just-couldn't-figure-out this would be much much harder. On top of that, thank you Lydia for becoming my friend and for being there when I just needed to talk to someone.

I have spent three amazing months of my PhD in Singapore. During this time I have gained a lot of new insights into urban climate of tropical cities. This is mostly thanks to Prof. Tan Puay Yok. I am very glad I could have cooperated with your research group in Singapore and to follow your course.

From the list of all the wonderful people I met in Singapore, I would like to more specifically thank Kathrin Schmiele. Thank you for introducing me to the local culture, for the hikes and good talks, and for letting me tag along with your research.

I would like to thank all the office-mates I had over the years. I believe I have been incredibly lucky, because the people who passed through thee room 4.96 of the civil engineering building were all amazing specimens of human beings!

Tim, thank you for being there the whole time...

Marja, with you it was a love on first sight! I still remember thinking "I want to be friends with this girl!". I am happy it worked out. (/textitplease, find a sentimental note attached to this thesis...:))

Aagje, thank you for showing me that people can be good friends, even if they have an opposite opinion about almost everything; except on roller-coasters. I enjoyed our discussions and they helped me to understand different points of view and the reasoning behind them.

Laurene, thank you for being the understanding friend who listens when I needed the most. Also, thank you for helping me with my Dutch motivation letters! I am sure I wouldn't be able to get a job without you...

Bart, thanks for making our office smell like basil! Also thank you for understanding, what is the perfect time to leave for a beer.

Gabi, thank you for taking care of the people I left behind in the office.

Boran, thank you for being "the most normal friend of mine", as Jeroen often puts it. Also, thank you for winning the fitterij with me.

Remco, Cesar, thanks for trying to defeat us, twice, tough luck...

Miriam, thanks for all the intel about cakes and cookies available for free consumption in our closest proximity. It is always good to have a soul-mate around.

Santiago, thank you for becoming a great friend, for trying to explain Python (sorry, I forgot it all by now), and for staying a friend even after you left Delft. Also, thank you for introducing me to your lovely wife.

Thank you Sandra dV. for making a beautiful poster skirt for me, it made me famous!

I also want to thank all the ladies that became my friends over the years, and then moved to another country (this is becoming a pattern, I wonder why). Tanja, Marie, and Sandra J., thank you!

Catherine, thank you for being the one friend who decided to return! The list of things I need to thank you for is quite long, so I just name two here, and the rest later in person. Thank you for doing the language editing of several (few? quite some, but not all?) of my papers. And thank you for being my wind shield during that night we slept in a tent when hurricane Irene blew over Iceland!

I would also like to thank all the people from volleyball, my teammates and trainers. We spent a great time together, and hitting whole lot of balls really hard provided me with some necessary emotional release. Thanks to this, I could go on through my days with a smile on my face.

More specifically, I would like to thank Anne and Nynke. You two became great friends. You offered new perspectives to old problems, and you were always there for me when needed.

Thank you, Carina, for being the voice of reason during the last year of my PhD. It is great to have you in my life and I trust you will always cover (for) me...

Big thanks to all my students! You taught me a lot and your great ideas, new perspectives, and enthusiasm made me hopeful about the future of this planet.

I would also like to thank all the people who took part at the press releases and "stories of science" related to my research. I enjoyed our cooperation and it is largely thanks to you that the Uchimizu research went viral!

The last year has been difficult. Lot of things went wrong and I wasn't in a happy place. During this time, there were two people who made these hard times better, even enjoyable. Bart and Rolf, thank you for being there.

Bart, thank you for all the tea, the bluegrass and cider in Mekelpark, delicious snacks, guitar music, and plaid fashion. Most importantly, thank you for the bluegrass version of "Oops I did it again", I'll never forget that!

Rolf, thank you for all the coffee and daiquiris, for introducing me to Sandman and reintroducing graphical novels and comic books to my life, and for convincing me that the comfort provided by broad trousers is just way too high to ignore. Most importantly, thank you for showing me that sometimes I can be wrong about people I don't like. On top of that, thank you both for providing a gossip topic to the whole department!

Samozřejmně bych chtěla poděkovat svojí rodině. Mojí milované sestřičce Olince, bez které by to stálo za prd! A mým rodičům za to, že při mě vždycky stáli a byli tu pro mě když jsem je potřebovala. Mám vás moc ráda a děkuju za všechno!

When it comes to family, I would also like to thank Jeroen. You were there with me every step of the way and I couldn't ask for more. Thank you! x

Všem kamarádům v Čechách a na Moravě! I přesto že se vidáme párkrát za rok, jsem ráda, že vás mám! Děkuju!

And, the best for last... Tim, thank you. Thank you for being there the whole four years. Thank you for co-authoring enough papers with me to make a whole new PhD. Thank you for being my friend and for all the moral support throughout the years. Thank you for sharing the exciting stories of your life with me and consequently being "my private soap opera". Thank you for setting an example and making me want to do more: to become a part of Young HS, to organize a short course at EGU. Thank you for the brilliant research ideas that mostly came while philosophizing with a cold beer in hand. I don't think I could have done this without you.

I hope I didn't forget anyone, but if I did, please, forgive me. It doesn't mean I value your contribution any less. I also hope I didn't insult anyone with the unbearable lightness of these acknowledgements. Please, know that I value your scientific contribution very much. I just wanted to let you know that you will all be remembered as people and as friends, not as stepping stones in my career.

CURRICULUM VITÆ

Anna Solcerova

anna.solcerova@gmail.com
+31 (0) 645 305 610

WORK EXPERIENCE

PHD WATER MANAGEMENT, *Researcher* 2013 - 2017
Role of water in the cooling effect of blue-green climate adaptation facilities in the urban environment. Focus on field work and data analysis.

KNMI, *Researcher* May - September 2012
Internship focused on analyzing radio-sounding profiles. The goal was to study under which conditions, concerning the atmospheric profiles, are observed the most intense precipitation events.

AOC TERRA, *Consultant* January - March 2012
Student consultancy project focused on integration of policies towards public space in municipalities of Dantumadiel (Friesland) and Zuidhorn (Groningen).

EDUCATION

IR. ENVIRONMENTAL MODELLING 2009 - 2013
Czech University of Life sciences, Faculty of Environmental Sciences
Comprehensive training in modeling of natural processes associated with inanimate nature, such as hydrological and hydraulic modeling, modeling of chemical processes and processes in the atmosphere.

MSC. METEOROLOGY AND CLIMATE 2010 - 2012
Wageningen University
Key elements of this specialization are the physics of atmospheric systems and climate processes, as well as computer skills and advanced statistics.

BSC. LANDSCAPING 2006 - 2009
Czech University of Life sciences, Faculty of Environmental Sciences
General overview of processes in landscape including hydrology, geodesy, urban planning, botany, dendrology, ecology, etc.
Thesis topis: El-Nino phenomenon.

LANGUAGES

Native Speaker
Professional Proficiency
Advanced level
Intermediate level

IELS Language (English) summer school (Sliema, Malta)
Direct Dutch Language school (Den Haag, The Netherlands)
LSI Language (German) summer school (Zürich, Switzerland)

SKILLS & INTERESTS

WRF (NCL)
Matlab
R
Adobe Illustrator

LaTex
HoBo ware
Pascal Lazarus
Linux

Hobbies: Volleyball (Czech National Junior League, now Promotieklasse), Snowboarding, Skiing, Traveling, Hiking, Reading, Oriental dance, Organizing social events

Driving license: B (since 2005)
Other: Climate-KIC Phd
Member of IntegraCie committee of the study association Pyrus at Wageningen University (position of secretary and PR)

List of Publications

8. **Solcerova, A.**, F. van de Ven, and N. van de Giesen, *Nighttime cooling of an urban pond*, submitted to Frontiers in Earth Science: Hydrosphere.

7. Lutz, S. R., A. Popp, T. van Emmerik, T. Gleeson, L. Kalaugher, K. Möbius, T. Mudde, B. Walton, R. Hut, H. Savenije, L. J. Slater, **A. Solcerova**, C. Stoof, and M. Zink, *"HESS Opinions: Science in today's media landscape–challenges and lessons from hydrologists and journalists.*, commentary in preparation for Hydrology and Earth System Sciences, 22 (2018): 3589-3599.

6. van Emmerik, T., A. Popp, **A. Solcerova**, H. Müller, and R. Hut, *Reporting negative results to stimulate experimental hydrology: discussion of "The role of experimental work in hydrological sciences–insights from a community survey"*, Hydrological Sciences Journal (2018): 1-4.

5. **Solcerova, A.**, T. van Emmerik, K. H. Hilgersom, F. van de Ven, and N. van de Giesen, *Uchimizu: A Cool (ing) Tradition to Locally Decrease Air Temperature.*, Water, 10.6 (2018): 741.

4. **Solcerova, A.**, T. van Emmerik, F. van de Ven, J. Selker, and N. van de Giesen, *Skin effect measured in fresh water bodies using distributed temperature sensing*, Water, 10.2 (2018): 2073-4441.

3. **Solcerova, A.**, M. Wang, M. Rijsdijk, F. van de Ven, and N. van de Giesen, *Do green roofs cool the air?*, Building and Environment, 111 (2017): 249 – 255 .

2. Hilgersom, K. H., T. van Emmerik, **A. Solcerova**, W. Berghuijs, J. Selker, and N. van de Giesen, *Practical Considerations for enhanced-resolution coil-wrapped Distributed Temperature Sensing setups*, Geoscientific Instrumentation, Methods and Data Systems, 5 (2016): 151 – 162 .

1. Theeuwes, N. E., **A. Solcerova**, and G. J. Steeneveld, *Modeling the influence of open water surfaces on the summertime temperature and thermal comfort in the city*, Journal of Geophysical Research: Atmospheres, 118.16 (2013): 8881 – 8896 .